LAPPEENRANTA-LAHTI UNIVERSITY OF TECHNOLOGY LUT
LUT School of Energy Systems
Degree Programme in Electrical Engineering

Jouni Kortelainen

UTILIZATION OF DIGITAL TWIN IN MODEL-BASED CONTROL OF FLOTATION CELLS

Examiners: Professor, D.Sc. (Tech.) Olli Pyrhönen
D.Sc. (Tech.) Niko Nevaranta

Supervisors: D.Sc. (Tech.) Mika Kosonen
D.Sc. (Tech.) Antti Remes
M.Sc. Sakari Kauvosaari

ABSTRACT

Lappeenranta – Lahti University of Technology LUT
LUT School of Energy Systems
Degree Programme in Electrical Technology

Jouni Kortelainen

Utilization of digital twin in model-based control of flotation cells

Master's thesis 2019
102 pages, 66 charts, 7 tables and 2 appendices

Examiner: Professor, D.Sc. (Tech.) Olli Pyrhönen
D.Sc. (Tech.) Niko Nevaranta

Keywords: froth flotation, froth speed control, optimization, digital twin, modeling, MPC, HSC

Optimization of flotation plants has become an important field of research as the demand for minerals is growing rapidly. The goal of the optimization is to reach the maximum recovery while keeping the grade of the product within limits. The trend in optimization controllers is moving towards model-based control as the long delays and time constants make it hard for other type of control laws to operate while getting the response models for the controllers requires long tests at the plant. In this thesis, a flotation model is created with HSC tool by Outotec and it was fitted according to real plant data. The model is then tested as a tool for producing the response models for the grade-recovery optimizer by making steps to froth speed models which are operated by controlling the air flowrates of the cells. Results showed that the model produced dynamics that were close to those of the real plant but estimation of the plant gain proved to be difficult with the available plant data. The gain is mostly affected by the relations between mineral kinetics, the change in air flowrate during the step and the cell by cell recovery. The results show that it is possible to use HSC to produce a priori model, but the gain of the response would have to be fitted with the traditional plant tests. Getting the model to produce correct gain would require more analysis points with more analyzed elements which would make kinetics fitting possible.

TIIVISTELMÄ

Lappeenrannan – Lahden teknillinen yliopisto LUT
LUT School of Energy Systems
Sähkötekniikan koulutusohjelma

Jouni Kortelainen

Utilization of digital twin in model-based control of flotation cells

Diplomityö 2019
102 sivua, 66 kuvaa, 7 taulukkoa ja 2 liitettä

Tarkastaja: Professori Olli Pyrhönen
TkT Niko Nevaranta

Hakusanat: vaahdotusrikastus, vaahdonnopeussäätö, optimointi, digitaalinen kaksonen, mallinnus, MPC, HSC

Vaahdotusrikastuksen optimoinnin merkitys on kasvanut, koska mineraalien tarve on kasvanut voimakkaasti. Optimoinnin tavoitteena on saavuttaa mahdollisimman korkea saanti pitäen mineraalipitoisuus sille asetettujen rajojen sisällä. Optimoinnin trendi on suuntautumassa mallipohjaisiin säätöihin sillä pitkät viiveet sekä aikavakiot tekevät prosessista vaikeasti säädettävän muille säätöratkaisuille, mutta mallien aikaansaaminen kuitenkin vaatii pitkiä testejä laitoksella. Tässä tutkielmassa tehtiin vaahdotusrikastuksen malli HSC-sovelluksella ja se sovitettiin saatavilla olevaan laitosdataan. Mallin soveltuvuutta pitoisuussaanti optimoijan tarvitsemien vastemallien tuottamiseen testattiin tekemällä askelmaisia muutoksia vaahdon nopeusmalliin, joka sääti rikastuskennojen ilmansyöttöä. Tuloksista selvisi, että malli tuotti laitosdataa vastaavat dynamiikat, mutta vahvistus oli vaikea saada oikeaksi. Vasteen vahvistukseen vaikuttaa voimakkaasti mineraalien kinetiikkojen suhde, vaadittava ilmavirtauksen muutos askeleen aikana sekä kennokohtaiset saannit. Tuloksien pohjalta HSC:llä on mahdollista tuottaa a priori mallit vasteille, jotka kuitenkin vaatisivat vahvistuksien sovituksen laitoksella. Vahvistuksen oikeaksi saaminen vaatisi lisää analyysipisteitä sekä enemmän analysoitavia elementtejä, jolloin kineettisten vakioiden sovitus olisi mahdollista.

ACKNOWLEDGEMENTS

I want to thank Outotec Oy for giving me the opportunity to write this thesis and giving me the resources I needed. This master's thesis was written whilst working at Outotec Oy Lappeenranta.

Firstly, I want to thank my examiners Professor D.Sc. Olli Pyrhönen an D.Sc. Niko Nevaranta at the university, who were active in arranging meetings and giving great questions, comments and guidance.

Secondly, I want to thank my supervisors D.Sc. Mika Kosonen, D.Sc. Antti Remes and M.Sc. Sakari Kauvosaari at Outotec Oy, for guiding me throughout the thesis by having regular meetings. I especially want to thank Mika Kosonen for his efforts in reading the drafts of the thesis, setting it higher standards and pushing me to improve.

Thanks to everyone else involved, regardless however small their part in making this thesis was, as all the help and effort was valuable. Thanks to Johanna Kortelainen and Julia Puustinen for always being there for me and showing that life is beautiful.

Jouni Kortelainen
Lappeenranta 5. November 2019

TABLE OF CONTENTS

ABSTRACT 2
TIIVISTELMÄ 3
ACKNOWLEDGEMENTS 4
TABLE OF CONTENTS 5
LIST OF SYMBOLS 7
LIST OF ABBREVIATIONS 9

1. Introduction 10
1.1. Research objectives and limitations 11
1.2. Structure of the thesis 12

2. Flotation 13
2.1. Flotation cells 13
2.1.1. Flotation circuits 15
2.1.2. Flotation circuit design 16
2.2. Forms of particle recovery 18
2.3. Flotation modeling 20
2.3.1. Micro-scale model 22
2.3.2. Flotation kinetics 25
2.4. Reagents 27
2.5. Grade and recovery 29

3. Control of Flotation Circuits 32
3.1. Base level control and instrumentation 33
3.1.1. Cell level measurement and control 34
3.1.2. Cell air flowrate measurement and control 35
3.1.3. Reagents 36
3.2. Element assaying 37
3.3. Froth speed and characteristics 39
3.4. Advanced control and optimization 40
3.4.1. Predictive control 40
3.4.2. Froth speed control 42
3.4.3. Grade-recovery optimization 43

4. HSC Sim Model as a Digital Twin 45
4.1. Digital twin 45
4.2. Components of the flotation model 46
4.3. Recovery model 48
4.4. Interaction between cells in a bank 51
4.5. Dynamics of the flotation cell model 53
4.5.1. Response to a level Step 53
4.5.2. Response to an air step 58
4.5.3. Response in the middle cell 61

5. Experimentation with HSC 63
5.1. Preliminary laboratory results 63
5.2. Gathering values from the plant data 64
5.3. Modeling froth speed 68
5.3.1. Constant hf model 68
5.3.2. Neural network structures 69
5.3.3. Training the neural netork model 70
5.4. Model parameterization with HSC 73
5.4.1. Nominal operating point 73
5.4.2. Fitting of the grades and the recovery 75

6. Responses from the Simulation 76
6.1. Measured responses from the plant test 76
6.2. Comparison of measured and simulated responses 77
6.3. Effect of the recovery in the simulation 79
6.4. Effect of the air flowrate in the simulation 80
6.5. Effect of the flotation kinetics in the simulation 81
6.6. Summary of the results 82

7. Discussion 84

8. Conclusion 87

References 89

Appendices

Appendix 1: HSC flotation circuit model

Appendix 2: Air flowrate, level and froth speed during the plant step tests 1 through 5

LIST OF SYMBOLS

A	area
α	froth recovery exponent
d_b	bubble size
d_i	particle size
δ	drainage parameter
E	energy
e	error
ϵ_g	air holdup
g	gravitational constant
h	height
H	height inside the tank
θ	contact angle
J_g	superficial gas velocity
k	flotation rate constant
λ_{air}	gas residence time
M	mass
m	mass fraction
P	mineral floatability
Q	flowrate
R	recovery
S	penalty
S_b	bubble surface area flux
t	time
τ	residence time
u	actuation
V	volume
W	work of adhesion
w	weight
X	input feed
ζ	entrainment parameter

Subscripts

μ	flow resistance
c	collection
e	entrainment
f	fast-floating / froth
fc	final concentrate
N	non-flotating
p	pulp
s	slow-floating
s/a	solid-air-interface
s/w	solid-water-interface
w	water
w/a	water-air-interface

LIST OF ABBREVIATIONS

ACT	Advance Control Tools
APC	Advanced Process Control
BSAF	Bubble Surface Area Flux
CCC	Critical Coalescence Concentration
GH	Gas Hold-up
GRO	Grade-Recovery Optimizer
HSC	Name of the process modeling software package supplied by Outotec
IEP	Isoelectric Point
MPC	Model Predictive Control
NN	Neural Network
NSG	Non-Sulphide Gangue
NSR	Net Smelter Return
PAX	Potassium Amyl Xanthate
PI	Proportional Integral
ReLu	Rectifier Linear Unit
XRF	X-Ray Fluorescence

1. Introduction

Froth flotation is an enrichment process which uses particles' different surface properties to selectively separate them from one another. The first commercial froth flotation plant was established over a hundred years ago and nowadays the process is seen as the most important invention in the field of mining (Bunyak, D, 2000) and it has become the standard method for selective mineral separation (King, R, 2012).

During the last ten years, the average grade of copper ore decreased by 25 % (Calvo, G., et al., 2016). The grades are decreasing because of the increasing demand for copper, which has been doubling every 25 years since 1900 (Meinert, L. et al., 2016). The high demand drives plants to use lower grade deposits, which are made profitable by high recovery and thus optimization.

Goal of the flotation optimization is to keep the concentrate grade above the acceptable limit while the recovery of the valuable minerals is maximized. Due to the long time delays and time constant of the process, model predictive control (MPC) is well suited for its control (Lundh, M., et al., 2009). Getting of the response models for the controller design however, require long step tests at the plant which may be intrusive to plant operation as non-optimal changes must to be done in order to get the response models.

As the flotation modeling has developed, simulation environments can offer a non-intrusive, disturbance free and precise testing environment with no measurement errors. Therefore, it is considered whether a simulator should replace the traditional step tests at the plant.

HSC Sim is Outotec's simulation software which includes simulation models for the flotation process. The simulator is mostly used as a static simulator which calculates the steady state of the system, but it also has a dynamic calculation mode which shows the intermediate states of the system. The dynamic model can be parameterized based on plant data, after which the model can be used to conduct an experiment to see how the simulated responses compare to step test measurements from a real plant. The comparison can then be used to estimate HSC's capabilities to calculate the response models for the MPC of the grade-recovery optimizer.

If the simulated tests are successful, they could partially replace the plant testing and become a standard method used in controls commissioning.

1.1. Research objectives and limitations

The objective of this paper is to study HSC Sim simulation software's capabilities in producing response models for a grade-recovery optimizer when a dynamic flotation circuit model is parameterized according to actual plant measurements.

The purpose of this thesis is to create an understanding about the general flotation process dynamics and response models for the grade-recovery optimizer. Additionally, the capabilities of the HSC simulator are studied and its suitability for response model testing is assessed based on whether:

- the simulator can produce the response models for the grade-recovery optimizer,
- the simulator can be used to create a priori response models which could be used as start-up models in control commissioning.

The study is conducted with a presumption that digital twins can be implemented using Outotec's HSC Sim simulation platform and by using the existing dynamic flotation cell, conditioner and pump sump models. It is also presumed that real plant data is available for model parameterization and plant step response tests results are available for the response comparison.

The experimentation in this thesis includes parameterizing of a simulation model according to the available plant data when no additional laboratory test campaigns are made. The parameterization is done on a hypothesis that if the concentrate and tailings grades are correct during steady state operation at the nominal operating point, the resulting response should be correct.

The plant data in use is from a control commissioning period at a real plant which includes the froth speed step test results. The fitting data has eight days of data with a sampling time of 15 seconds.

1.2. Structure of the thesis

The thesis is divided between a theoretical and an experimentational results section where the chapters two to four are the theoretical part and five to six are the experimental results part. The experimental section is followed by discussion and conclusion.

First, an understanding of the flotation process is developed by a literary research by studying its operational targets, subprocesses, modeling, control and measurements. The HSC Sim's flotation cell model is then studied in detail to create an understanding about the recovery model and the physical functions involved. The flotation cell's Air flowrate's and level's effect to concentrate and tailings grade is then studied by using the HSC Sim.

The grade-recovery optimizer uses froth speed, controlled by air flowrate and level, in its control scheme. As the HSC lacks an integrated froth speed model, a neural network model (NN-model) is developed for each cell in the flotation circuit in order to find a relationship between the process variables and the froth speed. A flotation circuit with eight cells is then modeled and fitted based on plant data.

Plant step tests are then replicated in the simulation environment and the simulated response models are compared to those of a real plant. The comparison is then used to assess whether the simulator can produce the response models for the grade-recovery optimizer. The simulators capability to create a priori models is assessed by studying the response dynamics and seeing whether there's usable similarities between the real response and the simulator's response models.

2. Flotation

Froth flotation is a selective separation process based on material's surface properties making it hydrophobic, meaning the material is repellent of water, or hydrophilic, meaning the material has affinity towards water. The technique is common in mineral processing, but the technology is also widely used in wastepaper deinking, water treatment and plastic separation (Nguyen, A., 2007).

Terms foam and froth are often interchangeable but in the mining industry, foam is known as a two-phase system consisting of water and gas whereas froth is a three-phase system consisting of macro-clusters of air and water with particles dispersed into it (Pugh, R., J., 2016)

2.1. Flotation cells

In froth flotation, slurry with finely crushed minerals is fed into a flotation cell. Air is fed into the tank from the bottom and the air bubbles start to rise to the surface. Hydrophobic minerals attach themselves to the rising bubbles whereas the hydrophilic do not. The hydrophobic particles float to the surface of the pulp where a layer of froth begins. As the layer of froth rises, some of it begins to overflow over the tank's lip. The overflowing pulp is known as concentrate and the leftover slurry that exists the cell from the bottom is known as tailings.

The flotation cells are typically either mechanical or pneumatic. Pneumatic machines rely upon a constant fluid flow that mixes the solids, liquids and air. Mechanical cells use an agitator which mixes and possible aerates the slurry. Mechanical cells are divided into multi- and single-chamber machines. A single-chamber machines are then further divided into self-aerating and externally aerated machines. Self-aerating machines use the negative pressure caused by the impeller's movement to induce air into the pulp and externally aerated machines use separate blowers to deliver the air into the pulp. Simplified visualization of a mechanical flotation cell is depicted in Fig. 1. The tanks studied in this thesis are Outotec's mechanical externally aerated TankCell – flotation tanks.

Movement of froth on top of a cylindrical flotation tanks is commonly modeled with simplified transportation zones: vertical, horizontal and stagnant, which are depicted in Fig. 2. Stagnant zone is located close to the impeller shaft and the froth stays stagnant due to direct contact with the shaft breaking the bubbles and due to added resistance caused by outer froth and eventually being overloaded with solids, both cases cause the froth to collapse. Vertical transportation zone acts as the main path for froth transportation and it is located close to the cell wall. Horizontal region is above the overflow lip and the height over the lip h_f is often uniform across the surface. (Zheng, X., et al., 2004)

Froth height over the lip, h_f, changes near the edges of the cell as operating conditions and the viscosity of the froth have large impact on the froth's behavior. (Shi, F. and Zheng, X., 2003)

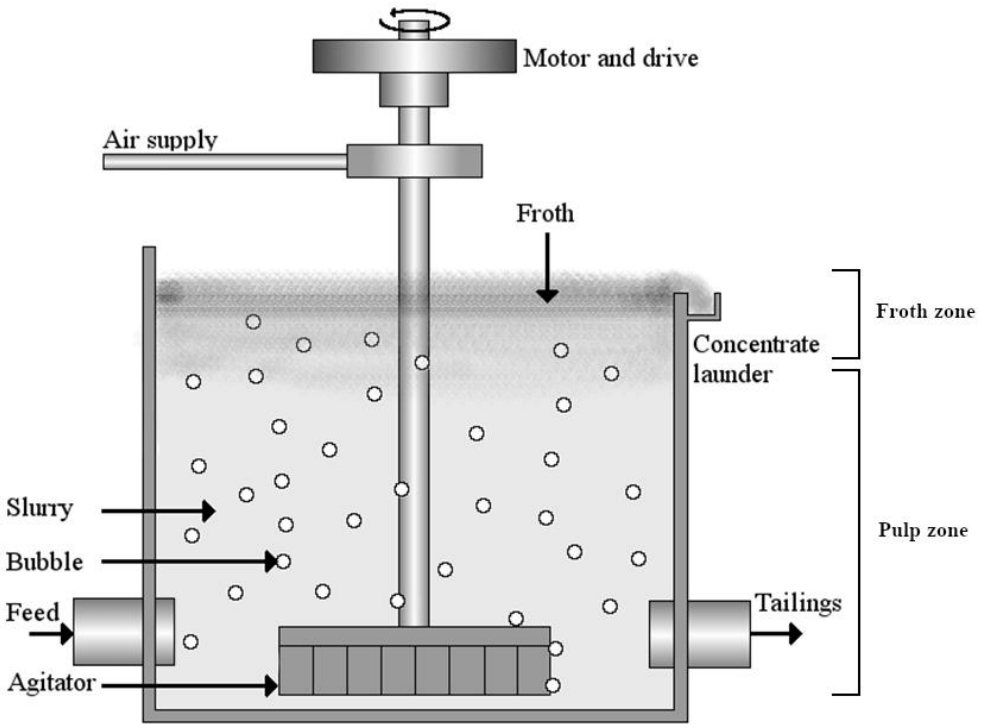

Figure 1. Simplified mechanical flotation cell. Feed comes in from the bottom left corner, concentrate overflows to the concentrate launder and tailings comes out from the bottom right. Agitator helps to suspend the particles in the slurry and the bubbles carry the mineral particles to the surface. As more bubbles rise, the froth overflows to the launder.

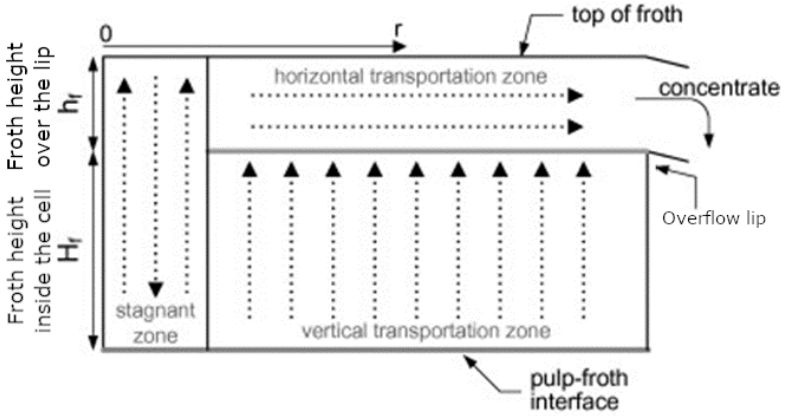

Figure 2. Froth transportation zones inside a cylindrical flotation tank. (Zheng, X., et al., 2004)

2.1.1. Flotation circuits

The flotation circuit has three specific stages: rougher, scavenger and cleaner. The setup of these stages varies depending on such parameters as the mineral type, degree of liberation of the valuable minerals, desired grade of the concentrate and the value of the product. Typically, each of the stages have multiple cells in series in them and the series of tanks is referred to as a bank. Simple setup is depicted in Fig. 3 but typically a flotation circuit has more interconnecting loops and multiple banks of different stages.

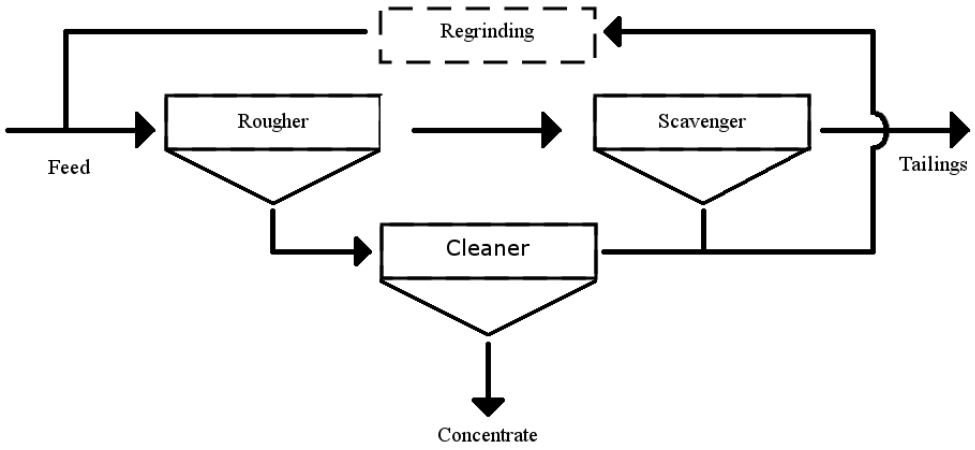

Figure 3. Stages of the flotation circuit. Rougher is fed with the fresh feed and the regrind and its tailings are fed to scavenger stage and its concentrate is fed to cleaner stage. Scavenger concentrate is fed to the regrind with cleaner tailings and its tailings are the final tailings. Cleaner stage produces the final concentrate.

Rougher stage is at the beginning of every flotation circuit and it receives the fresh feed and the recycled feed from the latter stages. The purpose of this stages is to remove the highly liberated minerals and to keep the recovery high. The froth depth is kept high so that the grade stays within limits while the recovery is maximized with high aeration. (Outotec, 2019a)

Scavenger stages follows the rougher stage and it receives the tailings from the rougher stage. The tailings from the scavenger are the final tailings, but the concentrate is usually recycled directly to the rougher or cleaner circuit with or without additional grinding. The scavenger stage is used to recovery the slow floating particles with the help of additional reagents. The forth depth is lower than in other stages because the rougher circuit recovers most of the minerals. (Outotec, 2019a)

Cleaner stage receives the rougher concentrate and the stage produces the final concentrate and the tailings are sent back to the rougher stage with or without additional regrinding. The main objective of this stage is to remove the waste material, hence increasing the grade of the final concentrate. The stage has highest froth dept out of the three stages. (Outotec, 2019a)

2.1.2. Flotation circuit design

Flotation circuit is designed based on cell size, their count and type, which are determined from the required residence time and froth transportation parameters: froth carry rate and lip loading. The residence time is the average duration that the pulp resides inside the tank or series of tanks before it flows out, the froth carry rate is the amount of dry concentrate that is recovered per square meter of froth, and lip loading is the amount of concentrate that can be recovered per meter of overflow lip.

The required residence time is based on ore types, their kinetics and liberation and the used reagents and their dosing and it is determined by doing laboratory tests to find out mineral specific recovery curves (Coleman, R., 2009). When the desired residence time and the target recovery are known, they can be used to estimate the required volume of the circuit.

The froth transportation parameters cannot be tested in laboratory due to unnatural froth behavior, and thus they must be calculated from cell parameters. The calculated values are compared to allowed maximums and minimums, which are based on an industrial rule of thumb. The reference values for froth carry rates are listed in Table 1 and the rule for lip loading is to keep it under 1.5 $t/m/h$. (Outotec, 2018)

Table 1. Froth carry rates in $t/m^2/h$ for each section of a typical flotation circuit. (Outotec, 2018)

	Rougher	Scavenger	Cleaner
Froth carry rate	0.8 – 1.5	0.3 – 0.8	1.0 – 2.0

Having the appropriate froth carry rate is essential since the froth is mostly made up of air and it has a limit on how much particles it can support before it collapses due to its weight. Higher carry rates lead to more probable dropback, weaker froth and worse transportation to launder lip and if it gets too high, solids loading becomes too high and the froth collapses due to its weight which is often associated with higher gangue entrainment. (Health, J., 2016)

The froth transportation parameters are designed using different launder setups which have different froth surface areas and overflow lip lengths. The three common configurations: external, internal and dougnut, are depicted in Fig. 4 (Outotec, 2018). All the designs have a central froth crowder which pushes the froth away from stagnant transportation zone, improving froth's stability and mobility.

The external launders have higher froth surface area, lip lengths and effective volume, resulting in lower lip loading and froth carry rate. Internal launders take up space inside the tank and they leave smaller froth surface area, lip length and effective volume and therefore have higher froth carry rate and lip loading. Donut launder have longer lip lengths due to having two overflowing edges, but they have low surface area. (Coleman, R., 2009)

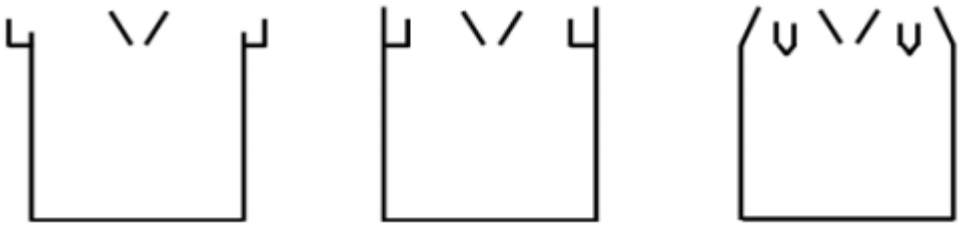

Figure 4. Different launder configurations. The types from left to right are external, internal and donut. Launder types affect the froth carry rate and lip loading by changing the froth area and overflow lip length. (Outotec, 2018)

2.2. Forms of particle recovery

The recovery of material by flotation from the pulp zone to froth zone happens due to three different mechanisms. The first is the selective attachment of particles to air bubbles, called true flotation, and the other two are entrainment and aggregation. Most of the valuable minerals are recovered using true flotation whereas entrainment and aggregation are the main ways for gangue to be recovered from the pulp.

As the particle enters the system, it enters the pulp phase, where the particle must have an adequate level of hydrophobicity, thus enabling an aggregation between the particle and an air bubble. For the attachment to happen, the particle must collide with an air bubble rising through the pulp and if the attachment happens, the particle must remain attached to the bubble as it rises through the pulp phase and enters the froth phase. If the particle remain attached to the bubble as it moves through the froth phase, it can overflow into a launder with the bubble and detach. (King, R., 2012)

Entrainment is the main way in which the non-flotating gangue is recovered to the concentrate. In entrainment, the material is dragged behind or next to the rising bubbles into the froth phase where it may be recovered into the concentrate or washed down into the pulp. Entrainment is non-selective, and it happens with all minerals equally. Washing the froth with water can decrease the recovery by entrainment but it may lessen the stability of the froth. (Wills, B. and Finch, J., 2015)

The three main theories of entrainment are the boundary layer theory, the bubble wake theory and the bubble swarm theory. In the bubble layer theory, the particles are transported in bubble lamella, which is a thin layer of water surrounding and following the air bubbles and in the wake theory, the particles are transported in the wakes forming behind the bubbles. The bubble swarm theory describes how a layer of gangue can be trapped between two layers of bubbles as the top layer is slowed down, crossing the interface between pulp and froth, and the bottom layer crowds behind the slowing layer, trapping gangue between the two. Fig. 5 shows main mechanisms behind entrainment. (Wang, L., et al., 2015)

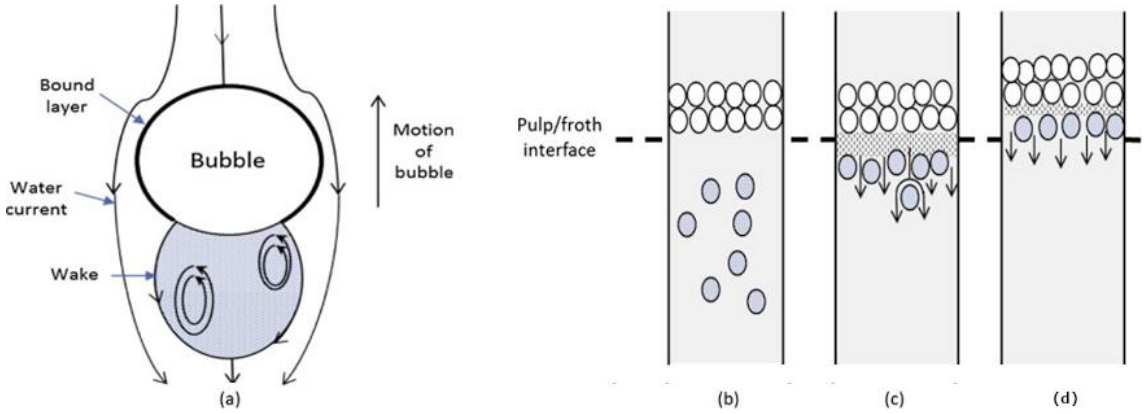

Figure 5. The mechanisms of entrainment. Image a describes the boundary layer theory and bubble wake theory whereas images b through d describe the bubble swarm theory. (Wang, L., et al., 2015)

The main function of the froth is to carry the valuable particles upwards and transfer them to the launder by overflowing. Secondarily, it increases the selectivity of the enrichment process by allowing the entrained particles to drain down with the water from the bursting bubbles while preferably holding on to the valuable particles. (Wills, B. and Finch, J., 2015)

In aggregation particles become attached to each other. Recovery by aggregation happens if particles attaches itself to a particle being recovered by true flotation. Aggregation due to electrostatic effects is known as coagulation and gangue is usually recovered due to heterocoagulation where two different types of particles are attached to each other. (Wills, B. and Finch, J., 2015)

Fig. 6 shows how the fine lizardite particles are coagulating with the pentlandite to block it from being coated by the collector, when aluminum ions are added into the mixture, the lizardite particles coagulate together, thus allowing the pentlandite to be coated with the collector. (Liu, C., et al., 2018)

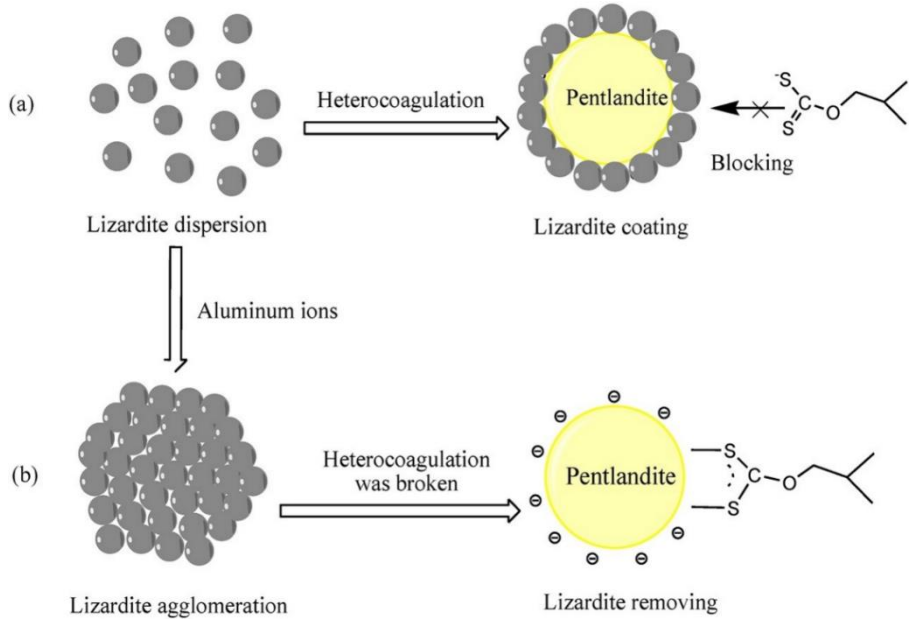

Figure 6. Heterocoagulation between pentlandite and lizardite. In image a, fine lizardite particles are coagulating with pentlandite and in b, heterocoagulation is blocked with added aluminum particles. (Liu, C., et al., 2018)

2.3. Flotation modeling

Flotation is a complex physico-chemical process consisting of both physical and chemical factors which are equally important and having significant interactions with each other (Wills, B. and Finch, J., 2015) and there is estimated to be about 100 variables which are required to characterize the flotation process (Jovanović, I., and Miljanović, I., 2015). The basic principles of flotation are well understood but the chaotic nature of particles make it difficult to produce accurate predictive models of typical operation of flotation cell in an industrial circuit (King, R, 2012; Laurila, H., et al., 2002). A categorization of flotation models is depicted in Fig. 7.

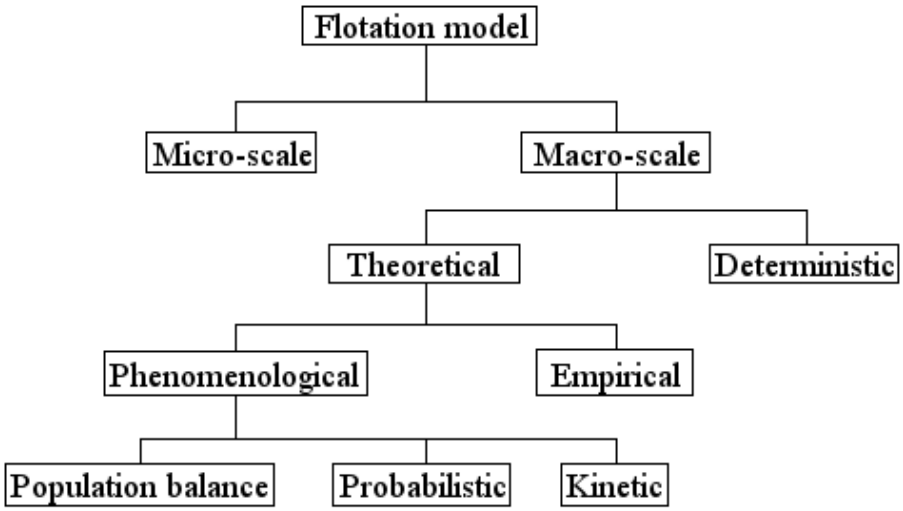

Figure 7. Categorization of flotation models. The models are divided into micro- and micro-scale models and the macro-scale models are further divided into subcategories. (Gharai, M. and Venugopal, R., 2015)

Models are categorized into micro- and macro-scale models. Micro scale models identify the underlying subprocesses in the system and they are used to find the relationship between the system variables in use. On the contrary, the macro-scale models work with the overall response of the system and the response is related to the system variables through equations and rules. (Jovanović, I. and Miljanović, I., 2015)

Macro-scale models can be divided into two subcategories: deterministic and theoretical. Deterministic models have always the same output to the same input and they give no room for randomness. Theoretical models, also known as first principle models, are based on the equations describing the laws of the system. The theoretical models can then further be divided into empirical models and phenomenological models. Empirical models, also known as black-box models, try to find the relationship between the given input and output, without describing the relationships between the phenomenon happening inside the system. Phenomenological models try to describe the relationship between each phenomenon inside the system in a way that fits the fundamentals of the system, without deriving the relationships from theory.

Phenomenological models can be divided into three subcategories: population balance, probabilistic and kinetic. Population balance models describe individual entities and the evolution of a system as these entities interact with the environment and each other. Probabilistic models make the use of random variables and probability distributions to model events and phenomenon happening in a system and the outcome is given as a probability distribution. Most of the flotation models are based on kinetics and the process is described with rate of flotation, which considers several chemical and physical factors. The focus of this thesis is on the kinetic models, since the simulator in use uses kinetic models.

2.3.1. Micro-scale model

Understanding of interactions between particles and air bubbles is essential in understanding the flotation process in a micro-scale. The principle enabling factor in flotation is that the particles and air bubbles form an aggregation, which happens by the work of adhesion:

$$W_{\mathrm{s/a}} = \gamma_{\mathrm{w/a}}(1 - \cos\theta), \quad (1)$$

where $\gamma_{\mathrm{w/a}}$ is the surface tension between water and θ is the contact angle between the particle surface and the air bubble. Fig. 8 depicts the interfaces between air, mineral particle and water. Interaction surface is said to be hydrophobic if $\theta > 90°$ in static water and hydrophilic if $\theta < 90°$ (Law, K., 2014). As the contact angle grows, the work of adhesion becomes greater and the system becomes more resilient against disruptive forces. Particles becoming more hydrophobic increases the contact angle and when particles have more affinity towards air than water, they are said to be aerophilic. (Wills, B. and Finch, J., 2015)

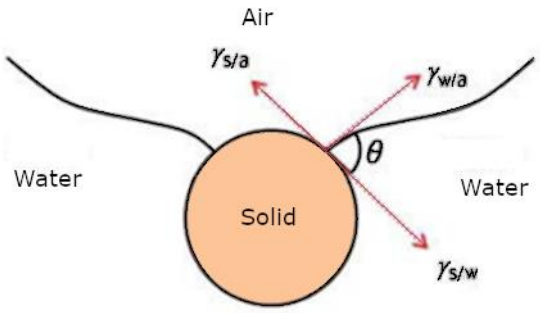

Figure 8. Interfaces between air, mineral particle and water. High contact angle means that more of the mineral particle is inside the air bubble. (Wills, B. and Finch, J., 2015)

The attachment between particles and bubbles is not instant during the collision and the time required for an attachment to happen is called induction time. If the contact is longer than the induction time, the particle becomes attached to the air bubble. Contact angle and induction time are the basic variables used to characterize the surface properties in flotation. (Chau, T.T., et al., 2009; Gu, G., et al., 2003)

Valuable minerals are often not hydrophobic by nature and their surface properties must be altered by adding chemicals, often referred to as reagents, into the slurry. The hydrophobicity can be controlled using reagents called collectors, which adsorb on the surface of the selected particles, making them more hydrophobic. The selectivity is controlled by the selection of the collector and the pH of the slurry, this way a selected group of minerals could become hydrophobic while another group remains hydrophilic.

Zeta potential, also known as electro kinetic potential, is used to measure the effectiveness of the collector. The potential results from an electrochemical phenomenon, electrical double layer, where an oppositely charged bound layer is formed on a charged surface. This bound layer is then compensated by another layer, known as diffuse layer.

Part of the diffuse layer is attached to the particle but there is a boundary called slipping plane after which the layer is mobile. In agitation, the bound layer remains as is but the diffuse layer and the slipping plane changes (Wills, B., and Napier-Munn, 2006). The electrical potential at the slipping plane is known as zeta potential (Park,S., and Seo, M., 2011). Fig. 9 shows the layers and the planes involved in determination of the zeta potential.

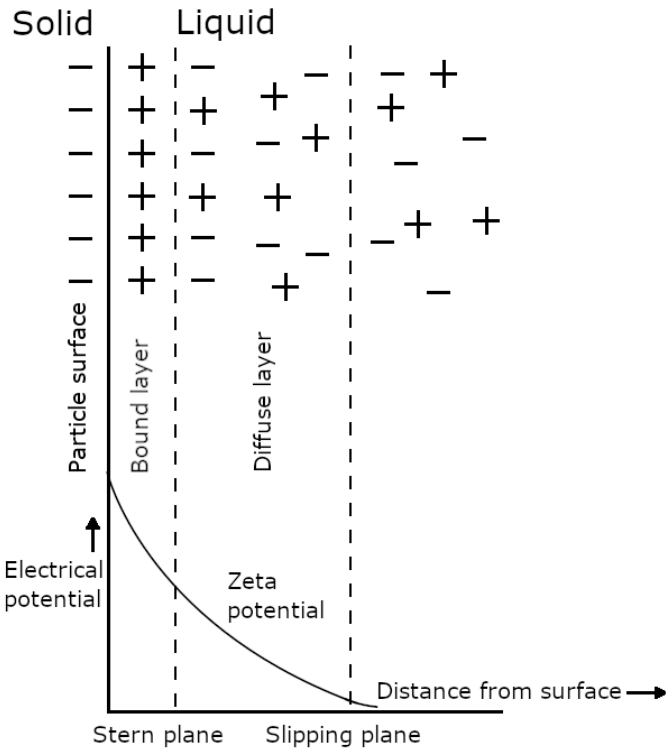

Figure 9. Zeta potential is the electrical potential at diffuse layer's slipping plane, after which the liquid is mobile and is not attached to the particle.

Zeta potential can be altered by increasing or decreasing the free electrodes of the system by the means of controlling the level of pH. The pH level at which the zeta potential is zero is known as isoelectric point (IEP). At pH levels below IEP, the zeta potential is over zero and anionic collectors are effective, and at pH levels above IEP, the zeta potential is under zero and cationic collectors may be used (Wills, B. and Finch, J., 2015).

Frothers are reagents which are mainly used for froth creation, but they also alter the dynamics of the flotation process. The size of the bubbles is measured using Sauter mean diameter D_{32} which means the average particle size in fluid dynamics. The optimal amount of frother is called critical coalescence concentration (CCC). Usually the maximum benefit of frother is reached when the concentration is slightly higher than CCC, because that is when the bubbles reach the optimal D_{32}. Adding more frother would make risk excess water being carried and recovered by the froth, which increases entrainment and lower than CCC amount of frother has large impact on bubble size. (Zhang, W., et al., 2010; Welsby, S.D.D, 2014)

Due to variation in the particle size in the feed, fine bubble size is not always optimal. Larger bubbles are more efficient at attaching with coarser particles and smaller bubbles are more efficient at attaching with finer particles (Wills, B. and Finch, J., 2015). If the comminution process is well controlled and the particle size remains stable, the smaller bubble size is significantly better due to higher collision probability and the benefit of being able to add more frother.

Making bubbles smaller also makes the bubbles rise slower (Clift, R., et al., 2005). The increased air retention time increases the air content of flotation cell which is referred to as air holdup ϵ_g or gas holdup (GH). Without frother, the gas holdup is typically less than 5 % but with the aid of the frother, it can rise as high as 15 % (Finch, J.A. and Dobby, G.S, 1990; Dahlke, R., et al., 2005). The linear velocity of rising bubbles in the pulp and froth are denoted by superficial gas velocity J_g and $J_{g,froth}$ respectively (Wills, B. and Finch, J., 2015).

Gas dispersion properties can be evaluated by bubble surface area flux (BSAF) which is given by

$$S_b = \frac{6J_g}{d_b}, \tag{2}$$

where d_b is the bubble size. The BSAF is linearly related to flotation rate constant, meaning that higher BSAF means higher recoveries. Too high BSAF values lead to turbulence which causes particles to tear away from the bubbles, resulting in lower recovery. (Wills, B. and Finch, J., 2015).

2.3.2. Flotation kinetics

Kinetic flotation models are typically based on flotation rates and residence times. Numerous models have been developed for describing the kinetics, but only four models are discussed here: one-, two- and three-component models and rectangular distribution. The models consider only the true flotation.

The one-component model, which is the continuous version of the classical method (Garcia-Zuniga, 1935),

$$R = \left(\frac{k\tau}{1 + k\tau}\right) \tag{3}$$

is the simplest model to describe the flotation process, where *R* is recovery, *k* is the flotation rate constant (unit 1/min) for given mineral and τ is the residence time. In practice, the flotation rate constant can be determined for given sample in a laboratory setting and it considers such things as bubble size, particle and fluid densities, turbulent conditions and collision-, attachment and particle-bubble stability-efficiencies (Duan, J., et al., 2003). The rate constant can also be determined based on plant data.

The two-component model, which is the continuous version of Klimpel's dual rate constant method (Klimpel, R. R., 1980),

$$R = m_f \left(\frac{k_f\tau}{1 + k_f\tau}\right) + m_s \left(\frac{k_s\tau}{1 + k_s\tau}\right) \tag{4}$$

divides the particles into slow and fast floating particles, denoted with subscripts *f* and *s*. The *m* parameters describe the mass fraction between the slow and fast floating particles, and they add up to one. The fast rate constants are also always higher than the flotation rate constants for the slow floating particles. The recovery of one- and two-component models reaches one as the residence time approaches infinite.

The three-component model can be expressed as

$$R = m_f \left(\frac{k_f\tau}{1 + k_f\tau}\right) + m_s \left(\frac{k_s\tau}{1 + k_s\tau}\right) + m_N \cdot 0 \tag{5}$$

and it adds a non-floating classification into the model. The m_N mass fraction is used to describe the proportion of particles that do not float. The recovery is limited to $m_f + m_s$ as the residence time approaches infinite.

The rectangular distribution model, which is the discretized version of the Klimpel model and it can be expressed as (Klimpel, R. R., 1980),

$$R = \frac{R_\infty}{n} \sum_{i=1}^{n} \left(\frac{k_i \tau}{1 + k_i \tau} \right), \tag{6}$$

calculates a sum for n evenly distributed flotation rate constant between k_{max} and $k_n = \frac{k_{max}}{n}$. The infinite recovery R_∞ limits the recovery as the residence time τ approaches infinity.

2.4. Reagents

The flotation reagents can be divided into two distinct groups: those used with sulfides and those used with non-sulfides. The basic reagents are collectors, frothers, activators, depressants, dispersants and pH modifiers.

Since most minerals are not hydrophobic by nature, it must be achieved by chemicals. Collectors are commonly added to the pulp during conditioning, so that the selected minerals become coated with it. The hydrophobicity is imparted by reducing the induction time, allowing bubble – particle collisions to become shorter. As there are often multiple collectors in the flotation circuit; highly selective collector is typically used during conditioning to recover highly hydrophobic particles at the beginning of the circuit whereas a stronger, not so selective collector, may be used downstream to recover slow floating particles. Adding too much collector results in a lower final grade on the concentrate due to better recovery of gangue material but much lower dosage than required drops the recovery significantly (Wills, B. and Finch, J., 2015).

For example, potassium amyl xanthate (PAX) is a collector, often used in copper flotation. It is the most powerful and the least selective of the xanthate types with a maximum stability at pH level of 10. Since the potassium amyl xanthate is not selective, a selective collector such as AERO 3894 may be used alongside with it. Xanthate then insures a good recovery when AERO 3894 makes sure that only the valuable particles are floated (Willard, T., 2010).

Frothers is another group that has an important role in the bubble – particle interaction by having three main functions: I) aiding in small bubble formation, II) reducing bubble rise velocity and III) aiding in formation of the froth (Klimpel, R.R. and Isherwood, S., 1991). The reduction in bubble size increases the collision probability because the total surface area of the bubbles grows as more small bubbles are formed. The reduction in rise velocity also increases the probability of collision by allowing the bubbles to reside in the pulp for a longer period. Formation of the froth increases because frothers decrease the bursting of bubbles as they reach the top of the pulp.

Frothers and collectors synergize with each other by uniting each other's alkyl chain by van der Waal's forces. This bond between collector on the mineral surface and frother on the bubble surface makes the froth more stable. (Shumba, T., C., 2014)

Activators activate the adsorption of other reagents by coating the mineral particle's surface and providing better adsorption sites. This way the collector is much more effective and the bubble – particle attachment becomes more probable. Overdosing the activator results in collapsing froth which leads to worse recovery and too little activator makes the collectors impact smaller which also leads to worse recovery.

Depressants can be used to make gangue hydrophilic, thus making it stay in the pulp phase. Addition of depressants has to be made with care since adding too much makes the valuable mineral particles hydrophilic as well. Dispersants instead are used coat the valuable particles so that the fine gangue particles cannot attach to them.

The pH modifiers are used to change the pH level of the slurry and change the surface charge of mineral particles. The pH of the slurry also affects the solubility of the collector. Lime (Calcium Oxide (CaO)) is universally used in copper flotation and it is used to keep the pH of the slurry between 9.5 – 10 in rougher circuit and 9.5 – 12 in cleaner circuits. (Willard, T., 2010)

The necessary chemical characteristics are obtained in a condition tank, where the slurry is fed before it enters the flotation circuit. Additional conditioning may occur during the circuit, for example, between rougher and scavenger stages. The tanks are also used as buffers between the stages so that the residence time in the circuit can be controlled. The stirring in the tank can also be used to remove gangue from the mineral surface. Effective conditioning is potentially the most economical way to increase the capacity of the plant due to decrease in flotation time if the conditioning is done adequately (Willard, T., 2010).

2.5. Grade and recovery

The performance of a flotation bank and the plant is represented by using grade-recovery curves that indicate the necessary trade-off between the two main performance measures in flotation (Neethling, S., and Cilliers, J., 2012). Grade refers to the weight percentage of valuable mineral or element in a stream, such as the feed or the concentrate:

$$\text{Grade} = \frac{\text{Tons of valuable element in sample}}{\text{Tons of sample}}, \tag{7}$$

whereas recovery is the percentage of the mineral or element collected from the feed stream to the concentrate:

$$\text{Recovery} = \frac{\text{Total metal in concentrate}}{\text{Total metal in feed ore}}. \tag{8}$$

The goal of a flotation plant is to achieve high grade without sacrificing recovery. The grade and recovery typically have an inverse relationship, meaning that as the recovery increases, grade decreases and vice versa. The inverse relationship between grade and recovery is due to the fact that when more valuable minerals get through to the concentrate, more gangue and other undesirable minerals get as well, which decreases the proportion of the desired valuable mineral in the final product. An example of a grade-recovery curve is depicted in Fig. 10.

The control points depict the basic steps taken in flotation process control. The first step is to stabilize the plant, which in practice means stabilization of the slurry level, adjustment of air rates and setting of the reagent flows. After the plant has been stabilized, the process is moved to a point where the grade of the concentrate is closer to the target. The final step maximizes the recovery while the grade remains close to its target. This is done by having better process conditions through optimizing control. If the process moves from one optimization curve to another, grade and recovery may change to the same direction.

The grade-recovery curves are often used to compare plant performance in different operation conditions, reagent regimes and circuit configurations. However, the results may vary a lot because of uncontrollable variables such as feed grade, which makes the comparison as a performance assessment demanding. (Neethling, S., and Cilliers, J., 2012)

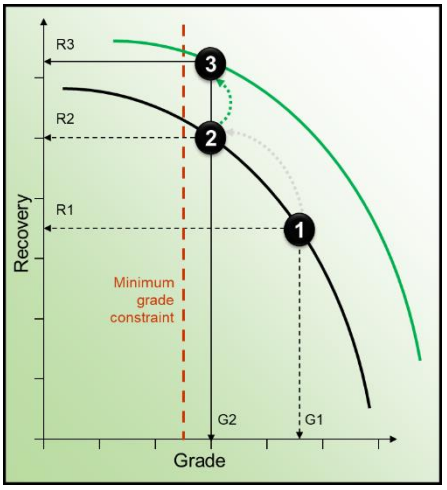

Figure 10. Grade-recovery curve. The curve shows the inverse relationship between grade and the recovery, as the grade increases, recovery decreases. Basics steps of flotation control are also shown: stabilizing control, set-point control and optimizing control. (Outotec, 2019b)

The degree of liberation is used to describe what percentage of the mineral occur as liberated particles in the ground ore, produced by the comminution process. The grade-recovery curve for perfectly separated ore is known as liberation limited grade-recovery curve, which can be compared to the actual process to see how well the plant operates and how far its performance is from the theoretical maximum. (Wills, B. and Finch, J., 2015)

Another important factor is the particle size, which effect can be observed from Fig. 11. The coarse particles are too heavy to float, their liberation is not sufficient, and the particle-bubble interaction is not stable enough for the particle to stay attached (Jameson, G. J., 2012). Too fine particles are less likely to collide with bubbles which leads to lower recovery. The recovery of the smaller particles can be controlled by decreasing the bubble size, therefore increasing the number of bubbles in the slurry. The size of the bubbles is limited by the gas hold up which can typically rise up to 15 % (Wills, B. and Finch, J., 2015). The fine particles are also prone to entrainment and the grinding to a size smaller than necessary wastes a lot of energy.

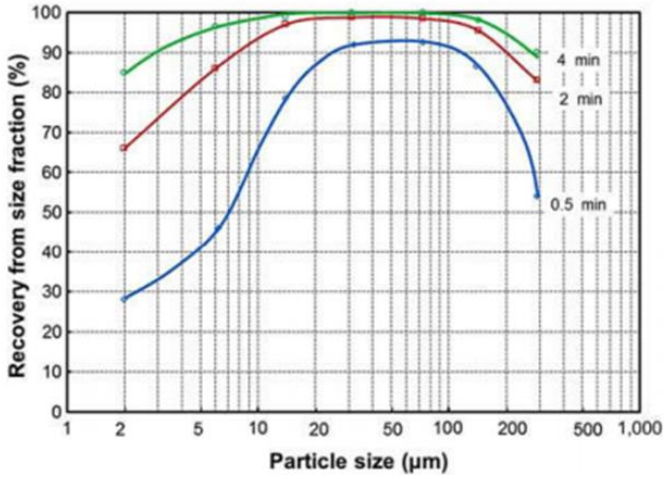

Figure 11. Recovery with different particle sizes and residence times. Too fine and coarse particles are impossible to float even with a long residence time. The green curve means a residence time of 4 minutes, the red means 2 minutes and the blue curve means 30 seconds. The optimal particle size is around 50 µm. (Trahar, W. J., 1981)

Since the goal of the mineral processing is to increase the value of the mined ore, the optimal point on the grade-recovery curve is calculated so that the final product gives the highest financial benefit (Wills, B. and Finch, J., 2015). As the economic state fluctuates, the optimal point on the curve changes and the plant must adapt to produce a product with given grade.

The optimal point is traditionally calculated using net return from the smelter (NSR), which considers the payment from the metal, smelter charges and the transportation costs (Malewski, J. and Krzeminska, M, 2012). The production of high-grade concentrate reduces the cost of smelting but as it is only achievable with lower recovery, it may result in a lower overall financial benefit. On the contrary, the production of low-grade, high recovery concentrate will have higher smelting and transportation costs and may incur penalties due to high gangue amount in the concentrate. Because of this balancing, it is essential that the plant can achieve its target grade and recovery. An illustrative example of the grade optimization by NSR can be seen from Fig. 12.

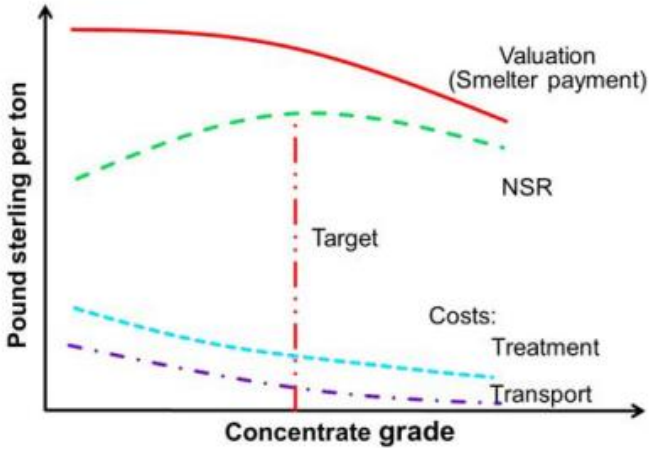

Figure 12. Optimizing the concentration grade by maximizing the NSR. The target grade is at the point where the dashed green NSR line reaches its maximum. (Willard, T., 2012)

3. Control of Flotation Circuits

Flotation is the most common beneficiation process and thus its performance has very high impact to the final product (King, R, 2012). The main difficulties in control of flotation process arises from its nonlinearities and complexity and typically a plant achieves recoveries in range of 85 - 95 %. Nowadays, one of the recognizable changes happening in modern flotation control is that the tank sizes are increasing, meaning that the circuits have less cells and it is easier to instrument each cell with higher quality instrumentation. The circuit configuration is also changing so that there are less recycle streams, making them more stable and reducing the self-compensation of the circuits. These changes make the control and optimization of the flotation circuits easier which allows new level of optimization and regulation. (Laurila, H., et al., 2002)

Currently Outotec's TankCell series flotation tank's volume range is from 5 to 630 m^3. The development of Outokumpu's and Outotec's combined tank size growth during the past decades can be seen from Fig. 13.

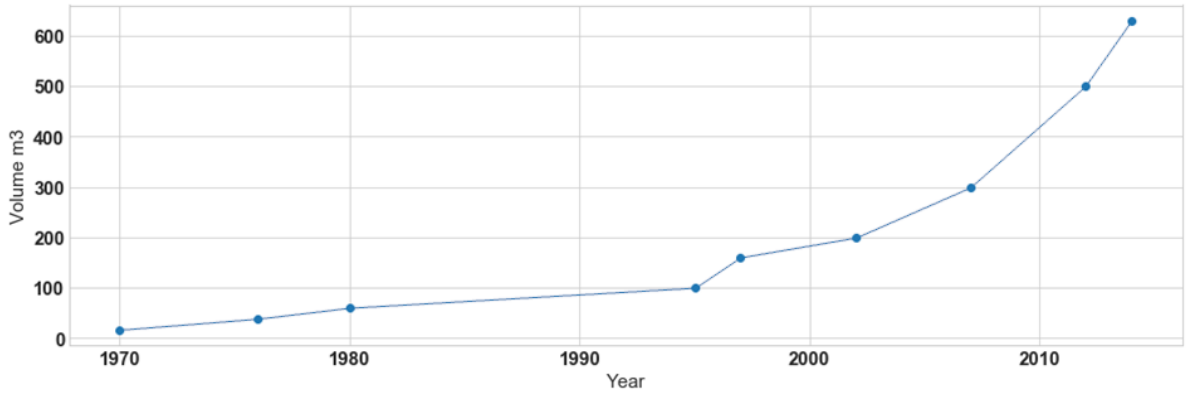

Figure 13. Increase in Outokumpu's and Outotec's largest available flotation tanks. Rapid volume increase starts in 1995 and TankCell 630 was introduced in 2014. Adapted from (Fuerstenau, M., et al., 2009).

Process control is often described with ISA95 (ISA95, 2019) standard that consists of several control layers. Fig. 14 shows four commonly used layers used in process control: instrumentation, base level control, advanced control and optimization. The layers can communicate with the adjacent layers, making the control design more coherent. The recent developments in instrumentation, such as the use of machine vision, have opened up new opportunities in base level control and therefore advanced control and optimization as well.

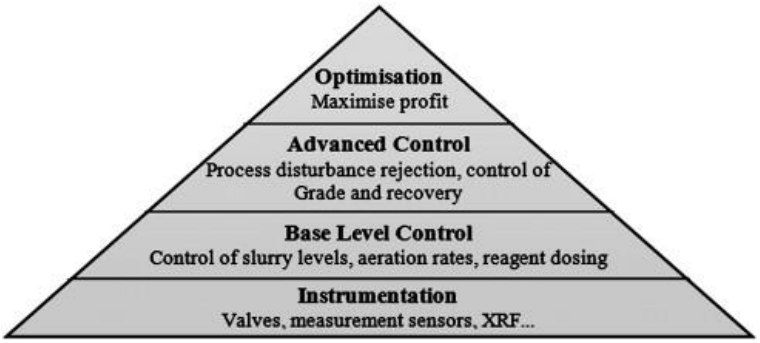

Figure 14. Process control system has four different layers, instrumentation, base level control, advanced control and optimization. Each of the layers communicate with the adjacent layers. (Laurila, H., et al., 2002)

3.1. Base level control and instrumentation

Reliable instrumentation and properly tuned base level control are the most crucial components in the plant operation. The fundamental base level control of a flotation plant includes: level, air and slurry flowrate, density, reagent addition and pH (Shean, B. and Cilliers, J., 2011). Of these variables, the level, air flowrate, elemental assaying and reagent dosing are discussed further. An example of the basic instrumentation locations in a flotation circuit are depicted in Fig. 15 which is a rougher and scavenger circuit from Pyhäsalmi mine.

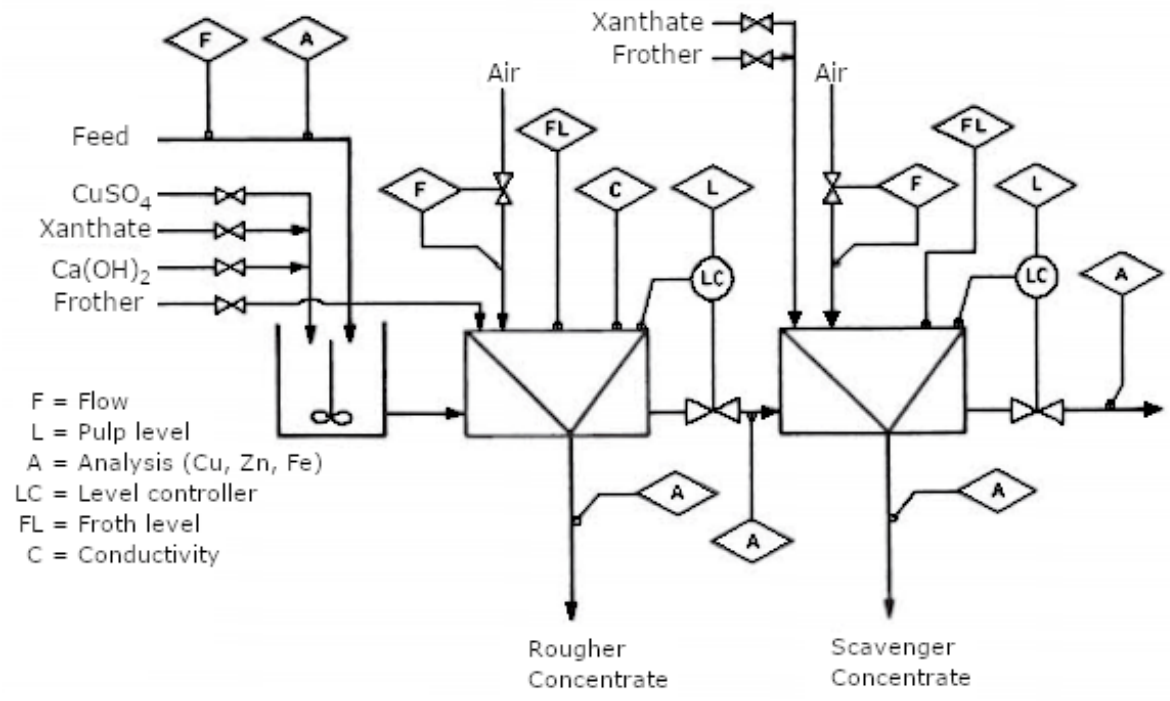

Figure 15. PI diagram showing the basic instrumentation in a flotation circuit. The flowsheet is of zing roughing and scavenging from Pyhäsalmi flotation plant (Miettunen, J., 1983)

3.1.1. Cell level measurement and control

Accurate measurement of the slurry level is difficult due to thick froth layer and a varying density of the slurry. The level is also hard to define because the transition from slurry with bubbles and froth with slurry is not instant. The typical level measurement methods are (Laurila, H., et al., 2002): I) a float with a target plate and ultrasonic level transmitter, II) a float with angle arm and a capacitive angle transmitter and III) reflex radar.

In the ultrasonic method, the transmitter emits a series of ultrasonic pulses which echo back after hitting the target plate and the level is calculated from the travel time. When the angle arm is used, the level can simply be calculated from the angle in the case when other dimensions are known. The reflex radar emits high frequency pulses which are reflected from the medium and the level is calculated from the travel time.

The level is controlled using dart or pinch valves. The pinch valves are used to control the flow by pinching a flexible sleeve to stop the flow of slurry and the dart valves are vertically moving cones, located on the base of a flotation cell. Depending on the case, the pinch valves can be troublesome due to the sleeve losing elasticity which results in the sleeve not following the pinch valves jaw correctly. Dart valves have larger operating range and control performance than pinch valves. Two valves are usually used in parallel, since smaller valves have more suitable control properties (Laurila, H., et al., 2002)

The level control is typically done with a feedback proportional-integral (PI) algorithm though feedforward algorithms are used to take upstream flowrate variations. (Shean, B. and Cilliers, J., 2011). Single cell's level control is straightforward but when a series of cells are controlled it becomes more difficult due to the feed disturbances moving slowly through the bank of cells. As one cell maintains the setpoint independently, it acts as a disturbance for the other cells in the bank and offsets those cell's levels (Laurila, H., et al., 2002).

Multivariable control techniques, such as Mintek's FloatStar Level Stabilizer (Mintek, 2011) and Outotec's ExactLevel, exist to control all the levels same time but individual level control is still widely used.

3.1.2. Cell air flowrate measurement and control

Aeration control is used more to control the flotation process than the level due to its faster response times. Air flowrate is also much easier to control than level and it does not cause disturbances in other cells. The most common ways to measure airflow are (Laurila, H., et al., 2002): I) differential pressure flow meter and a venturi tube, II) differential pressure transmitter and a pitot tube or annubar tube and III) pitot-tube or a thermal gas flow sensor

Venturi tubes are tubes with constrictions that change the velocity of the flowing liquid or gas. As the material passes through the constriction and its velocity changes, it creates a pressure difference between the tube inlet and the constricting throat. The two pressures are measured, and the resulting difference can be used to calculate the flow rate though the tube. The venturi tube is simple, long-term reliable with no moving parts, but however it is an expensive measurement solution. (Boyes, W., 2010)

Pitot-tube measures the flow rate using two pressures: total impact pressure and a static pressure. The static pressure is the operating pressure of the pipe and the total impact pressure is the sum of the static pressure and the kinetic pressure of the flowing material. The annubar tube works in same manner to the pitot-tube but it calculates the average flow by taking multiple measurements. The pitot-tube is desirable measurement method since it is inexpensive, does not have any moving parts and the resulting pressure loss is low but, on the downside, the accuracy is relatively low, and the pitot tube can get clogged easily. (Shean, B. and Cilliers, J., 2011)

Thermal gas flow sensors measure the flow rate based on the cooling effect of the flowing material. The change in the temperature is then used to calculate the flow rate. These sensors do not obscure the flow, but they are expensive and difficult to calibrate. (Shean, B. and Cilliers, J., 2011)

The venturi-tube, pitot-tube and the thermal gas flow sensor are depicted in Fig. 16.

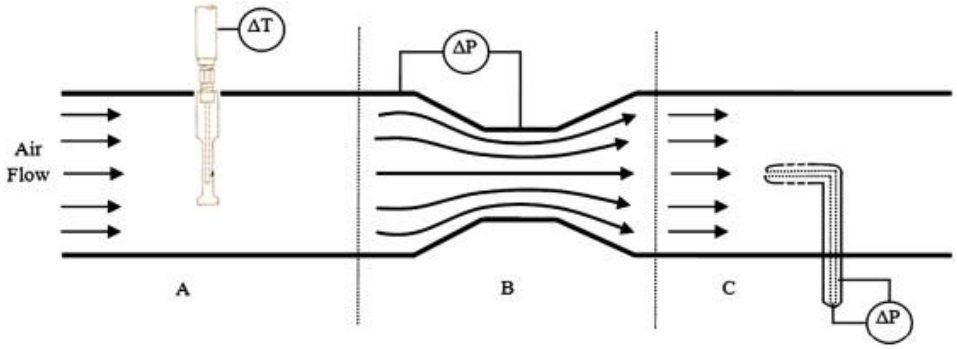

Figure 16. A-section shows the thermal gas flow sensor, B-section is the venturi-tube and the C-section has the pitot-tube. (Shean, B. and Cilliers, J., 2011)

The pressure flow meter and the pressure transmitter are the most commonly used methods in flotation circuits. Of those two, the pressure flow meter is often selected because of their low cost, simplicity and relatively low need for maintenance. The airflow to the tank is controlled with butterfly valves and a PI/PID-algorithm. (Laurila, H., et al., 2002)

3.1.3. Reagents

Reagents are controlled to achieve selective environment in which the desired minerals float better than those that are undesirable. Typical control methods are on-off switching where a dosing the valve is opened periodically and metering pumps. The on-off switching is highly inaccurate, and it requires regular checks to ensure correct dosing. The metering pumps are accurate, but the cost is much higher than that of on-off switching and they require regular maintenance. Addition rate is based on the feed flowrate, but it may be altered according to other quality measurements such as elemental composition of concentrate, analyzed by the x-ray fluorescence analyzer. (Shean, B. and Cilliers, J., 2011)

3.2. Element assaying

Element assaying is a crucial part in flotation circuit grade and recovery control as it can be used to measure the elemental composition of the streams going in and out of the system and as such it's the most important type of measurement in flotation optimization.

The principle of elemental assaying is based on material's properties to get excited from radiation. The use of radiation with high energy and low wavelength such as X-ray, excites the material and it becomes ionized. Powerful enough radiation can remove an electron from the inner layer of an atom which makes the atom unstable, and make the atom replace its missing inner layer electron with an outer layer electron. As this happens, energy is released since the binding energy decreases. The released radiation is called fluorescent radiation and it has lower energy which can be used to detect a presence of an element because the energy is characteristic to the transition which happened in the atom's orbits. Two transitions are often needed to confirm the presence, the energies of which are called K_α and K_β. Fig. 17 shows results from an X-ray fluorescence analyzer and Fig. 18 shows how the K-values are formed.

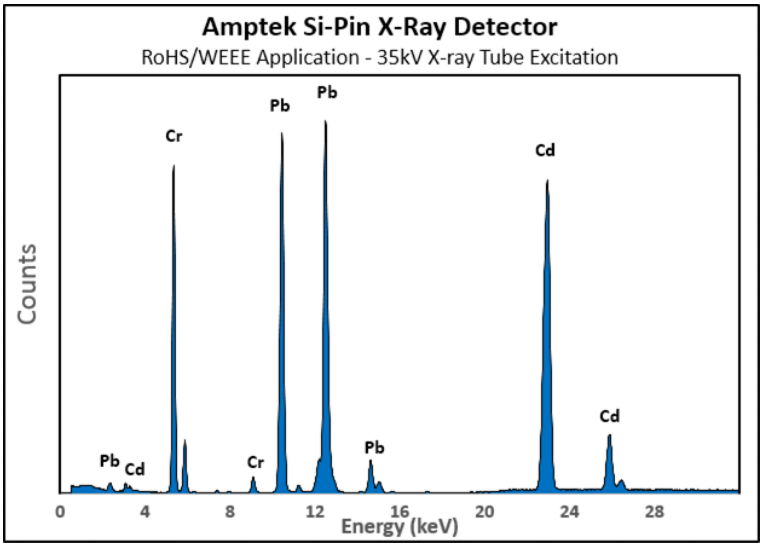

Figure 17. Results from X-ray fluorescence analyzer. Peaks are formed when transitions are detected. Each element has at least two peaks, K_α and K_β. K_α forms when an electron moves from L to K shield and K_β forms when an electron moves from M to K shield. (AMETEK)

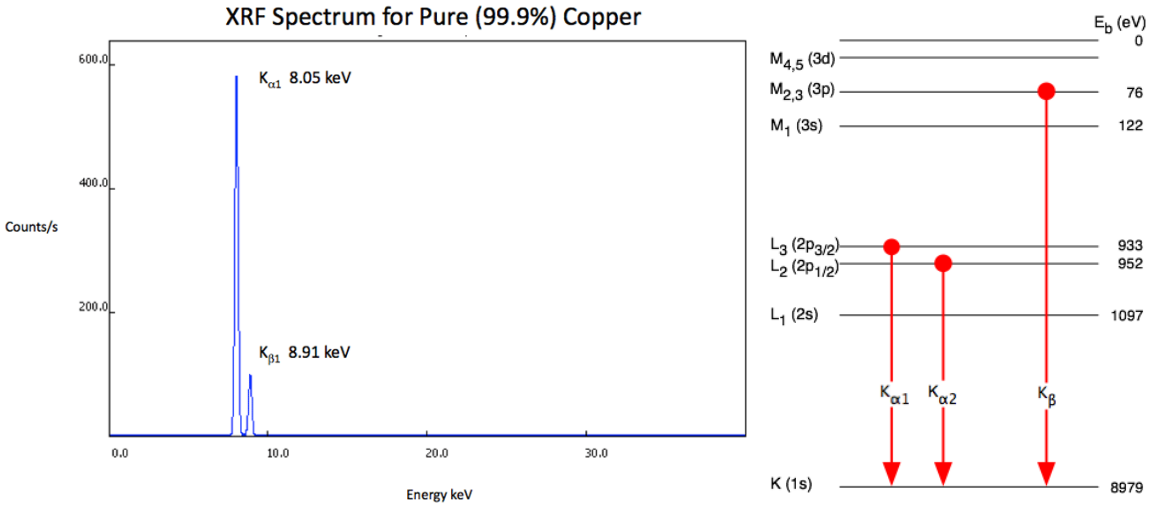

Figure 18. XRF spectrum for copper with K_α and K_β and the transitions involved in producing the values.

The sampling cycle on an on-line X-ray fluorescence analyzer (XRF) is typically between 10 and 25 minutes, varying with the number of sampling points attached to the analyzer as the sampling itself can range between 15 and 60 seconds (Laurila, H., et al., 2002). The analysis accuracy can vary between 1 and 10 % relative to measurement, depending on the variations in particle size, sample composition, mineralization and the density of the sampled slurry (Remes, A., et al., 2005). Long sampling cycle makes it difficult to control fast changes and to detect oscillations.

Faster measurements such as reflectance spectroscopy, with a sampling time as fast as 10 seconds exist, but XRF analyzer is still the state of the art due to difficulties in interpreting the reflectance spectroscopy results and the need for frequent calibration. It has been considered that XRF analyzer could act as an automatic calibrator for the reflectance spectrum information, resulting in a continuous stream of measurements. (Kejonen, I., et al., 2018)

The reflectance spectroscopy technique has been tested at Kevitsa's copper rougher-scavenger control and it resulted in a 22.7 % smaller deviation from the target grade. Feed's grade and its deviation were recorded during the testing period and there was no significant difference during the XRF and rapid measurement tests. The deviation was higher during the rapid measurement period and it was also able to detect oscillations in the grades. (Kejonen, I., et al., 2018)

3.3. Froth speed and characteristics

Study of the froth layer can give feedback about the performance of the flotation process and process variables (Liu, J., et al., 2013). For a long time, the plant operators observed the froth by themselves and the performance of the process was heavily dependent on operators experience and many times optimal adjustments are not found.

Machine vision-based process monitoring can be used to extract information from the froth surface images. Static feature extraction includes morphological measurements such as bubble size and shape and their distributions, bubble color and froth texture and dynamic extraction include froth speed and bubble stability. (Liu, J., et al., 2013)

The main control benefit from machine vision is the froth speed since the process performance is heavily dependent of it. The froth velocity determines the froth retention time, meaning that with high froth speed, there is less time for dropback of particles to happen which leads to higher recovery but lower grade and respectively, low froth speed leads to lower recovery and higher grade. (Liu, J., et al., 2013)

Froth's stability is defined as its ability to resist bubble coalescence and bursting (Farrokhpay, S., 2011). Froth stability is used to estimate the selectivity and recovery of the flotation process. With high froth retention time, there's more time for drainage to occur which leads to bubble coalescence because the water layer between the bubbles disappear. Large coalesced bubbles have higher burst rate which leads to hydrophobic particles dropping back into the pulp. On the other hand, too stable froth leads to higher entrainment of hydrophilic particles. Therefore, small stable bubbles improve recovery and large unstable bubbles improve grade (Subrahmanyam and Forssberg, 1988). Having enough particles in the froth also improves its stability, froth height, drainage capacity and its ability to support more particles (Johansson and Pugh, 1992).

Froth height over the lip and therefore froth speed has been proven to vary according to the froth properties and the flotation conditions (Harris, M., C. 2013). Rheology studies matter flow by means of viscosity, the resistance of flow, and yield stress, the resistance of deformation As the froth rheology changes, froths flow resistance E_{μ} changes and the froth requires more gravitational energy E_g above the lip so that it has enough kinetic energy E_k to overflow, as shown in (9) (Chao, L., 2016).

$$E_k = E_g - E_{\mu} \tag{9}$$

3.4. Advanced control and optimization

Advanced control and optimization take place on level three and four of the process control hierarchy. Advanced control approaches are needed to control the quality of the concentrate by monitoring grade and recovery and calculating appropriate setpoints for regulatory controllers. The optimization is done by fourth layer which sets grade and recovery setpoints according to economic state and hence, maximizing the profit. (Laurila, H., et al., 2002)

The basic structure of the four-layer process control is depicted in Fig. 19. The real-time optimization is carried out by the fourth, where economic factors are used as references, and process controller is carried out by the third layer.

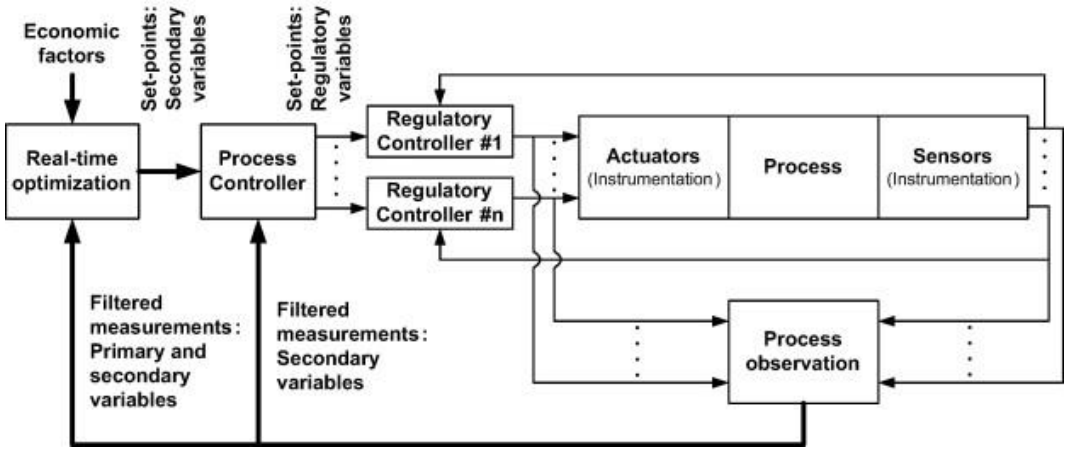

Figure 19. Four-layer model of process control. Left most block, real-time optimization, is fourth layer whereas the actuators on the right form the first layer.

3.4.1. Predictive control

Model predictive control (MPC), uses dynamic model to predict the process outputs at discrete times in the future over a defined prediction horizon. Depending on the application, the models do not necessarily need to be high fidelity and often the related gains, time constants and delays are enough due to the need of predicting only the relevant time horizon, which is given by the process time (Lundh et al., 2009). Robustness is ideal for flotation control, since the models are often rough estimates based on empirical data.

The prediction of the future behavior is based on the process model, past control actions and the movements of the disturbance variables. The control actions are optimized using a cost function, which finds the actions that achieve the minimal deviation from the setpoint with the minimal cost. The optimization problem is the same at every cycle of the calculation except the initial state changes according to past values.

There are numerous different MPC algorithms available which differ in how they handle the process, disturbances, cost function and constraints (Sbárbaro, D. and Del Villar, R., 2010). The typical cost function of an MPC controller is

$$J = \int \boldsymbol{w_1 e_1^2} + \int \boldsymbol{w_2 e_2^2} + \int \boldsymbol{w_3 \Delta u} + \boldsymbol{w_4 S}, \quad (10)$$

which consists of four parts. The first part is for output reference tracking, which is the cost of deviating from the setpoints of the controlled variables. The second part is for manipulated variable tracking, which is the cost of deviating from the setpoints of the manipulated variables. The third part is for manipulated variable move suppression, which is the cost for actuating the manipulated variables and the fourth part is the constraints violation, which adds a cost if minimum or maximum constraints are reached. The **w**'s correspond to different weights and $\boldsymbol{e_1}$ and $\mathbf{e_2}$ are errors from the setpoints of controlled variables and manipulated variables, respectively. The $\Delta\mathbf{u}$ is the actuation and **S** is the penalties for the constraints.

Weights are used to emphasize the importance of variables. By designing a large weight for variable tracking, they become more important and they are controlled more aggressively. Having a large weight on the manipulated variable tracking makes the control more limited since the controller tries to keep the variable at its set point, or it tries to minimize or maximize it. The weights for the actuator move suppression indicate which variable should be used when the controller is making a correction and having high weight on suppression limits the actuator swinging.

Constraints are divided into hard and soft constraints. The hard constraints cannot be violated at all, but the soft constraints can be exceeded but a penalty is still added to the cost function. The constraints can be used to ensure that the process stays within its limits, around certain operating point or they can be used to limit step sizes of the manipulated variables. The controller can be used to work with control objectives such as trying to minimize or maximize certain variables. For example, the chemical usage could be minimized while the flow speed could be maximized.

3.4.2. Froth speed control

In this thesis, a control strategy called mass pull control is investigated. The mass pull describes how much concentrate is collected proportional to the input stream and it can be calculated from concentrate streams if density and flowrate measurements are available, but often times it is estimated from cell's froth speed (Shean, B. and Cilliers, J., 2011). The control of the mass pull is achieved by controlling froth speed with both air and level, where the level is often used to make larger changes and the air is regarded as the primary control variable.

In Outotec's froth speed controllers, air is typically chosen to be the primary control variable due to ease of control and its effect on both the pulp and froth phase recoveries. Level control is difficult due to its nature to disturb other cells in the bank and therefore its often kept constant. The setpoint for the level is determined by the purpose of the cell; rougher cells often have thicker froth beds to keep the gangue away as the easily floatable minerals are recovered and scavengers have thinner froth beds to allow recovery of coarser particles before they are carried to the final tailings. Simplistically, recovery can then be increased and decreased by only increasing and decreasing the air flowrate to a cell, which then changes froth speed. In practice, there exists a point called peak air recovery (Hadler, K. and Cilliers, J. J., 2009), which gives the maximum recovery, and after which increase in air flowrate starts to decrease the recovery as froth stability decreases (Hadler, K. et al., 2010). The point is reached at lower air flowrates when shallower froth beds are used and therefore cells with different froth thicknesses must be operated at different air flowrates. Too low air flowrate however has deteriorating effects on the pulp phase as its kinetic rate constant increases linearly with bubble surface area flux (Gorain B. K., et al., 1998) and exponentially with superficial gas velocity (Harris, A. et al., 2013). To combat the two extremities, air flowrate is given high and low limits.

In a rougher bank, the goal of the mass pull control is often to keep the banks mass pull at a level which meets the capacity of the retreatment banks such as cleaners or grinding capacity of regrind. Instead of controlling cells by themselves, a froth speed profile is set to the whole bank and the profile is then controlled by rising and lowering the profile as one. Target froth speed is then achieved by controlling level and air on individual cells. (Supomo, A., et al., 2008). The control scheme for cell by cell froth speed is depicted in Fig. 20.

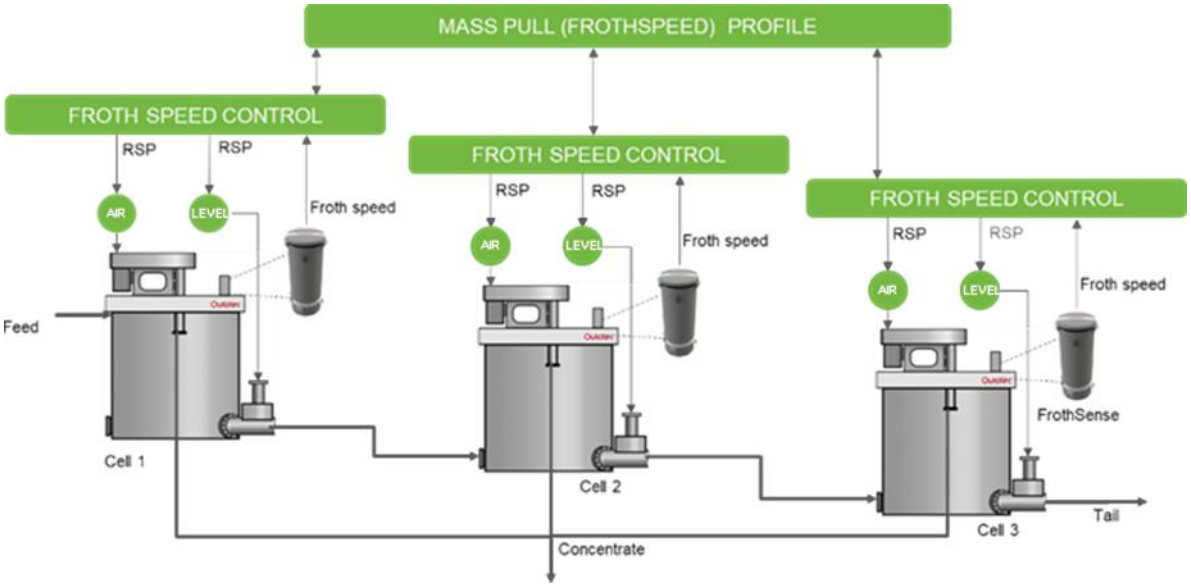

Figure 20. Control structure for GRO solution. GRO gives a mass pull, or froth speed, profile that is achieved by air and level control on the base level.

Reagent dosing also has a role in froth speed control as the conditions inside the tank can be altered using different chemicals. For example, frother increases the froth formation and water recovery while the solids recovery can stay relatively stable and collector increases the recovery of the selected mineral. Both of the situations alter the froth strength and mobility and thus have an impact on the overall froth speed.

3.4.3. Grade-recovery optimization

Optimization with conventional PID algorithms are not enough to control the flotation process due to its multivariable and non-linear nature. Additionally, the process has long delays in its responses and the time constants in the grade changes are long. Optimization has been done for decades and for example, a minimum variance controller was successfully installed in a Canadian mine in 1986 (Suichies et al., 2000). After the nonintrusive method for froth speed measurement and on-stream XRF analyzers were established, the optimization of the grade and recovery has become more common and the controlled design has been moving towards model based and expert system control with good results. (Suichies et al., 2000)

The target mass pull for the unit and therefore the froth speed profile is given by grade recovery optimizer (GRO). The goal of GRO is to maximize the recovery of valuable minerals while keeping the quality of the final product sufficient. This is achieved by minimizing the grade of valuable minerals in the tailings stream and keeping the grade of the concentrate streams within set limits. The measurements used in the optimization are obtained from the online XRF analyzers, Courier analyzers, which typically measure the elemental compositions from input feed and the streams connecting different banks. Along with the froth speed profile, the GRO also controls reagent dosing.

The GRO is built using MPC algorithm with reagent dosing and froth speed profiles 1 and 2 as its manipulated variables, feed's copper grade as its disturbance variable and concentrate and tails grades as its controlled variables. The response models are typically obtained by doing bump tests on site and first order transfer function models are fitted to the measured data. The basic structure of a GRO driven control system for flotation bank is depicted in Fig. 21.

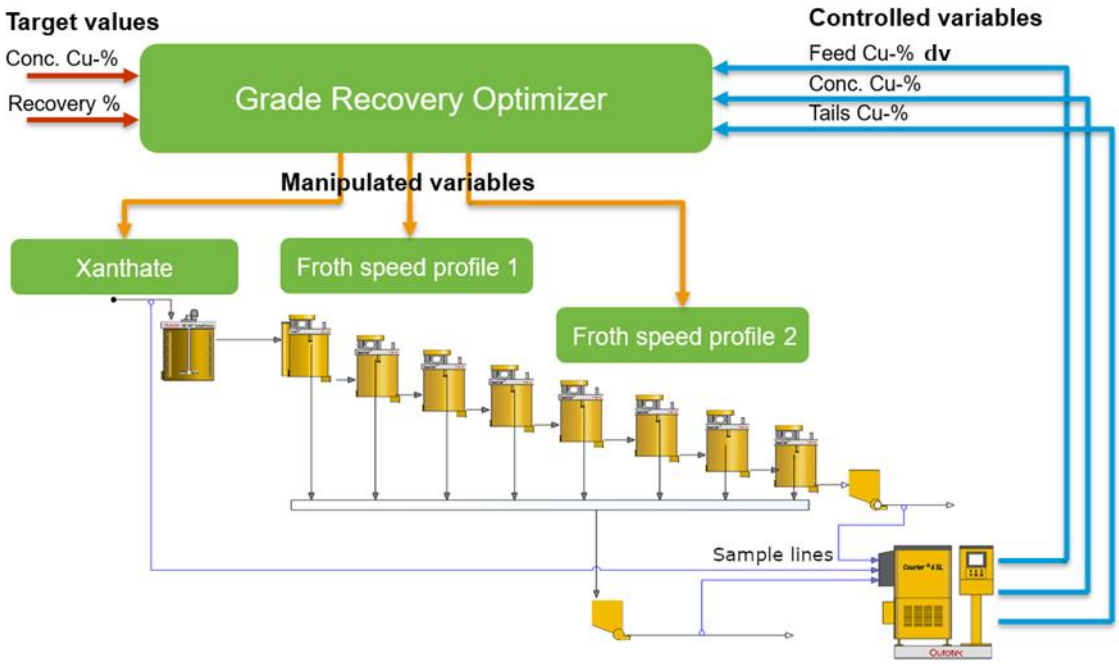

Figure 21. Control principle of the grade-recovery optimizer. The copper grade in the concentrate is kept within limits while maximizing the recovery. The process is controlled through setting setpoints for xanthate dosing and forth speed profiles. Copper grades are measured from feed, concentrate and tailings and they are used in decision making.

4. HSC Sim Model as a Digital Twin

HSC Sim is Outotec's process simulator tool with a focus on mining and mineral industry. The simulator is based on HSC Chemistry software, which was has been in development since the 60s and the first version was launched in 1974 (Outotec, 2015). The HSC Chemistry was designed for chemical reaction and equilibrium calculations and simulations, but later the HSC Sim was developed for general simulation purposes. The HSC software is capable of dynamic simulation and real-time communication with the Advanced Control Tools (ACT) software which can then interact with the real process. Thus, HSC is capable of two-way communication between the process.

4.1. Digital twin

A digital twin as a term was first introduced by NASA in 2010 and it was used to describe model with three common components: robust simulation environment, high fidelity models and real-time two-way communication with the physical process. The models are used in multiple purposes such as optimization, virtual instrumentation and condition monitoring. In mineral processing, the main goal of the model is the optimization, which improves operation performance by increasing efficiency and decreasing operating costs. (Nazari, S. and Cristonffanini, C., 2018)

The digital twin is seen as the optimal plant model and the inefficiencies of the real plant are detected by identifying deviations between the optimal model's outputs and the real plant's measurements. The deviations then trigger actions in the control system that try to drive the plant towards more optimal performance. (Oliver, S. and Tooher, R., 2018)

Aside from control purposes, the predictions can be used in decision making during shorter periods such as shifts or longer periods when larger decisions such as maintenance plans or stockpile changes are made. The model can also be used to test the plant in abnormal situations or for operator training without risking loss of profit.

The model can be used as a soft sensor where the model gives additional measurements from the system, which are not measurable from the real system or that have a long sampling time. For example, sampling time in XRF analyzes are typically 15 minutes but the model could be used to estimate them between the samples, or it could be used to give estimates between cells, which are not analyzed. These measurements are available in real-time and offer a low-cost alternative to physical hardware.

4.2. Components of the flotation model

Fig. 22 contains the basic unit models: conditioner, flotation cell and pump sump, which are used in the rougher circuit model. The conditioner units are used to select the kinetic model and it holds the required rate constants and infinite recoveries for each mineral. It also acts as a buffer and it adds delay to feed variations. The pump sump is similar to the conditioner in that it holds the slurry and acts as a delay and buffer. Each model contains its own runtime values which can be logged during a simulation.

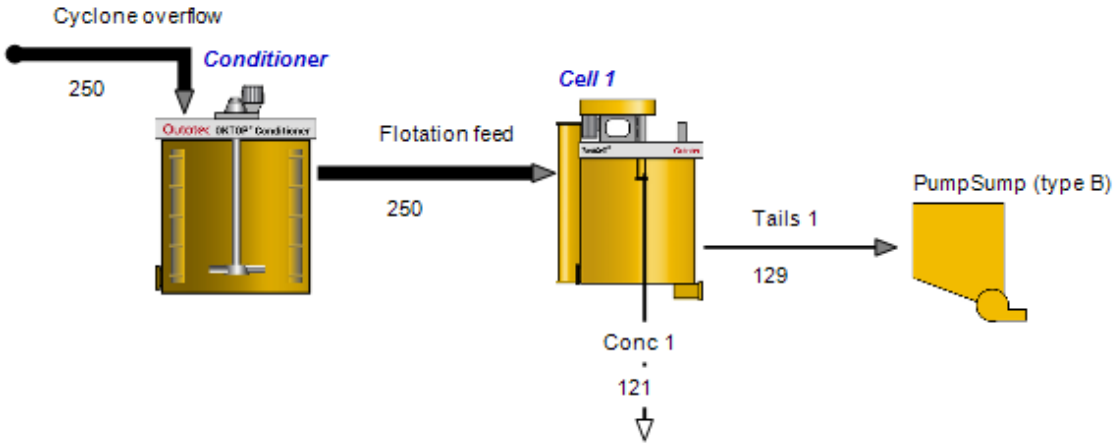

Figure 22. An example HSC model with one flotation cell, conditioner and pump sump.

The fresh feed to the system comes from the cyclone overflow at a constant solids and liquid flow rates and mineral composition. The numbers near the streams are used to visualize the current state of the system and they are currently showing solids flowrate. In the figure the Tails 1 is the discharged material that comes out of the discharge valve, located at the bottom of the tank and the Conc 1 is the froth concentrate that flows over the lip of the cell.

The two main control variables in a flotation cell are level and air rate. The level is measured as the froth thickness, meaning that the measurement describes the distance from the water level to the cell's overflow lip and the slurry level in the tank is called cell hydrostatic height.

Both the air and level are controlled with PID controllers. The level is controlled by controlling the dart valve opening percentage which changes the flowrate of the slurry. Air flowrate has a linear relationship between the valve opening, where an opening of % sets the air flow to 0 and opening of 100 % sets the air flow rate to the maximum value.

The rougher model, shown in appendix 1, includes eight flotation cells and two conditioners and pump sumps. The parameters for the flotation cells used in the model are listed in Table 2. The volumes of conditioners are set to 100 m^3 and pump sumps' volumes are set to 5 m^3. The four first cells have a froth surface area of 16.12 m^2 and the last four 8.66 m^2. This is due to four last cells having internal launders.

Table 2. Some of the parameter set for the rougher bank's flotation cell unit models. The valve in the last cell is smaller than in the other cells with a diameter of 200 mm. Smaller valve is used to compensate the lack of next cell.

	Value	Unit	Description
Net volume	58.05	m^3	Cell's net volume
Pulp area	16.62	m^2	Area of the pulp
Lip height	3.5	m	Height from cell bottom to lip level
Lip length	14.45	m	Length of the froth collection launders
Rotor diameter	900	mm	Rotor impeller size
Rotor speed	126	rpm	Rotation speed of the rotor
Step to next cell	0.6	m	Vertical step-down to the next cell in the bank
Number of valves	2		Number of tails valves
Valve type	Dart		Type of the tails valve (dart/pinch)
Valve size	250	mm	Valve diameter
d32	1	mm	Bubble Sauter diameter in the pulp phase

4.3. Recovery model

The flotation model in the HSC is divided into two parts: pulp and forth, which are connected into a series. The pulp phase, often referred to as collection cone is where the mineral particles have a chance to be recovered into the froth phase by being attached to the rising bubbles and rising into the froth zone. The froth zone is where the particles, still attached to the rising bubbles, have a chance to be recovered into the concentrate stream by being carried over the cell lip along with the overflowing froth. The interaction between these two zones is depicted in Fig. 23.

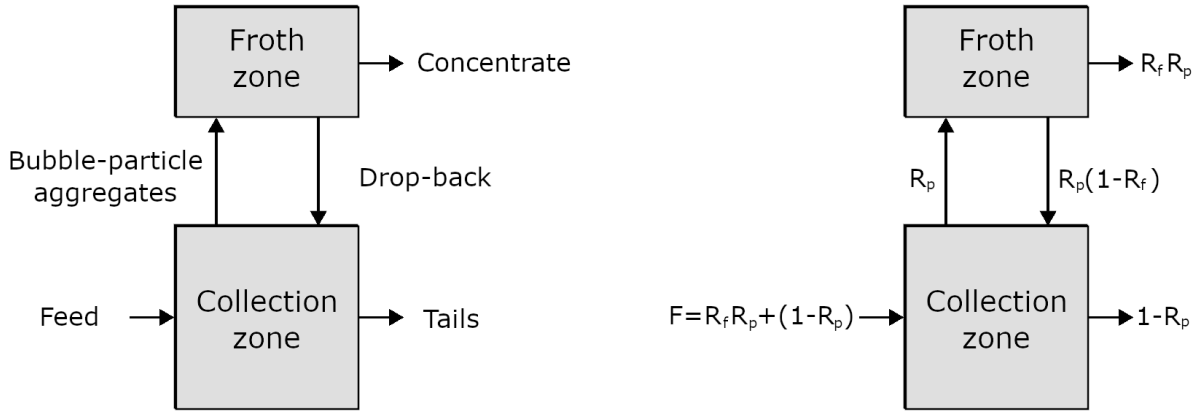

Figure 23. Interaction between collection and froth zones. The diagram on the left has the stream names and the diagram on the right has the recoveries of the streams. The input feed F is concentrate $R_f R_p$ and tails $1 - R_p$ streams summed together, and the dropback is the multiplication of what gets through the collection zone, R_p, to the froth zone but does not get pass the froth zone $1 - R_f$. (Gómez, C. et al. 2017)

The recoveries in the system, R_p and R_f, are pulp and froth recoveries. The froth recovery is defined as the proportion of particles that pass into the concentrate after passing through the pulp-froth interface (Ata, S., 2012). It has been found that froth recovery correlate strongly with the time the particles spend inside the froth phase (Gorain et al., 1998) and thus, the recovery can be calculated using froth retention equation:

$$R_f = 1 - e^{-\alpha \lambda_{air}}, \tag{11}$$

where α is froth recovery exponent and it can be adjusted to achieve desirable recovery and λ_{air} is the gas residence time in the froth.

The kinetic rate constant inside the pulp zone is calculated using the given mineral specific rate constants P and the bubble surface area flux and its nominal value as in (Remes, A., Izart, C., et al., 2019)

$$k_c = P \frac{S_b}{S_{b,nominal}}. \tag{12}$$

Since the bubble surface area flux is calculated from the superficial gas velocity J_g and bubble size d_b as in (2), the use of it makes it possible to simulate different bubble sizes and air flowrates. If the nominal value is not known, the value of k_c defaults to P.

In a static calculation the pulp recovery would be calculated using the models described in section 3, but in dynamic calculation it is assumed that the particle removal rate is proportional to the mass available in the pulp zone (Gómez, C. et al. 2017),

$$\frac{dM}{dt} = k_c M = \frac{PMS_b}{S_{b,nominal}}, \tag{13}$$

where the M is the mass of particles in the pulp, the t is the flotation time and the k_c is the kinetic rate constant in the collection zone. This can be rewritten to a similar form as the continuous version of the first order equation in (3), described in the section 3:

$$\frac{M}{M_0} = e^{-\frac{PS_b t}{S_{b,nominal}}}, \tag{14}$$

where M_0 is the initial particle mass in the pulp. Floatability distribution can be used by choosing rectangular distribution as the flotation model. In this case the floatability P is replaced with the maximum floatability P_m and the above equation takes the form

$$\frac{M}{M_0} = \frac{1}{P_m S_b t} e^{-\frac{P_m S_b t}{S_{b,nominal}}}. \tag{15}$$

The pulp zone recovery can then be calculated as

$$R_p = 1 - \frac{M}{M_0}. \tag{16}$$

Recoveries in pulp phase are difficult to measure in an industrial flotation cell but typical values for the froth recovery are between 40 and 80 % and can get as high as 90 % (Yianatos, J., et al., 2008; Savassi, O., N., et al., 1997).

The feed to coming in to the system is written as the sum of concentrate and tails recoveries, as in

$$F = R_p R_f + \left(1 - R_p\right), \tag{17}$$

where $R_p R_f$ is the concentrate and $\left(1 - R_p\right)$ is the tails recovery. The final concentrate recovery is proportional to the feed (Remes, A., Izart, C., et al., 2019),

$$R_{fc} = \frac{R_p R_f}{R_p R_f + (1 - R_p)}. \tag{18}$$

Along with the pulp and froth recoveries, the recovery by entrainment can be simulated as well. The recovery by entrainment is calculated from the Savassi entrainment and water recovery. The water recovery for the given industrial cell is hard to estimate from laboratory tests and the recovery is usually estimated from the concentrate or tails solids content (Kawatra, S. and Young, C., 2019). The Savassi entrainment equation can be expressed as

$$Ent_i = \frac{2}{e^{2.292\left(\frac{d_i}{\zeta}\right)^{adj}} + e^{-2.292\left(\frac{d_i}{\zeta}\right)^{adj}}},$$
$$adj = 1 - \frac{\ln(\delta)}{e^{\frac{d_i}{\zeta}}} \tag{19}$$

where ζ is known as the entrainment parameter which is the particle size with entrainment degree of 20 %, d_i is the particle size and δ is the drainage parameter. Entrainment and drainage parameters have a linear relationship with the gas residence time and the best fit is achieved with

$$\zeta = -0.667\lambda_{air} + 40.416$$
$$\delta = 0.020\lambda_{air} + 0.534. \tag{20}$$

The recovery by entrainment is then given by

$$R_e = Ent \cdot R_w, \tag{21}$$

where R_w is water recovery. (Savassi, O. N., et al., 1998)

With the recovery by entrainment added to the final concentrate recovery in (17), it becomes

$$R_{fc} = \frac{R_p R_f R_e}{R_p R_f + (1 - R_p)}. \tag{22}$$

4.4. Interaction between cells in a bank

The cells can disturb each other by varying the flowrate. The changes in the flowrate can happen due to the changes in recovery, level or feed flow disturbances. If the level is increased, the controller increases the opening of the dart valve and respectively if the level is decreased, the opening is decreased. The recovery of the cell can be affected by changing the level and air flow and the change in the flowrate occurs due to more or less material making it to the following cells. The flowrate is calculated from (Remes, A., Izart, C., et al., 2019)

$$Q = A_{valve} C_v \sqrt{2g\Delta h}, \tag{23}$$

where the A_{valve} is the opening area of the dart valve, the C_v is the flow coefficient of the slurry, the g is the gravitational constant and the Δh is the hydrostatic head. The flow coefficient is a constant thus the flowrate can be controlled only by changing the valve opening and the hydrostatic head.

The Figs. 24, 25 and 26 shows an example of how a step input affects to one cell's level as disturbs the following cell's level. As the hydrostatic height drops in cell 2, it makes it easier for slurry to flow from cell 1 to cell 2 due to increased hydrostatic head. Since the slurry flows easier from cell 1 to cell 2, the level drops in cell 1.

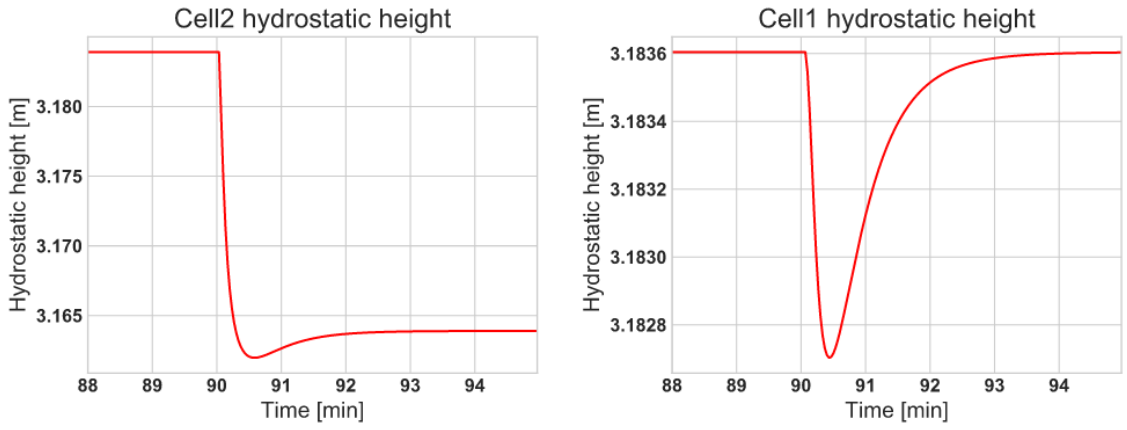

Figure 24. On the left is the hydrostatic height of cell 2 and on the right is the hydrostatic height of cell 1. As the hydrostatic height is decreased on cell 2, the hydrostatic height decreases on cell 1 before the controller fixes the error.

To compensate the increase in hydrostatic head, the valve between the cells decreases its opening to maintain the level in cell 1 which can be seen from Fig. 25.

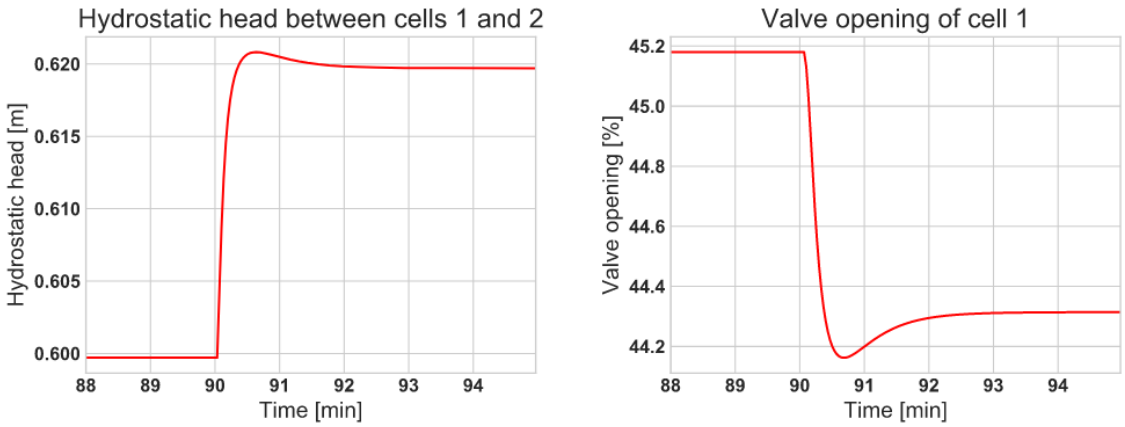

Figure 25. On the left is the hydrostatic head and on the right is the valve opening between cells 1 and 2. Increasing the hydrostatic head makes it easier for the slurry to flow through the valve and the increased flow is suppressed by decreasing the valve opening.

This results in a spike in the flowrate which travels through the following cells and the oscillation gets longer further away from the causing cell. If the disturbance was cause in the middle of the bank, the cells upstream would have an inverse disturbance in the flowrate since the hydrostatic head decreases. The change in the flowrate between cells 1 and 2 is depicted in Fig. 26.

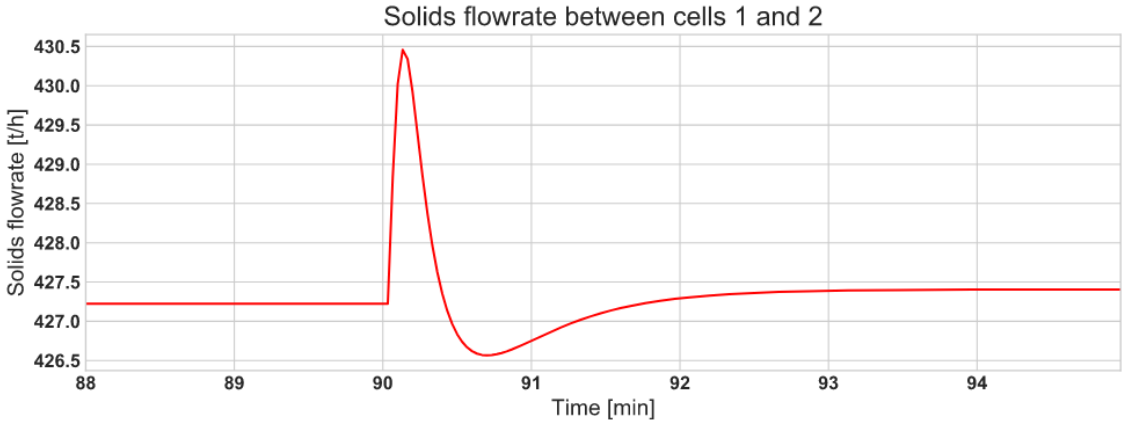

Figure 26. The step in cell 2's level results in a spike in solids flowrate between cells 1 and 2.

It is worth noticing that the changing flowrate influences the recovery of all the cells since it changes the residence time.

4.5. Dynamics of the flotation cell model

To evaluate the dynamics of the model, step tests were made to the level and air rate and the simulated data was used to interpret the changes in the final concentrate and tailing recoveries and the concentrate grade. The steps were made to cells 1 and 5. The cell 1 was selected because it is not as impacted by the changes happening in the following cells and cell 5 was selected because it is in the middle of the process and upstream and downstream changes can be seen at the same time. The equations shown in this section are from the HSC manual (Remes, A., Izart, C., et al., 2019).

4.5.1. Response to a level Step

The step test was made only to the first cell of the series and other cells were left as they were. Fig. 27 shows the step response from 217 mm to 227 mm, meaning that the thickness of the froth bed was increased by 1 cm.

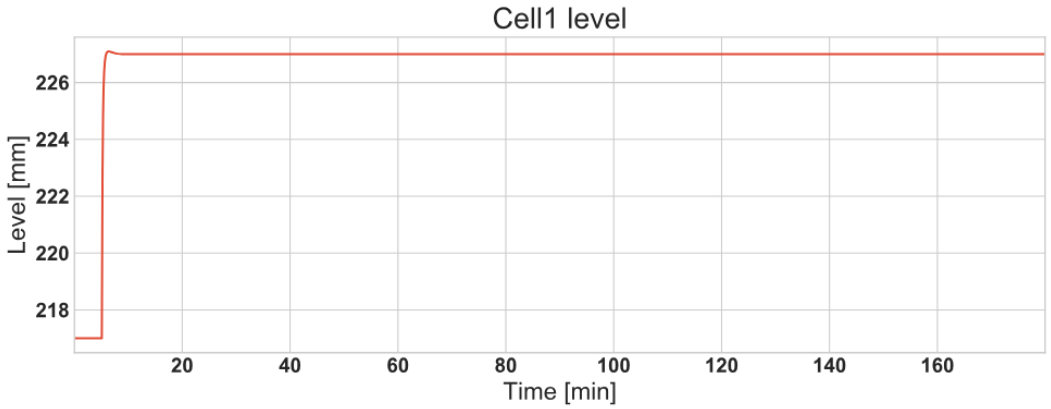

Figure 27. Step response resulting in an increase of 1 cm to the thickness of the first cell's froth bed at 5 minutes.

The control adjusts the level by opening the tails valve of the cell which makes the slurry level, hydrostatic height, drop and leaving more space for the froth layer. The hydrostatic height is calculated from the fill volume V_{Fill} and the lip height h_{lip} as:

$$h_{HydrostaticHeight} = \frac{V_{Fill}}{100} \cdot h_{lip} = \frac{V_{Effective}/V_{Total}}{100} \cdot h_{lip}, \quad (24)$$

where the fill volume is calculated from the effective volume $V_{Effective}$ and the total volume of the cell V_{total} as:

$$V_{Fill} = \frac{V_{Effective}}{V_{Total}}. \quad (25)$$

The thickness of the froth layer is then calculated by subtracting the hydrostatic height from the lip height as:

$$h_{froth} = h_{lip} - h_{HydrostaticHeight}. \quad (26)$$

Since the air flowrate is not changed, bubbles' rise velocity stays constant. As the layer of the froth thickens, the bubbles spend more time in the froth. The gas residence time is calculated as follows:

$$\lambda_{air} = \frac{h_{froth}}{J_{g,froth}}, \tag{27}$$

where h_{froth} is the thickness of the froth layer and $J_{g,froth}$ is the superficial gas velocity of the bubbles in the froth layer. According to the froth recovery (10), the recovery drops due to increase in gas residence time. The changes in the hydrostatic height, gas residence time and froth recovery are depicted in Fig. 28.

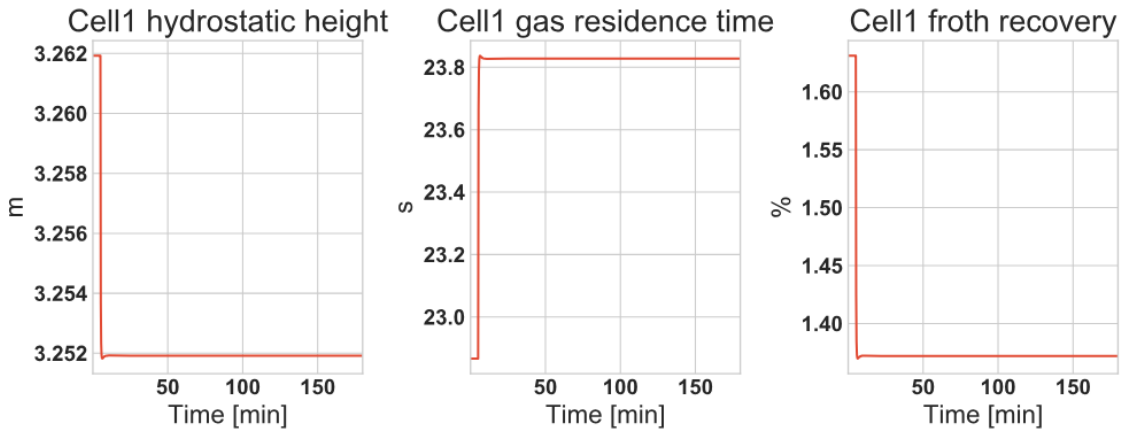

Figure 28. Hydrostatic height, gas residence time and froth recovery of cell 1. Increased level leads to Decreased hydrostatic height, increased gas residence time and decreased froth recovery.

As the forth takes more space in the cell, the effective volume decreases. The effective volume is calculated by subtracting the froth and the gas volumes out of the total cell volume:

$$V_{Effective} = V_{Total} - V_{Froth} - V_{GasHoldup}. \tag{28}$$

The gas holdup is constant and set to 10 percent in cell parameters. When the feed to the tank stays constant and the effective volume decreases, the residence time in the cell

$$\tau = \frac{V_{Effective}}{Q_{Feed}}, \tag{29}$$

decreases.

Pulp recovery or masses inside the cells are not available measurements in HSC and instead overall flotation rate:

$$k = \frac{R}{\tau(100 - R)}, \tag{30}$$

calculated from overall recovery R and cell residence time τ, shows how the change in residence time impacts the overall recovery. The recovery in the pulp phase can also be estimated to decrease due to less mineral mass being in the cell since there's less pulp in the

tank after the level change. Fig. 29 shows how increase in the level leads to decrease in the effective volume, residence time and overall flotation rate.

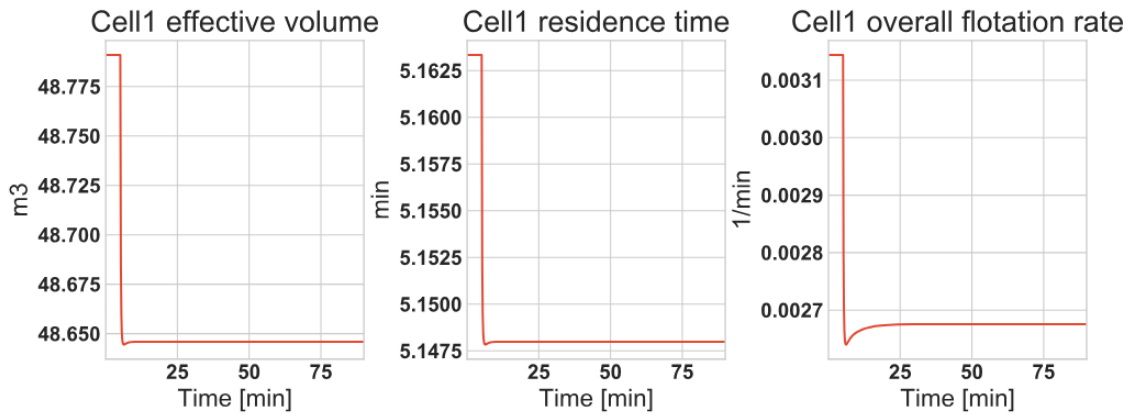

Figure 29. An increase in the level decreases cell's effective volume whih leads to decrease in residence time and pulp recovery.

Lowering of the hydrostatic height requires that the valve opening is increased, which results in a spike in tails flowrate. The spike travels through the downstream cells, hence increasing their hydrostatic heights and lowering the residence times. The hydrostatic heights stabilize to the same level and only a momentary spike can be seen in the froth recoveries, but the residence times decrease slightly since the tails flow of cell 1 stabilizes to higher value.

Impact of the decreased residence time is over powered by the increasing particle mass in the cells and thus the recoveries of cells 2 through 8 are increased. The effect of the tails flow is depicted in Fig. 30.

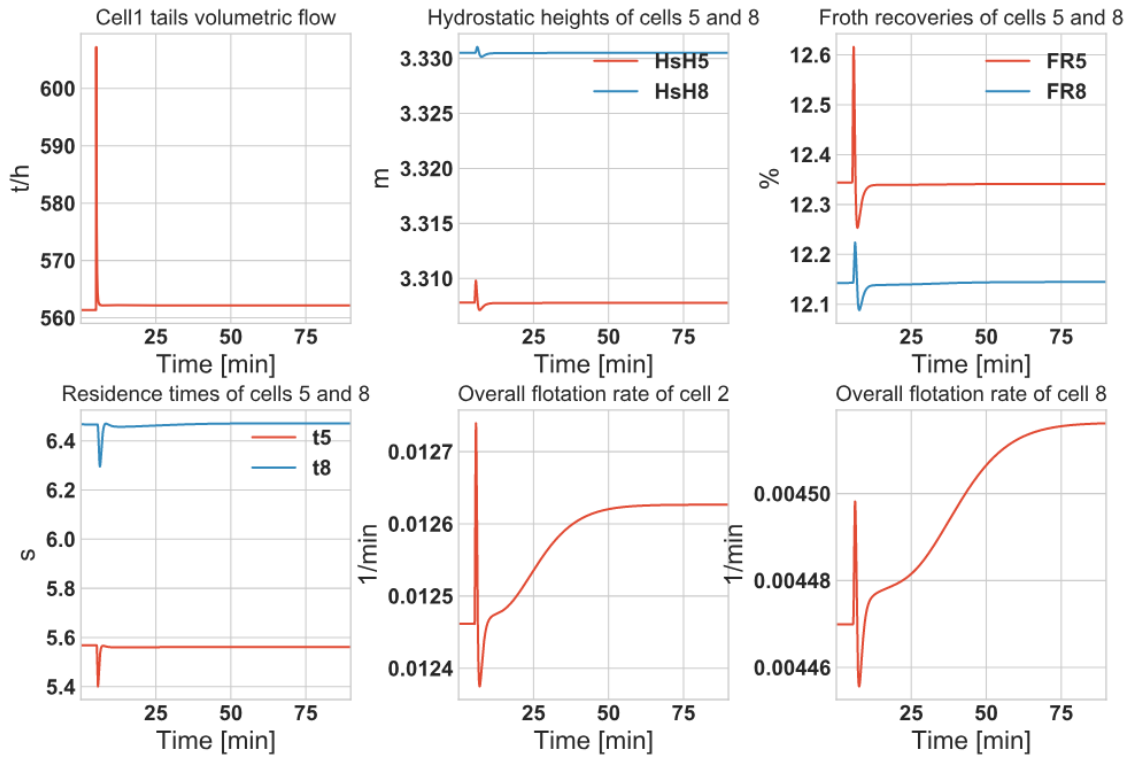

Figure 30. Impact of the changing tails stream flowrate. Froth recoveries have a short increase but stabilize to the same level and pulp recoveries rise slightly.

Increase in the level results in a lower recovery in cell 1, but it increases in the following cells, due to more recoverable material making its way into them. The overall recovery drops which is depicted in Fig. 31

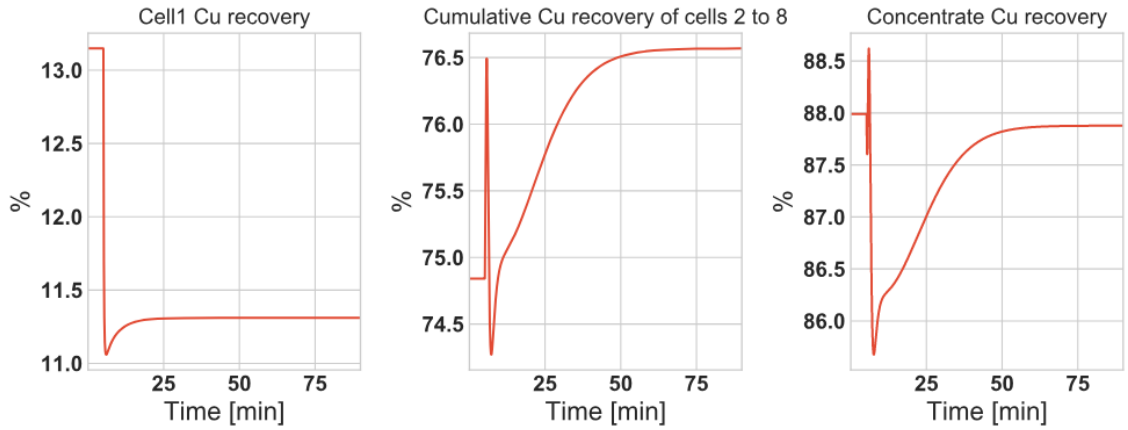

Figure 31. Copper recoveries of cell 1, cells 2 through 8 and the final concentrate. The recovery of the cell 1 decreases but cells 2 through 8 make up for the loss with increased recovery. The final recovery is slightly decreased.

As the overall recovery drops, the grade increases in both the concentrate and the tails. The shape of the tailings curve comes from all the cells stabilizing to a new point one after another and minerals having to make it through all the cells in different phases. The grades are depicted in Fig. 32.

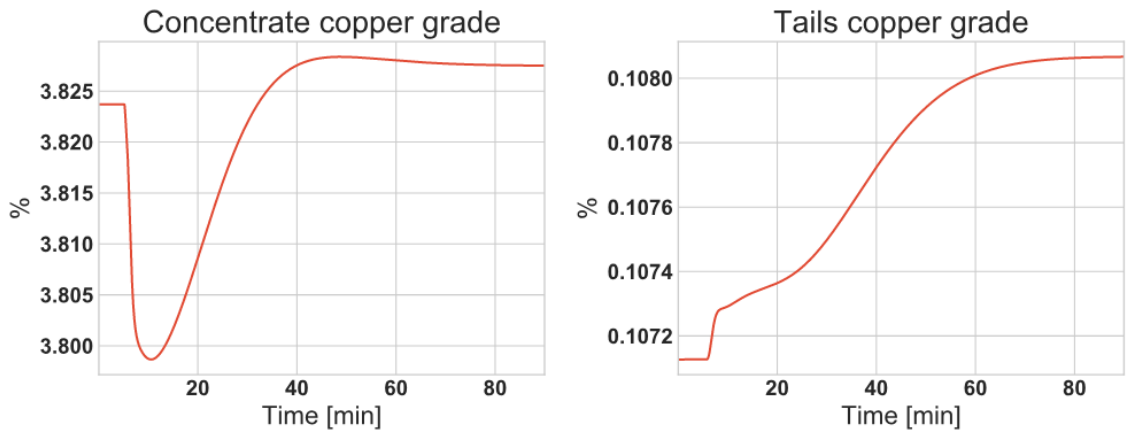

Figure 32. Rougher circuit's concentrate and tail grades. Both grades increase.

Increase in concentrate grade is mainly due to less pyrite making it to the concentrate which increases the copper proportion in the stream. Increase in tailings is more complicated but it is mainly due to the large amount of gangue already present in there. The gangue has small maximum flotation rate constant which means that it is already difficult for it to get into the concentrate, and thus increasing the level in the first cell has little effect on it. On the other hand, copper has is more affected by the level increase as it can make it through the pulp phase easily due to high maximum flotation rate, but it is more easily dropped back to the pulp due to higher level. Thus, the small increase of copper in the tailings can increase its grade as the main bulk of the tailings stays the same tonnage wise. The increase in grade is seen in all elements except those unique to the gangue: silicon and oxygen.

A simple method to calculate froth speed is to calculate the speed of concentrate pulp flowing through a constant area. Fig. 33 shows how the increase in level results in a decrease in concentrate pulp's volumetric flow and since the overflow area is kept constant, the decrease in froth speed is dictated by the decrease in flowrate.

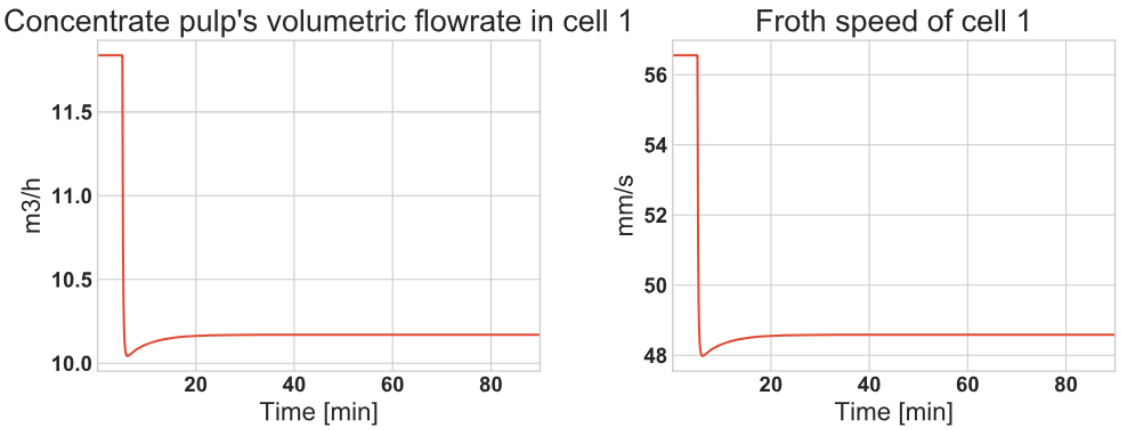

Figure 33. Resulting froth speed change in cell 1. Increase in level decreases the recovery and therefore the pulp's volumetric flow. As the overflow area is kept constant, the froth speed decreases with the pulp volumetric flowrate.

4.5.2. Response to an air step

As with the level step test, all cells start with a level of 300 mm and air flowrate of 20. The step was made to the first cell and it increases the air flowrate from 9.1 m^3/h to 10.1 m^3/h. The step is depicted in Fig. 34.

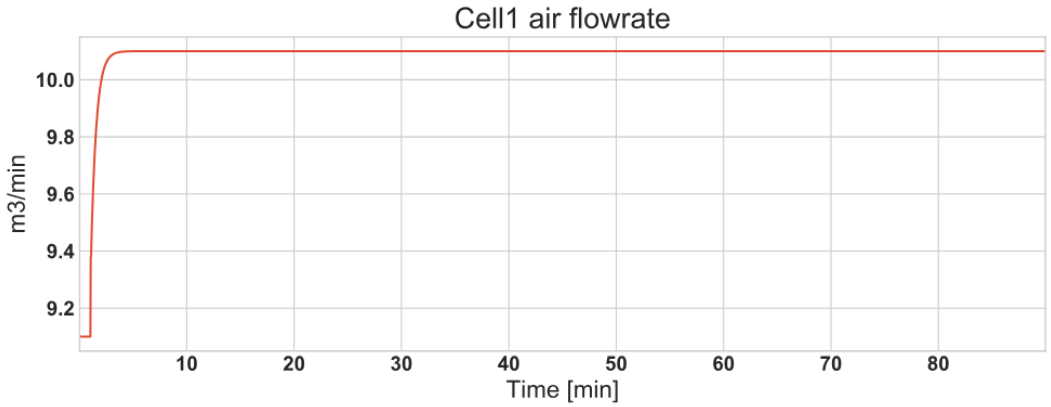

Figure 34. Step to cell 1's air flowrate.

Increasing the air flowrate increases the superficial gas velocity in the froth zone:

$$J_{g,froth} = \frac{5}{3} \cdot \frac{Q_{Air}}{A_{Froth}}. \tag{31}$$

The increase in velocity decreases the gas residence time according to (27), when the thickness of the froth layer remains constant. The decreased gas residence time leads to an increase in the froth recovery, the responses are depicted in Fig. 35.

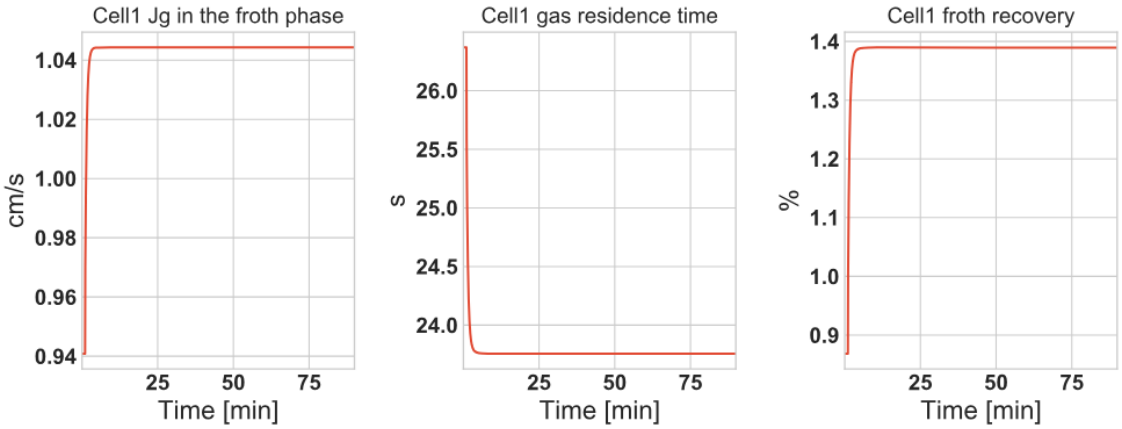

Figure 35. Increasing superficial gas velocity in the froth phase leads to decreasing gas residence time and increasing froth recovery.

The pulp phase has an increase in superficial gas velocity:

$$J_g = \frac{5}{3} \cdot \frac{Q_{Air}}{A_{Pulp}}, \tag{32}$$

which leads to an increase in bubble surface area flux:

$$S_b = 60 \cdot \frac{J_g}{d_{32}}, \tag{33}$$

where d_{32} is the Sauter mean distance with a constant value of 1 mm. Increasing BSAF

leads to better flotation conditions in the pulp phase and increases the collection zone kinetic rate constant:

$$k_c = P \cdot \frac{S_b}{S_{b,nominal}}. \tag{34}$$

The responses are depicted in Fig. 36.

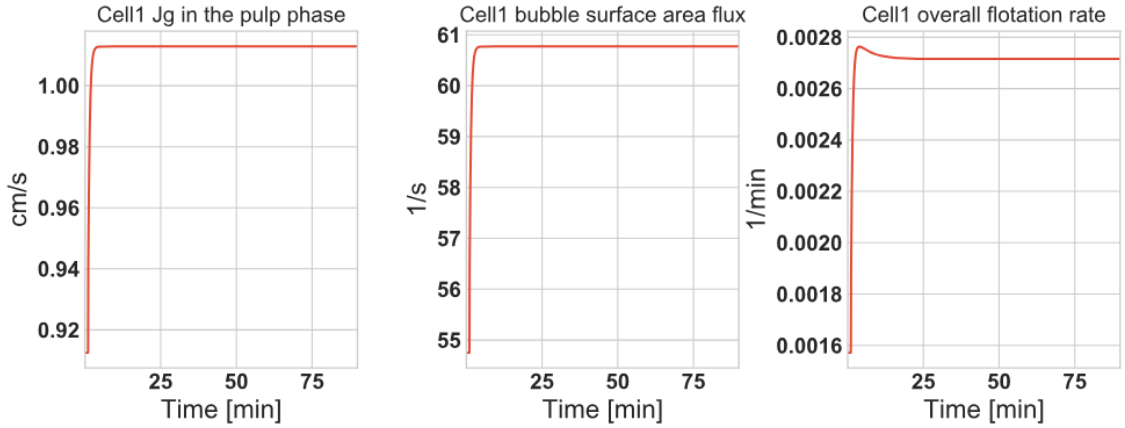

Figure 36. Increasing superficial gas velocity, bubble surface area flux and overall flotation rate.

As the volumetric flowrate decreases, cells 2 through 8 have a slight increase in hydrostatic height and increase in the residence times. The change in the hydrostatic height lowers the froth recoveries and the increase in residence times increases the pulp recovery but the drop in froth recovery overpowers it and the overall recovery drops. This is depicted in Fig. 37.

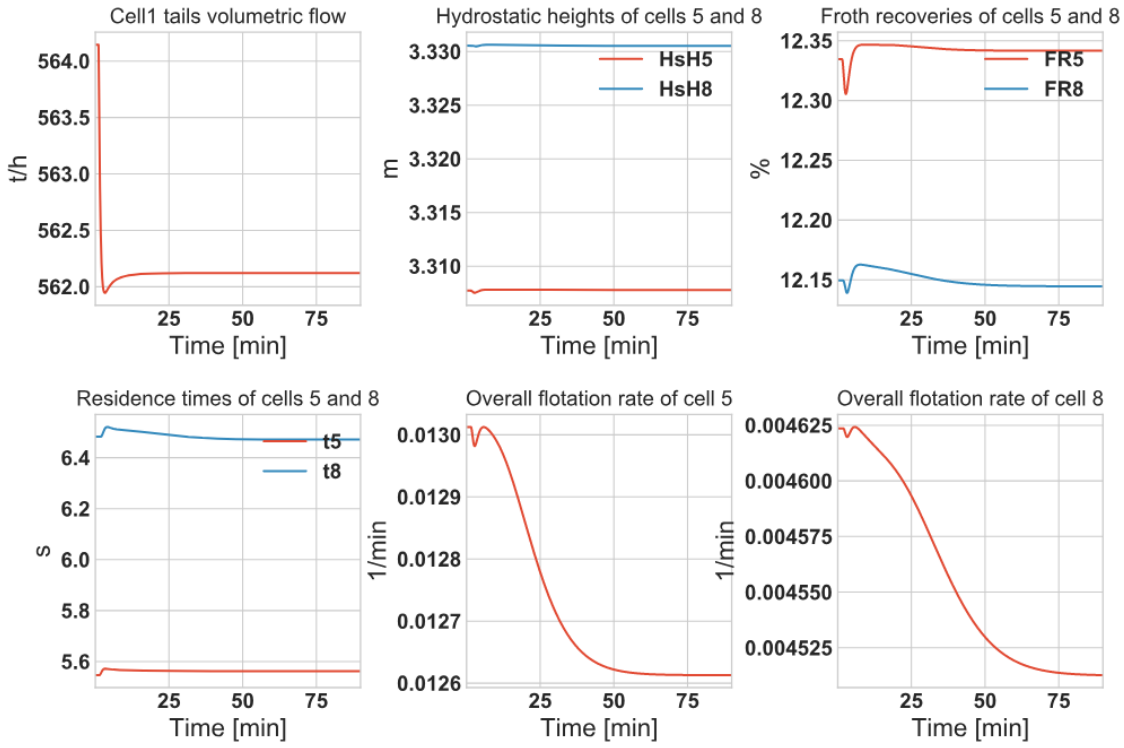

Figure 37. As the recovery in cell 1 changes, the tail's volumetric flowrate changes as well.

Increase in air the flowrate leads to higher recovery due to increase in both froth and pulp recoveries. Overall recovery rises and thus the grade decreases in concentrate and tails, these are depicted in Figs. 38 and 39.

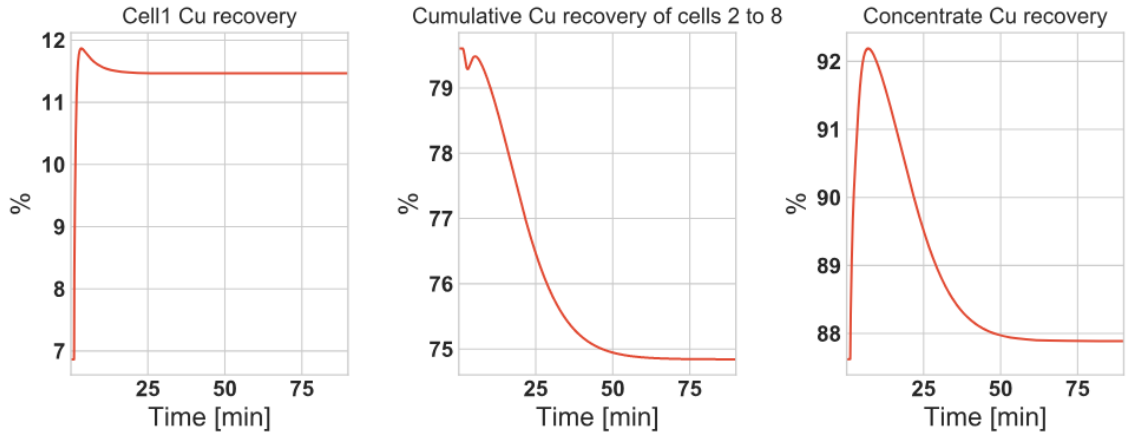

Figure 38. Air step leads to an increase in copper recovery in cell 1 but lowered recovery in cells 2 through 8. The final recovery rises.

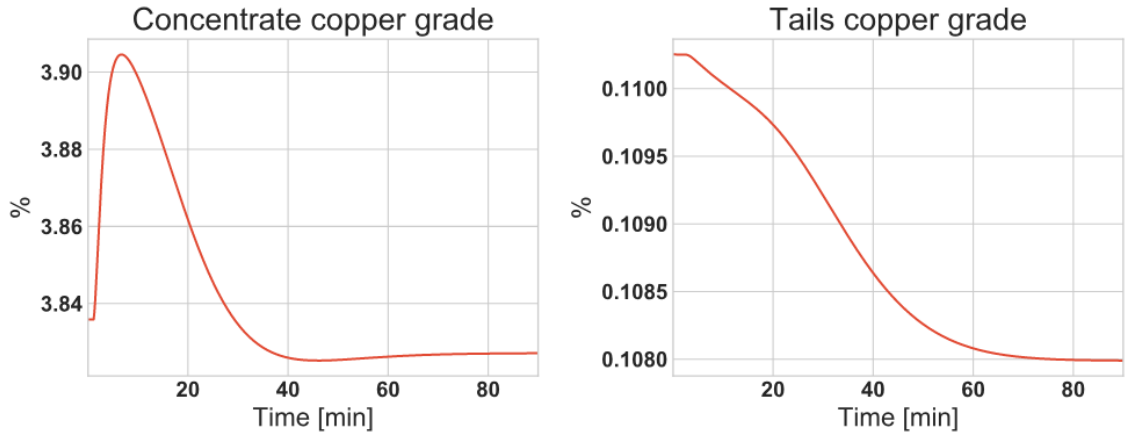

Figure 39. Since the final recovery increases, there's a decrease of grade in both the final concentrate and tailings.

Increase in air flowrate leads to higher recovery and thus higher flowrate of concentrate pulp. The increase in froth speed due to the step in air flowrate is depicted in Fig. 40.

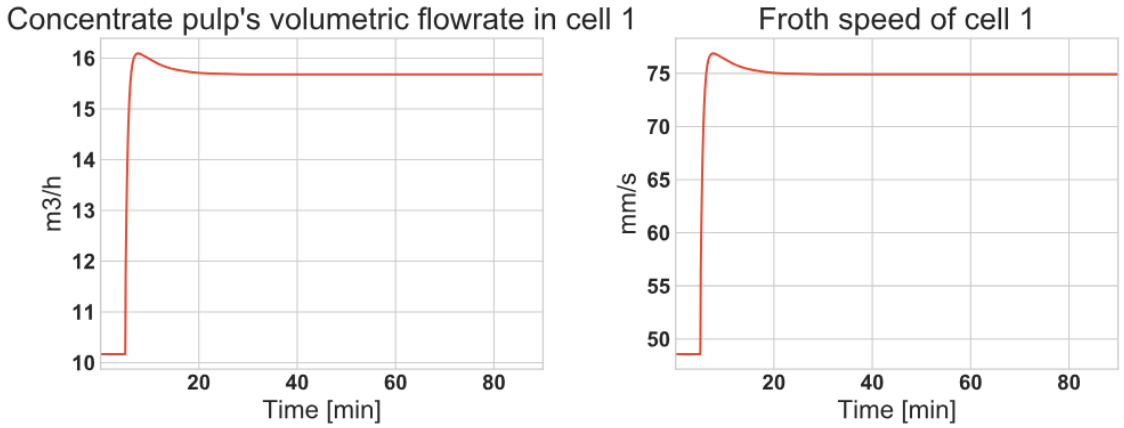

Figure 40. Increase in air flowrate leads to an increased recovery. As more particles get recovered into the concentrate, the volumetric flowrate of concentrate pulp increases and thus the froth speed increases.

4.5.3. Response in the middle cell

Step test to the air and level have in middle of a bank have the same lasting effect on other cells. When the level or air flowrate are changed in a middle cell, they have an impact in other cell's because of changes in flowrates. Following the change in the cell's hydrostatic heights they stabilize to new values due to only having very small error, resulting from new flowrate, which the level controller cannot remove during the simulation. Volumetric flowrates in cell 4 and 5 tailings are depicted in Fig. 41.

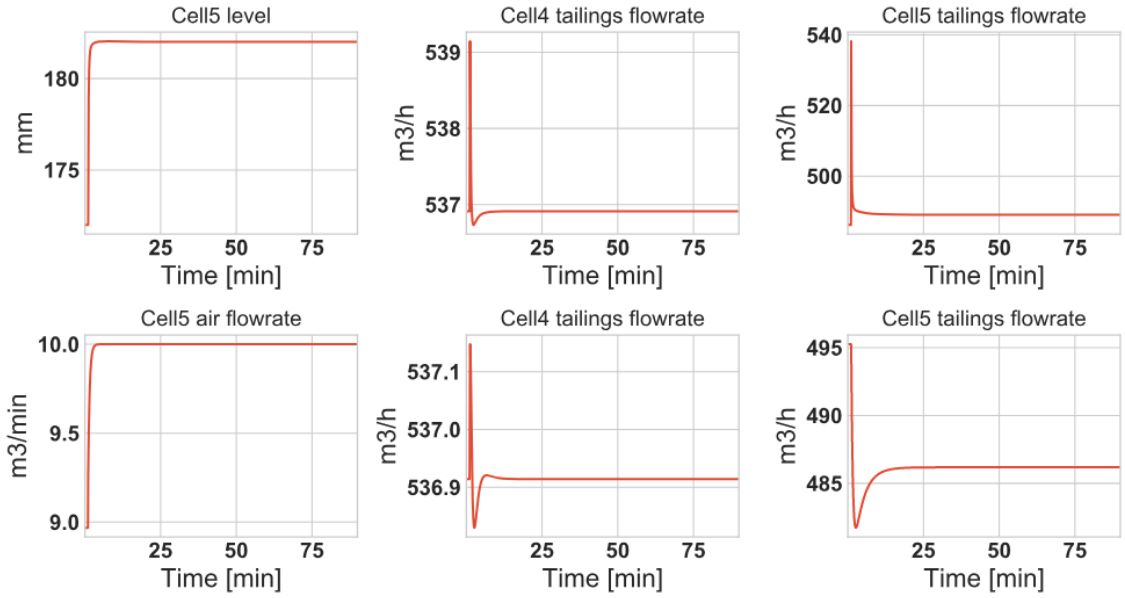

Figure 41. Increasing the level in cell 5 makes the hydrostatic height drop momentarily in cell 1. In cells 6 to 8 it stabilizes to a lower level.

The lasting effect comes from the change in recovery which changes the flow of minerals in the tailings. When the air rate increases, recovery increases and less minerals get through to the other cells. This simultaneously increases the residence time due to decreased flowrate of the tailings and decreases the pulp recovery because less mass comes in to the cell. The froth recovery changes due to small error in hydrostatic height and the overall recovery in the cells 6 through 8 increases. The same effect can be seen when level is changed, and this is depicted in Fig. 42.

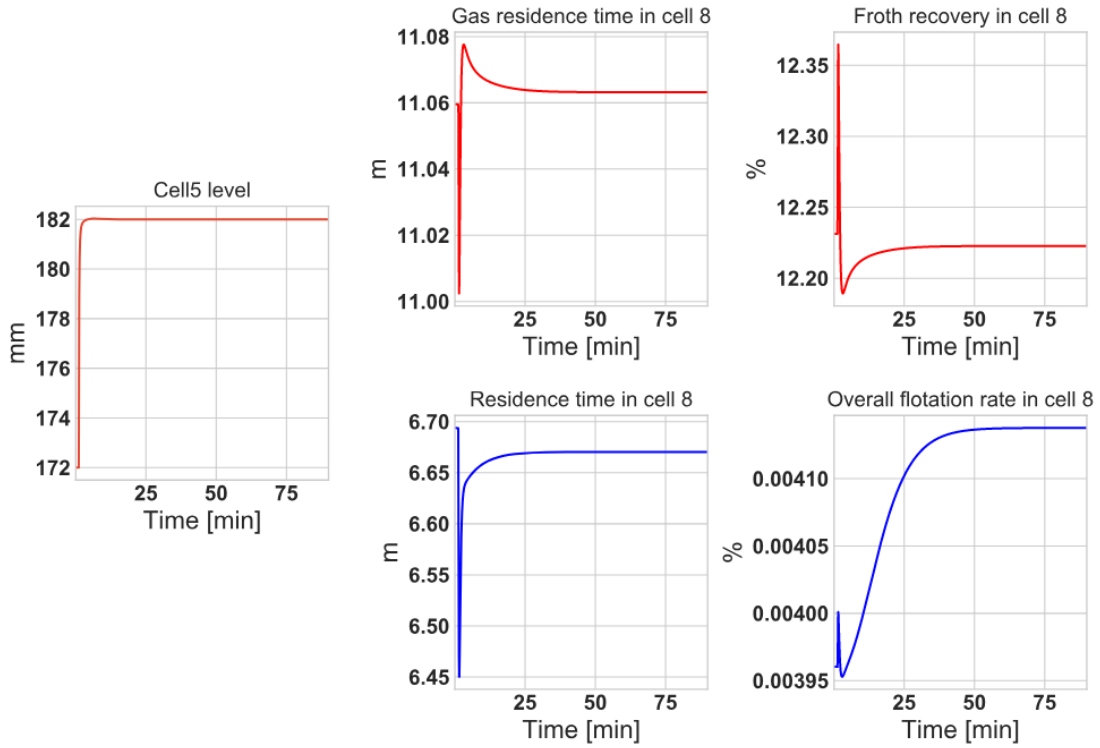

Figure 42. Increase in the level decreases the froth recovery and increases the pulp recovery in proceeding cells.

The comparison of step tests made to cells 1 and 5, depicted in Fig. 43, shows that a step made upstream leads to higher recovery and thus lower grade, as the overall residence time of the bank increases. Step made in cell 5 leads to faster stabilization of the bank since there's less tanks for disturbance to travel through.

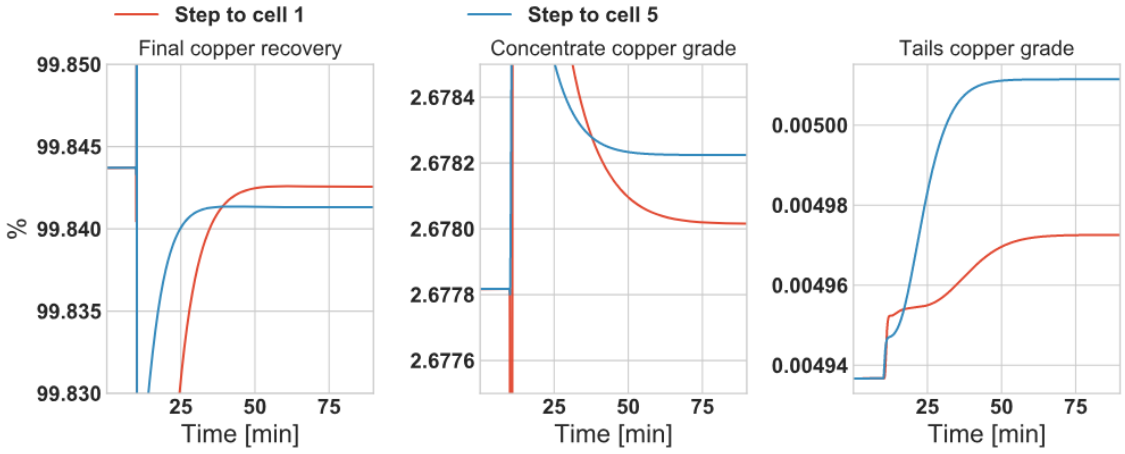

Figure 43. Copper recovery stabilizes to higher level when the step is done at cell 1 but the grade is higher when done in cell 5.

5. Experimentation with HSC

This section describes how the HSC model is parameterized according to the preliminary laboratory work which was used to design the actual plant and the plant data which was recorded during step tests at the said plant. As HSC lacks an integrated froth speed model, it is designed with a neural network (NN) and the design process is described. The values concerning the size and profitability of the plant are scaled or hidden due to confidentiality reasons.

5.1. Preliminary laboratory results

Before a plant is built, laboratory work is done in order to understand the feed composition and flotation kinetics for each of the major mineral type. These results are then used to design the plant. In this case, the mineral types are chalcopyrite, sphalerite, pyrite and Non-Sulphide Gangue (NSG) and their compositions are described in Table 3. All the minerals contain iron and copper is unique to chalcopyrite, zinc is unique to sphalerite and oxygen and silicon are unique to NSG.

Table 3. Major minerals of the feed slurry and their elemental distributions. The feed contains four different mineral types which amount to six different elements.

		Mineral			
		Chalcopyrite	Sphalerite	Pyrite	NSG
Element	Cu %	20.60	-	-	-
	Fe %	26.42	1.96	40.32	5.47
	S %	30.37	28.48	45.36	-
	Zn %	-	41.84	-	-
	O %	-	-	-	50.35
	Si %	-	-	-	44.18

The flotation model is based on rectangular distribution and the laboratory determined flotation kinetics are in Table 4. The pH during the test was 9.5.All the minerals except NSG have an infinite recovery close to 100 %. Chalcopyrite is the fastest floating and NSG the slowest floating mineral.

Table 4. Flotation kinetics based on the laboratory work.

	Chalcopyrite	Sphalerite	Pyrite	NSG
R_{inf}	99.9	97.2	100	2.4
kmax	3.39	1.845	1.467	0.897

The laboratory testing showed that the rougher circuit doubles the copper and iron grades from feed to concentrate and copper recovery is above 95 % and iron's is above 80 %.

5.2. Gathering values from the plant data

The timespan for the plant data from the Advance Control Tools (ACT) database is 77 days, majority of that being average data over 600 seconds. Latest eight days had average data over 15 seconds, and they were used in the model fitting. The most important variables in the data are the courier analyzes and the levels, air rates and froth speeds. Additionally, some variables such the reagent dosing and the flow rates are obtained from the distributed control systems database and some additional grade analyzes are obtained from periodical laboratory tests.

The iron and copper grade averages for the feed, concentrate and tailings are calculated from seven days of the eight-day period, as one day had problems with the courier analyses. The grades for zinc are calculated from the periodical laboratory results as it is not included in the courier analysis. Fig. 44 shows the measured copper and iron grades and it can be seen that copper grade increases from feed to concentrate and tailings grade is lower than that of the feed. There is also a lot more iron than copper in the feed and the iron grade is similar to feed's grade, but tailings grade is almost half of that of the feed. Talings grades are low since mostly made of NSG and thus oxygen and silicon have high grades.

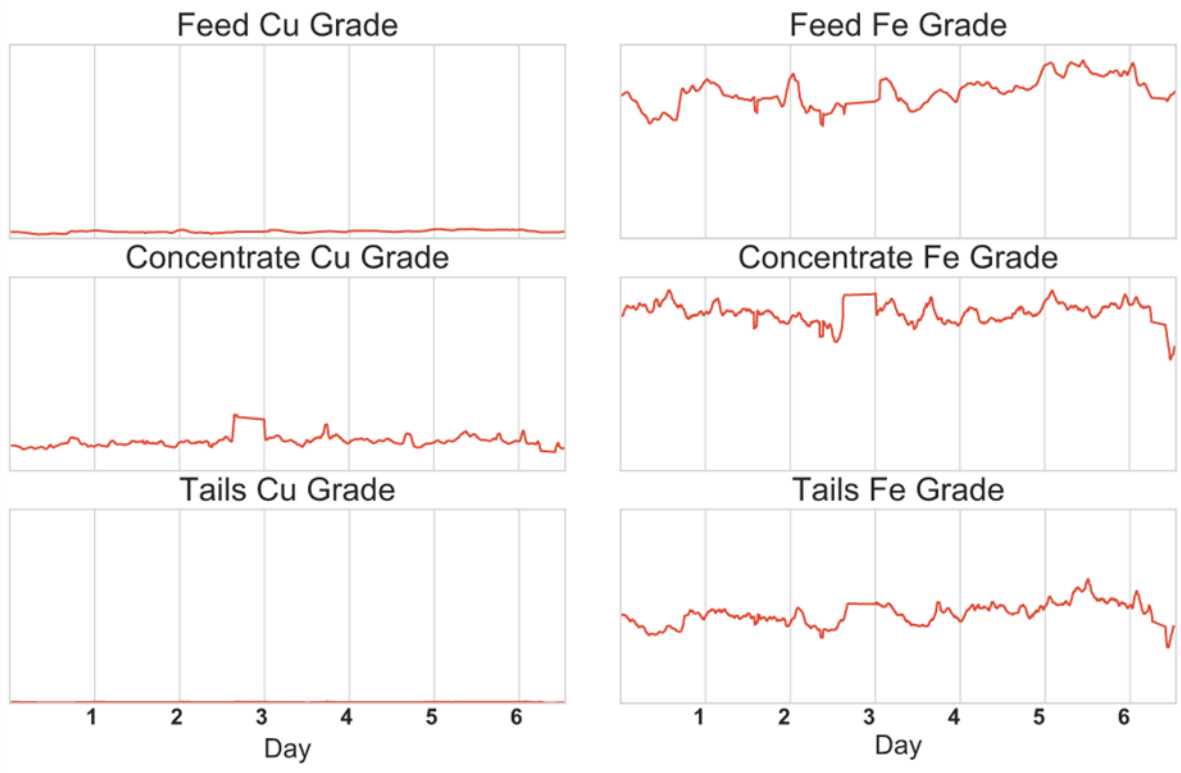

Figure 44. Copper and iron grades during seven-day period. Their averages were calculated for parameterization of the model. The same y-scale is used in all figures.

The averages from the plant data and the periodic laboratory tests showed that the plant performed better than during the preliminary laboratory testing as both show that the copper grade quadruples from feed to concentrate. Iron grade has large differences in concentrate between the two and the one used in the fitting is selected to be from the plant data as it has more measurements.

The pH level of the circuit is controlled by adding lime to the first conditioner and the fifth flotation cell. Fig. 45 shows that the pH level remains between 8.5 and 9.5 during normal operation of the plant, meaning that PAX operates optimally. The average pH level is 8.76 with the spikes removed.

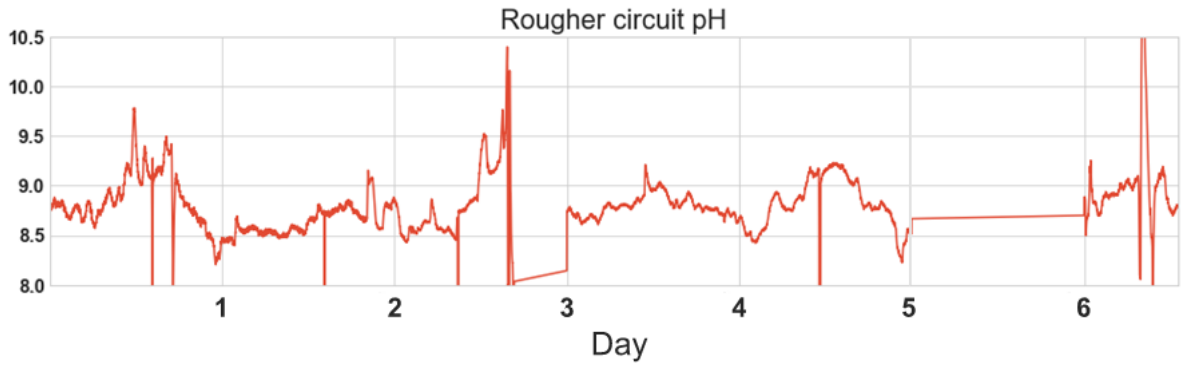

Figure 45. pH data is available only for a three-day period during which the average value is around 8.76. The pH level is controlled by adding lime to the first conditioner and the fifth flotation cell.

The feed solids flowrate and solids content are determined by taking an average over a 22-day period and by removing the downtime values. The average flowrate is 0.86 % of the nominal flowrate and the solids content is 44.24 %.

Figure 46. Feed's solids flowrate and solids content. The average for flowrate was 0.86 % of the nominal solids flowrate and 44.24 % for the solids content.

Average solids content for the concentrate was also calculated but it was missing for tailings. For concentrate, the average is 31.07 % and the measurements are depicted in Fig. 47.

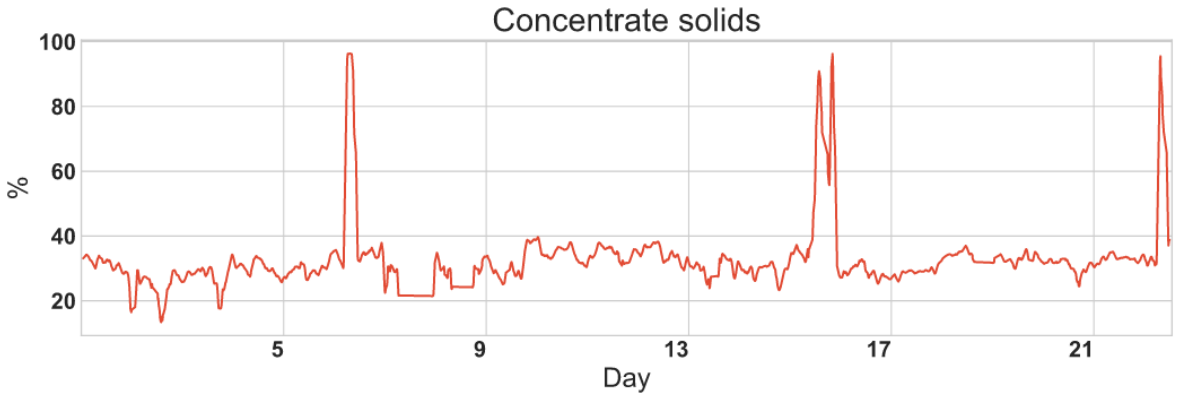

Figure 47. Concentrate solids content. The average value was 31.07 % when the values above 50 were removed.

Volumetric flowrate was not available for the feed and it was estimated using the flowrates for concentrate and tailings. The feed flowrate was then calculated as a total flowrate of the two. Fig. 48 shows both the concentrate and tailings flowrates, scaled by the total flowrate. The average volumetric flowrate for the feed is necessary for getting the residence times correct.

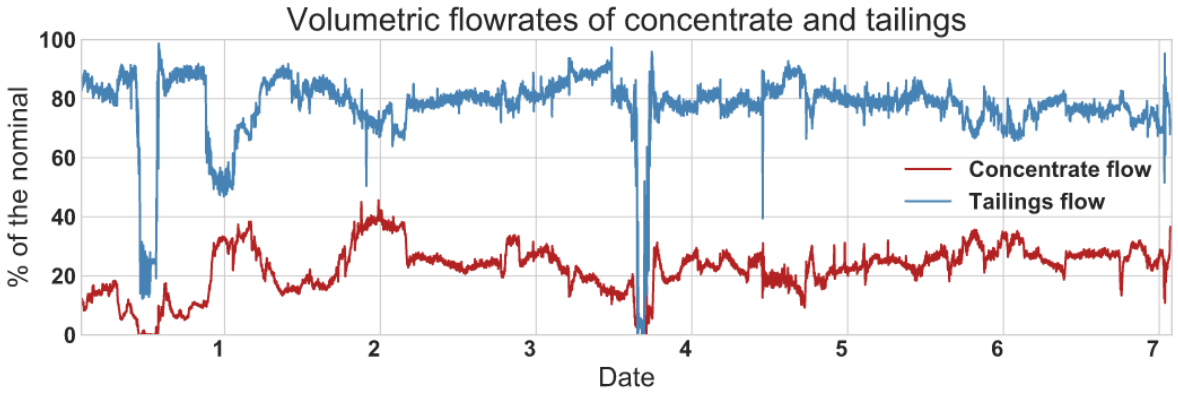

Figure 48. Flowrates of concentrate and tailings streams. About fourth of the total volume flows into concentrate while the rest are processed into tailings.

The copper recovery of the circuit is also monitored during the tests and it has an average value of 91.31 %. The six-day period can be seen from Fig. 49. The recovery stays between 85 and 95 % during the normal operation, and the only observable changes are caused by interrupts in the feed.

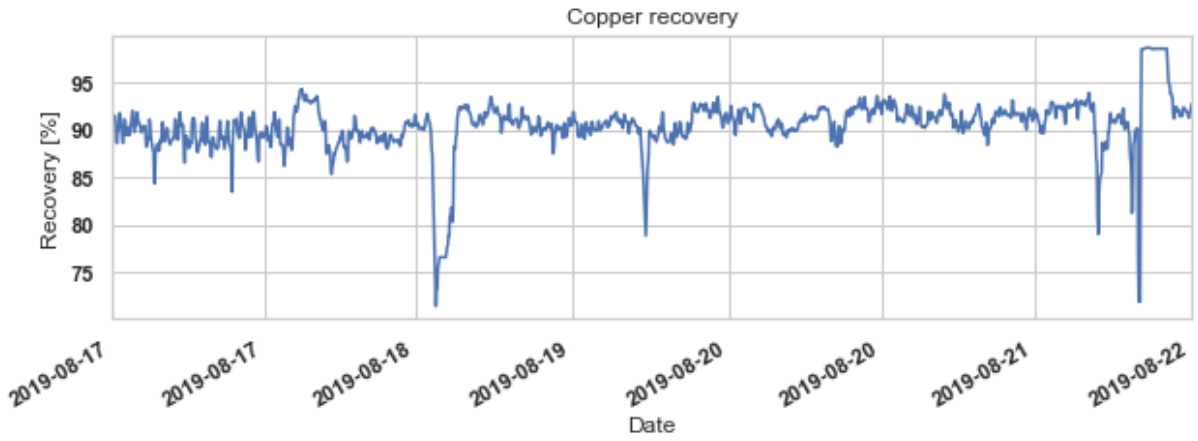

Figure 49. The copper recovery of the circuit. The recovery stays mostly between 85 and 95 %, and an average value of 91.31 % is obtained between that range.

5.3. Modeling froth speed

As HSC lacks integrated froth speed model, one had to be developed for the simulated step tests. Here a simple approach of calculating the forth speed is described after which a model is made with a neural network, based on the plant data. The main idea behind creating a NN-model is to find a relation between air flowrate and froth speed and thus being able to produce similar air flowrates during the froth speed steps made to the cells.

5.3.1. Constant hf model

The simplest froth speed model was made by assuming that the gas hold-up was 85 % and the forth height over the overflow lip was selected so that the nominal froth speed of a cell as reached with nominal air flowrate and level. The speed was then calculated from the overflow area $A_{Overflow}$ and the froth flowrate Q_{Froth}

$$v_{Froth} = \frac{Q_{Froth}}{A_{Overflow}}. \tag{35}$$

The overflow area can be calculated with the constant height over the lip h_f and the lip length l_{lip} as:

$$A_{Overflow} = h_f l_{lip}, \tag{36}$$

and the froth flowrate can be calculated from the flowrate of the air escaping from the top of the cell, along with the froth Q_{Air}, and the concentrate flowrate $Q_{Concentrate}$

$$Q_{Froth} = Q_{Air} + Q_{Concentrate} = \frac{Q_{Concentrate}}{1 - \epsilon_g} + Q_{Concentrate}. \tag{37}$$

When compared to the plant data, the model produced smaller air flowrate changes than in the real life, as the froth speed was changed. The model is also not valid as it uses constant froth height over the lip although it has been proven to change during plant operation.

As the froth height over the lip is not known, the froth speed must be estimated using a different method. Thus, a neural network is used to find a relationship between air flowrate and froth speed at different operating conditions. The modeling is done using HSC's data processing unit which can model feed forward neural networks. The contributing attributes in froth speed estimation are considered to be: air flowrate, level, reagent dosing, grades for input feed, tailings and concentrate, feed's solids flowrate and pH level. The variables are collected from the actual plant data and their ability to predict the froth speed is investigated.

5.3.2. Neural network structures

Grade for concentrate is neglected because it is impossible to argue which tank made the change in the stream since all of the tanks are under constant change. The flowrate is not selected for modeling because the models made with it turned out very sensitive to it and the correlation was changing cell to cell. The uncertain correlation is produced by tight flowrate control which allowed it to move within a really small range. The pH level has the same issue as it moves between 8.4 and 9.4, which does not have a considerable impact on PAX and thus it is discarded from the models.

Three differently structured models are made for the eight flotation cells. The basic structure consists of level, air flowrate, grade, previous froth speed and reagent dosing. The different input combinations summarized in Table 5 and Fig. 50 shows the basic structure.

Table 5. Summarization of model inputs.

Cell	Level	Air	Feed grade	Tailings grade	Previous froth speed	Reagent dosing
1	x	x	x			x
2	x	x	x		x	
3	x	x	x		x	x
4	x	x	x		x	x
5	x	x		x	x	
6	x	x		x	x	x
7	x	x		x	x	x
8	x	x		x	x	x

All the models have one hidden layer with neuron count matching the input count. Activation functions used in the model ‘s hidden layer is leaky rectifier linear unit (Leaky ReLu):

$$y = \max(0.1x, x) \tag{38}$$

and linear function for the output layer:

$$y = x. \tag{39}$$

Use of the linear activation functions makes it impossible for saturation to happen and it also makes the computation much faster. Using a leaky ReLu instead of regular ReLu means that the neuron cannot deactivate during the training since the derivative is non zero at $x \leq 0$.

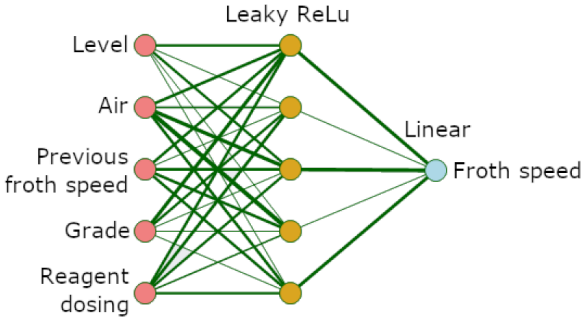

Figure 50. Basic structure of the neural network. Input layer is shown in red, hidden in yellow and output in blue.

5.3.3. Training the neural network model

The data is filtered by removing outliers, mainly zeros at levels, air flowrates and froth speeds. Additionally, many cells did not have much measurements for low and high froth speeds which are removed, as the models cannot predict those while simultaneously estimating the normal operating range.

After the basic filtering is done, initial model is trained with HSC's neural network tool. The training and validation are done with the same dataset where 70 % of the data is picked randomly for the training and the remaining 30 % is used in model validation. After the training, the errors between the predicted and the measured values are calculated and data points with an error above 15 % are removed. The filtered attributes are depicted in Fig. 51.

The scatter plot shows that the level has no correlation to froth speed as it moves between 200 and 250 mm and covers the whole froth speed range in that area. The air flowrate shows a clear curve, which rises linearly from 7 to 11 m3/min but after that point, the measurements become scarce and the behavior is hard to discern. The copper grade shows some positive correlation as froth speeds over 70 mm/s are achieved only with the highest third while values below 50 mm/s are not seen. The medium and low grades can still reach 70 mm/s. Correlation with reagent dosing cannot be seen.

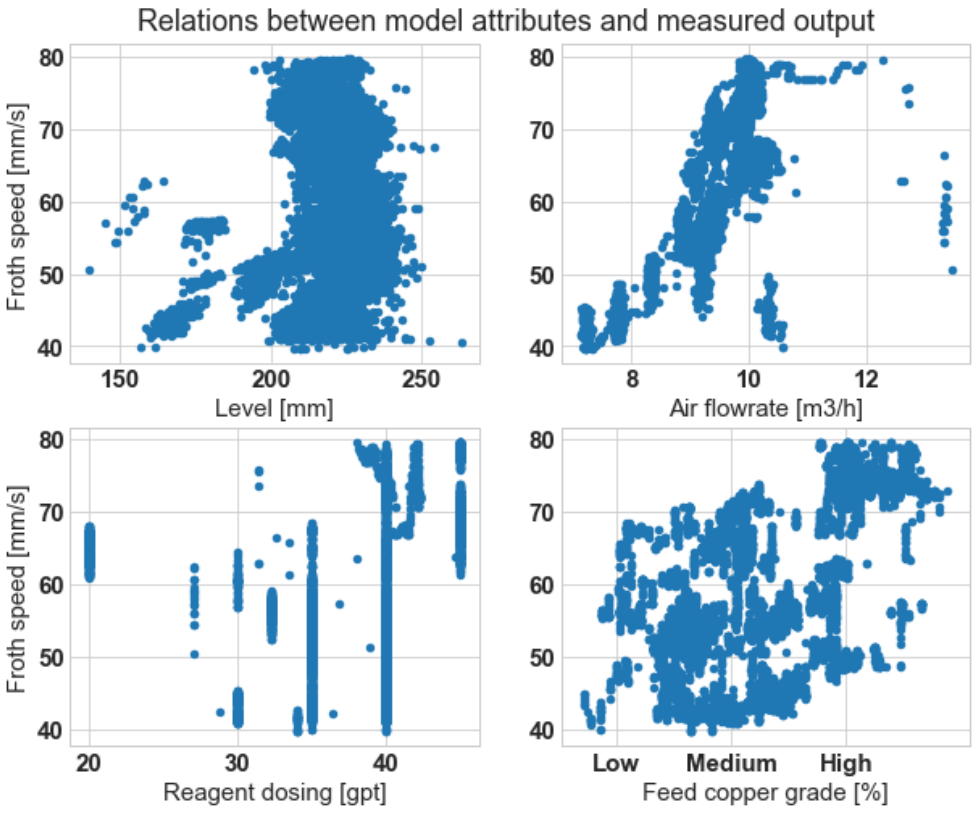

Figure 51. Froth speed as a function of filtered model attributes.

The reagent dosing's correlation to the froth speed cannot be seen from the figure as the frequent setpoints cover most of the froth speed range. The cell 6 has regent dosing for PAX and the dosing shows correlation to froth speed, as depicted in Fig. 52. From the figure it can be seen that when higher reagent dosing is used, less air has to be used to get higher froth speeds.

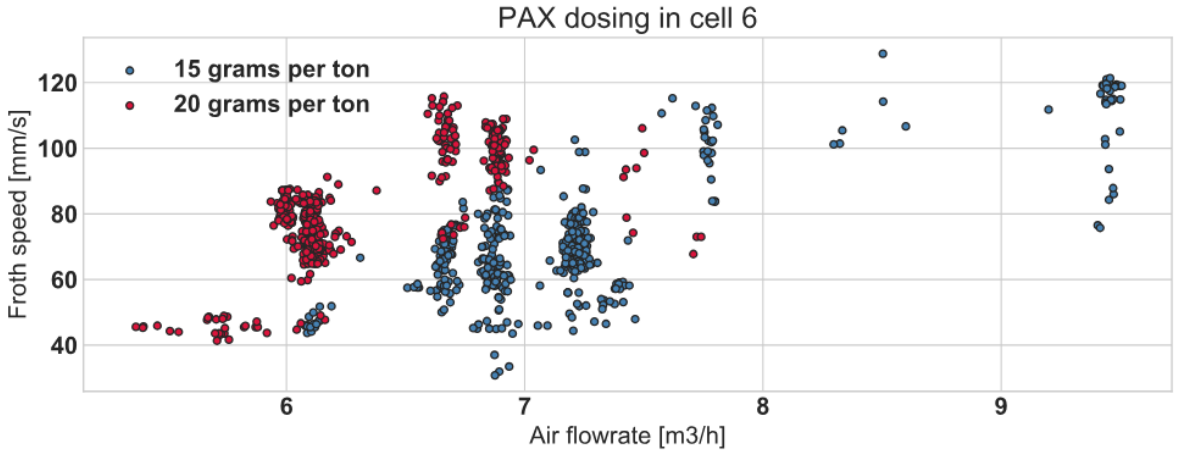

Figure 52. Comparison of two reagent doses in cell6. Lower air flowrates are needed to produce higher froth speeds when the reagent dosing is larger.

After the training has been done, the resulting predictions from the model are compared agains the actual values. Fig. 53 shows that there is still a lot of error but the estimates follows the measured values with a mean squared error of 7.86.

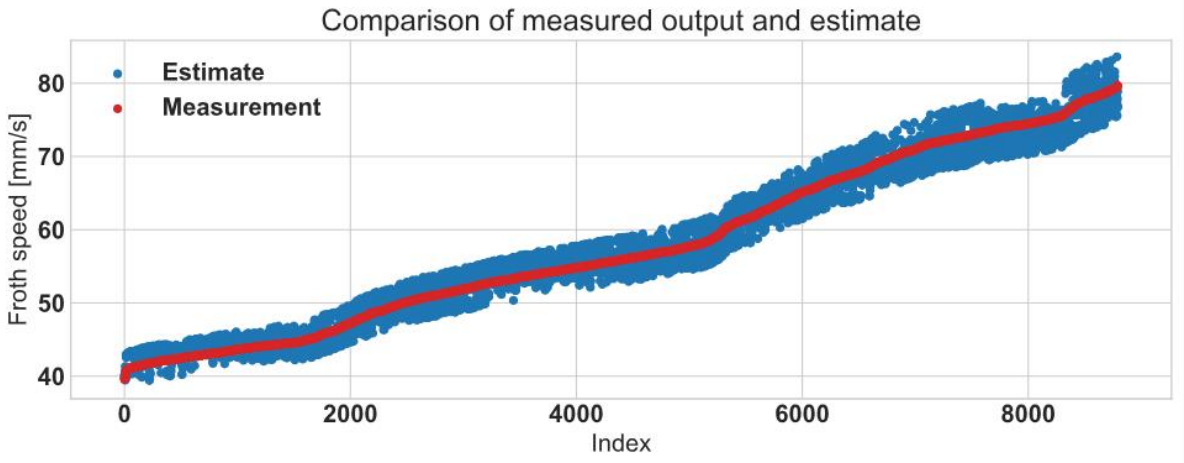

Figure 53. Predictions from the model versus the actual values. There's still a lot of error and the mean squared error was 7.86.

When all the other model attributes are kept constant, the froth speed as a function of air flowrate can be calculated. The resulting air flowrate curves with different feed copper grades is depicted in Fig. 54. The figure shows three different grades, low, middle and high, which produce different froth speeds at the same air flowrate. Low and middle curves follow each other until 9.2 m3/min after which the low grade curve deviates downwards. The high curve is 5 mm/s higher than the middle grade on all the air flowrates.

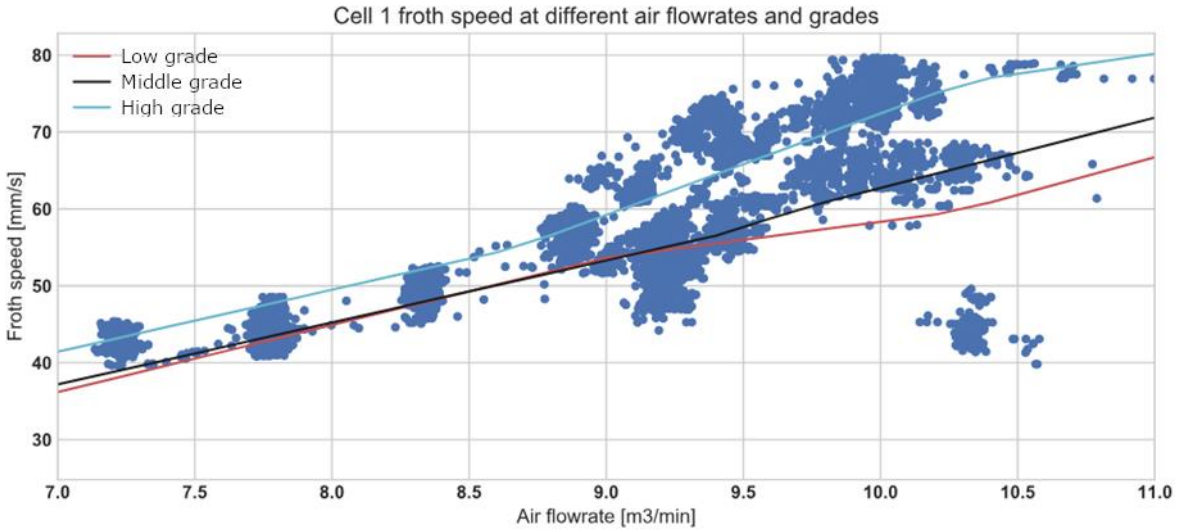

Figure 54. Air flowrate and the corresponding froth speed with nominal level and reagent dosage in cell 1 when three different feed copper grades are used.

The models use data from the same timespan for training and validation and they can predict the values within this timespan at a reasonable accuracy. The predictions do not work when other data sets are used however. Additionally, only air flowrate and reagent dosing showed correlation with froth speed whereas the correlation with grade is loose and level did not have any.

The air flowrate changes to produce a step of 5 mm/s in each of the cells are shown in Table 6 for both the neural network and the constant h_f model. The changes are considerably smaller in all cells when the constant h_f model is used. From the plant data, it was estimated that the change in air flowrate should be between 0.5 and 1.5 m3/min, meaning that the neural network makes more realistic changes to the air flowrate.

Table 6. Required air flowrate change [m3/min] to produce a 5 mm/s step to froth speed. The basic model with a constant froth height over the lip produced lower changes in all cells.

Cell	1	2	3	4	5	6	7	8
Neural network	0.62	1.12	1.52	1.36	0.86	0.99	0.34	1.78
Constant h_f	0.29	0.35	0.40	0.76	0.64	0.21	0.29	0.5

5.4. Model parameterization with HSC

After the required data has been gathered from the plant data, the model can be parameterized to produce the same copper grades and recovery as the real plant. This is done using methods approved by Outotec's specialists in process modeling, simulation and metallurgy. First, a meeting was held where a static model was set to its nominal operating point and made to produce the correct grades and recovery. This section shows the dynamic model is fitted afterwards. (Remes, A. and Klemetti, M., personal communication, 11 September)

5.4.1. Nominal operating point

Before the model is fitted, the cells are set to their nominal levels, air flowrates and bubble surface fluxes which are calculated by taking averages of every cell during the plant test period. The nominal levels and air flowrates are depicted in Fig. 55 and they show a decreasing profile downstream. This is because the first four cells are roughers, recovering most of the product, whereas the last four are scavengers, recovering the valuable material from the rougher tailings while sending gangue to the final tailings. The nominal bubble surface fluxes are calculated from the nominal air flowrates and they are depicted in g. 56.

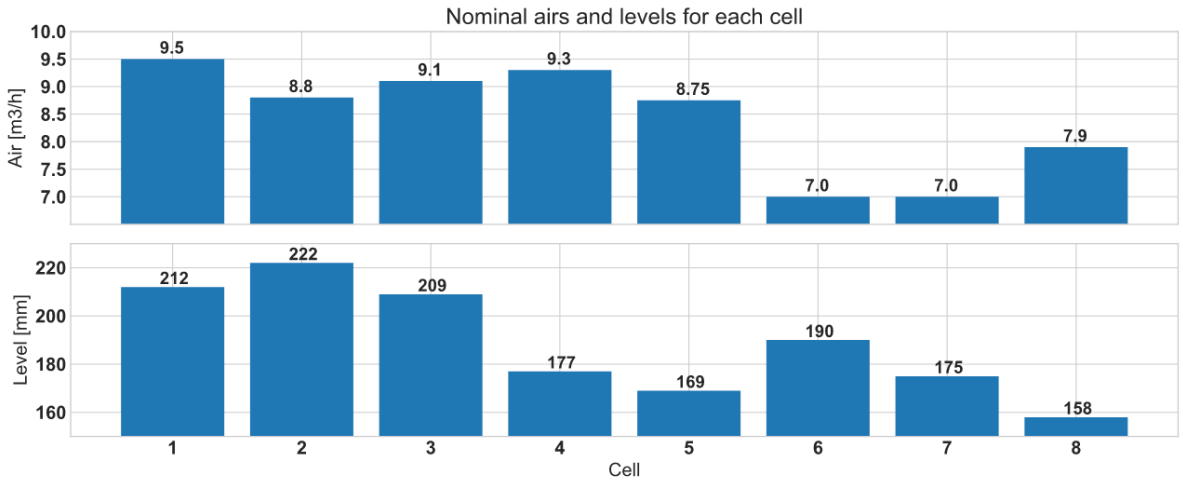

Figure 55. The nominal air flowrates and level for each cell. The values are calculated by taking a mean value over the eight last days of running the plant.

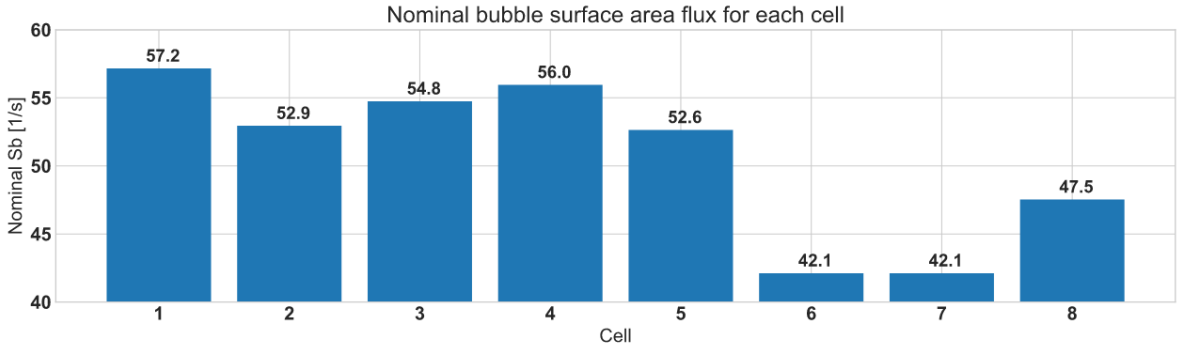

Figure 56. The nominal Sb values for the eight cells. Values are calculated from the nominal air flowrates.

As the levels and air flowrates are set, the froth speed models are connected to the cells. The grades and the reagent doses are given as constant values and levels and air flowrates are linked to the neural network models' inputs. The comparison of the nominal froth speeds and estimates given by the neural network models are depicted in Fig. 57. It can be observed that the neural network's estimates are close to the average froth speeds. The highest deviation is in the cell 7 where the average is 53.0 mm/s while the estimate is 56.4 mm/s.

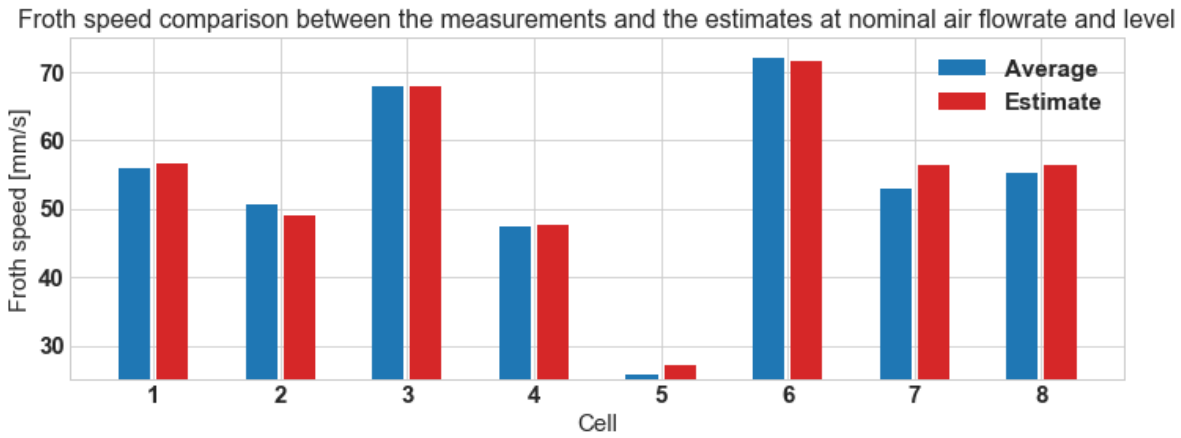

Figure 57. Comparison between the measured and estimated froth speeds at nominal levels and air flowrates. All the estimates are close to their targets.

5.4.2. Fitting of the grades and the recovery

Fitting of the grades and the recovery is done by using two parameters; the froth recovery exponent and the pyrite grade of the feed. Firstly, the feed of the model and the mineral specific kinetics are set according to the preliminary laboratory tests. After this, the copper recovery is corrected by increasing the froth recovery exponent and the grades by decreasing the pyrite grade of the feed.

The residence time of the process has a considerable effect on the recovery, and therefore it is fitted first. This is done by setting feed's volumetric flowrate to its nominal value by giving it the wanted solids flowrate, after which the solids contents percent is used to get the volume correct. Water recovery of the flotation cells are then used to get the volumes right in the concentrate and tailings.

After the residence time is set, the recovery on the concentrate stream is fitted increasing the froth recovery exponents of the cells. Every cell is set to have the same exponent value, and the correct copper recovery is reached with 0.16. The cumulative recoveries for the first four cells became 52.3 % and 39.4 % for the last four. The final copper recovery is therefore 91.7 %.

The correct copper grade is reached by changing the pyrite content, as it is the dominant mineral type in the concentrate and thus has a large effect on the iron grade. The correct copper grades for the concentrate and the tailings are reached when the iron grade of the feed is 5 % lower than that of the plant average. The iron grade became much higher and lower in concentrate and tailings respectively, compared to the plant and laboratory averages. Zinc grade is correct in all the streams and it was reached with the preliminary value for the feed's sphalerite grade.

The high froth recovery exponent leaves the first four cells' froth recovery under 4 % whereas cell's 5 and 8 have froth recovery values of 14 and 15 %, which means that particles are more easily recovered in the last half of the circuit. The increase is due to the internal launder which decreases the froth surface area and therefore the superficial gas velocity and froth residence time.

6. Responses from the Simulation

In this chapter the fitted model is compared against the measured grade responses from the plant tests. After the comparison against the base model, the model's parameters are varied to see how they affect the simulation. The experiments focus on three uncertainty factors that were found to affect the simulation model's response the most: recovery balance, change in the air flowrate and the flotation kinetics.

6.1. Measured responses from the plant test

The bank of eight cells is divided into two froth speed profiles, frothSpeed1 and frothSpeed2, where the first is the profile for the first four cells and the second is the profile for the last four. These profiles can be adjusted independently from each other, so that when a step is done to frothSpeed1, the set points change for cells 1 through 4 while the set points for the others remain constant. The two profiles are depicted in Fig. 58.

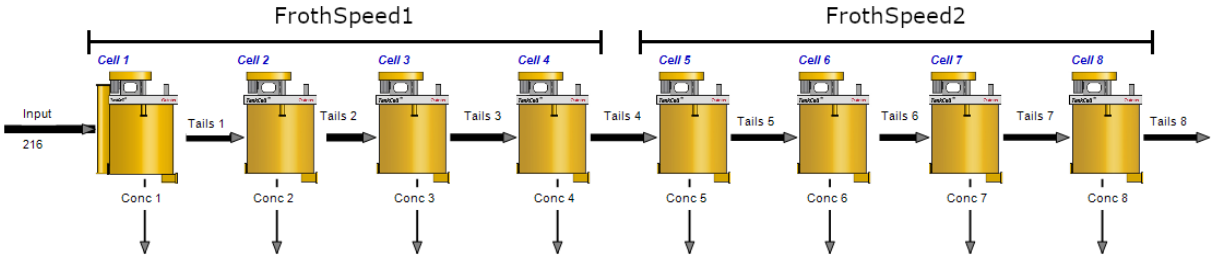

Figure 58. FrothSpeed1 is the profile for the first four cells and frothSpeed2 is the profile for the four last cells.

During the experimental testing at the real plant, five step response tests were made to the bank where the first four are made to frothSpeed1 and the last one to frothSpeed2. During 15 mm/s steps to profile, control limits for air flowrate are reached on all the steps except the third step, which was the only step where froth speed set points were fully reached. Step 5 reached the set points on all cells except one. The air flowrates, levels and the froth speeds during the five steps are shown in appendix 2. The measured grade responses at the plant are depicted in Fig. 59, where the y-axis shows the amplitude of:

$$G(s) = \frac{Y(s)}{U(s)} = \frac{\text{Copper grade [\%]}}{\text{Froth speed [mm/s]}}. \tag{40}$$

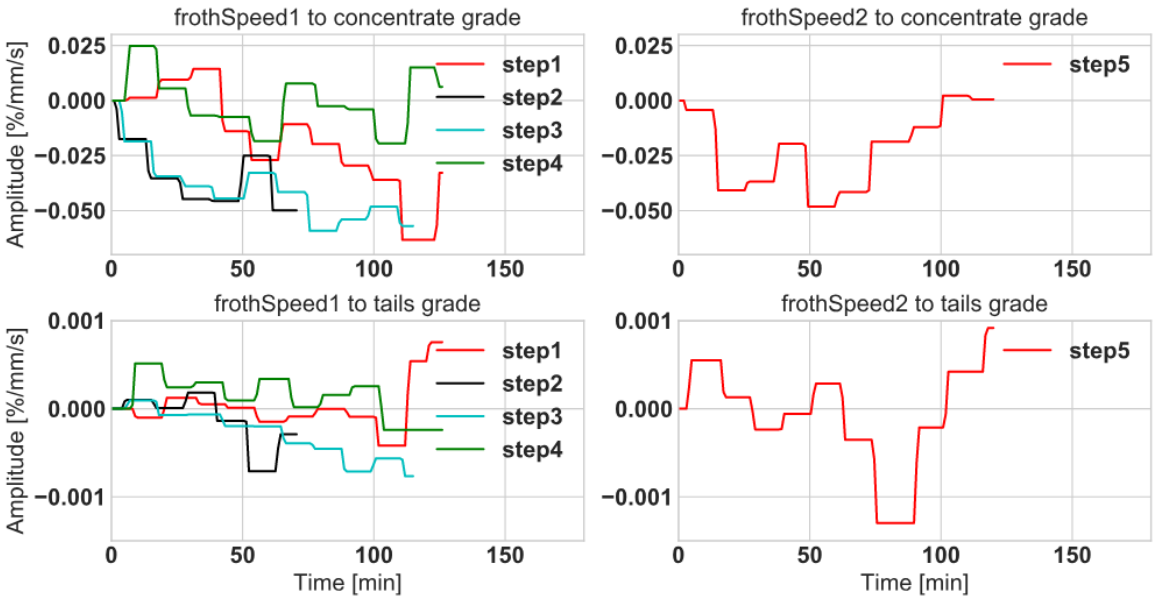

Figure 59. Deviation in copper grade after a step has been made. Four steps were made to frothSpeed1 and only one to frothSpeed2.

6.2. Comparison of measured and simulated responses

Simulated step responses are produced by increasing and decreasing the froth speed profiles by 5 mm/s. The target froth speed is reached by changing the air flowrate while cell levels are kept constant. The resulting grade responses in concentrate and tailings are then scaled to unit step responses and compared against the measured responses from the plant step tests.

Fig. 60 shows the comparison between the simulated responses and the steps 3 and 5 which are the most representative measured responses. The overall dynamics of the simulated responses fit the measured process responses. Especially the response from frothSpeed2 to concentrate grade fits very well. The simulated response follows the measurement for 60 minutes, achieving a gain close to that of the measured, after which the measurement starts to rise towards zero which is not produced by the step. The other responses have a considerable error in gain as frothSpeed1 to concentrate is half way to the measured response and tailings responses are both much higher than the measured. FrothSpeed1 to concentrate also has a non-minimum phase response which is not seen in the most representative measurement.

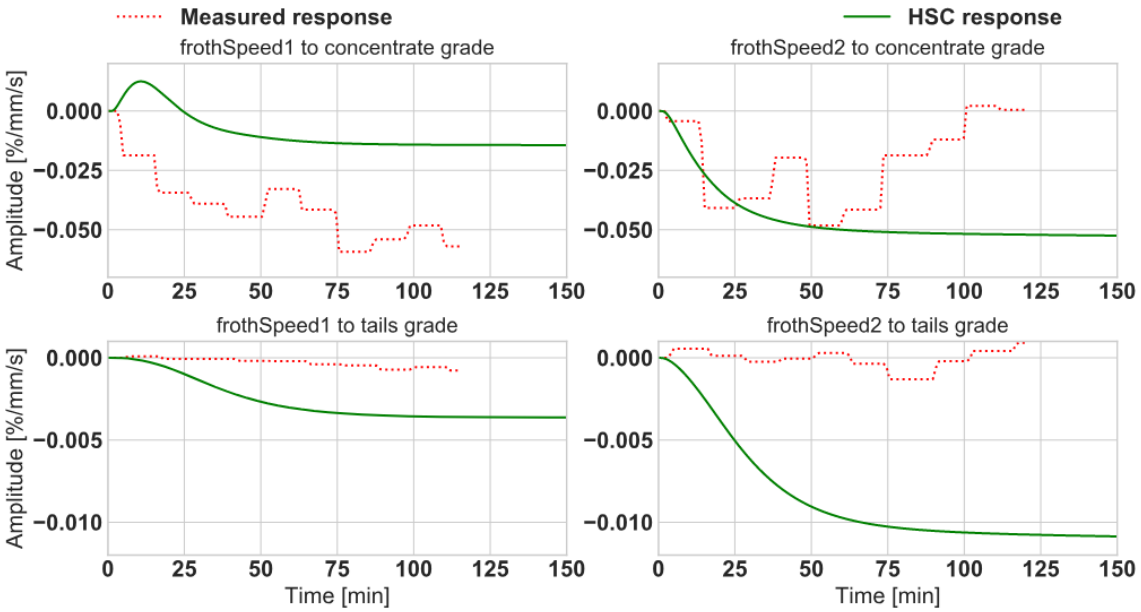

Figure 60. The response models from HSC compared to the plant measurements. Simulated gains on frothSpeed1 and 2 are 6 and 20 times higher on the tailing. FrothSpeed2 to concentrate fits the measurements and frothSpeed1 to concentrate has a non-minimum response and too low gain.

The measured steps 1 and 4 in Fig. 59 also show a non-minimum phase response and step 4 has a gain close to that of the simulated frothSpeed1 to concentrate response. These steps were however excluded from the comparison because two cells' froth speeds were not changed during the step. In overall the simulated gains on the tailings responses are far from every measured tailing response. Thus, HSC requires more comprehensive plant operation or on-site laboratory testing for adequate model calibration as producing representative response models for neither of the tailings or from frothSpeed1 to concentrate grade succeeded. Especially the froth recovery should be examined at the plant as the froth recovery in the model is much higher in the frothSpeed2's cells than on the frothSpeed1's cells, which makes the last cells too effective.

6.3. Effect of the recovery in the simulation

The non-minimum phase response is due to the balance of recoveries between the frothSpeed 1 and 2. The recoveries of the two units are close to each other but the grade of frothSpeed1 is considerably higher. As frothSpeed1's profile is lowered, its recovery decreases which leads to more copper making it to the frothSpeed2, increasing its recovery. The non-minimum phase response is then formed due to the response time of the copper recovery being lower than that of the grade. As less high-grade concentrate from frothSpeed1 and more low-grade concentrate from frothSpeed2 are added to the final concentrate, the grade starts to move to the wrong direction. The gain then switches direction as frothSpeed1's grade begins to increase.

The non-minimum phase response and the gain error in frothSpeed1 to concentrate can be removed by setting frothSpeed1's recovery higher than that of the frothSpeed2. The resulting response is depicted in Fig. 61 along with the original simulation. The recoveries were set so that the recovery of frothSpeed1 was five times higher than that of the frothSpeed2 by lowering and increasing the froth recovery exponents of the two cell groups.

Moving the recovery balance towards the front of the bank removes the non-minimum phase response and gives an appropriate gain in frothSpeed1 to concentrate. However, this also gives worse fits for frothSpeed1 to tailings and frothSpeed2 to concentrate. FrothSpeed2 to tailings however, is closer to the measured response. It can be observed that having lower gains in the concentrate, also produces lower gains in the tailings and vice versa.

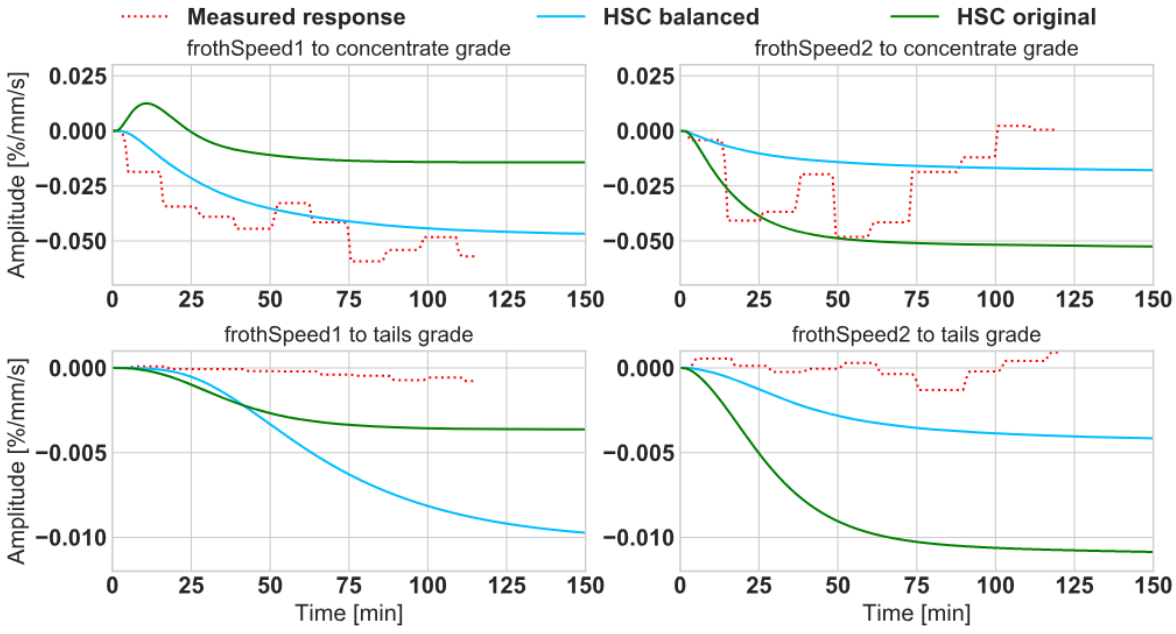

Figure 61. Attempt to produce similar response in frothSpeed1 to concentrate grade. Error on frothSpeed1 to concentrate was reduced but it grew on frothSpeed2 to concentrate.

6.4. Effect of the air flowrate in the simulation

It was also thought whether the error could be due to too small air flowrate changes in frothSpeed1, resulting to lower grade increase and thus lower gain. As shown in Table 6, the constant h_f model produces considerably lower changes in the air flowrate than the neural network does. Hence, simulations were run with the two forth speed models, the constant h_f and the neural network, using the original model. The comparison proved that making a larger change to the air flowrates does not necessarily mean that the gain becomes higher.

Fig. 62 shows the results from the two models and the gain for frothSpeed1 to concentrate is slightly higher with the constant h_f model. The frothSpeed2 responses show the expected outcome where the gains are lower with the constant h_f model. The similar gains in frothsSpeed1's responses are due to frothSpeed2's ideal performance which causes it to recover the minerals which were not recovered in frothSpeed1.

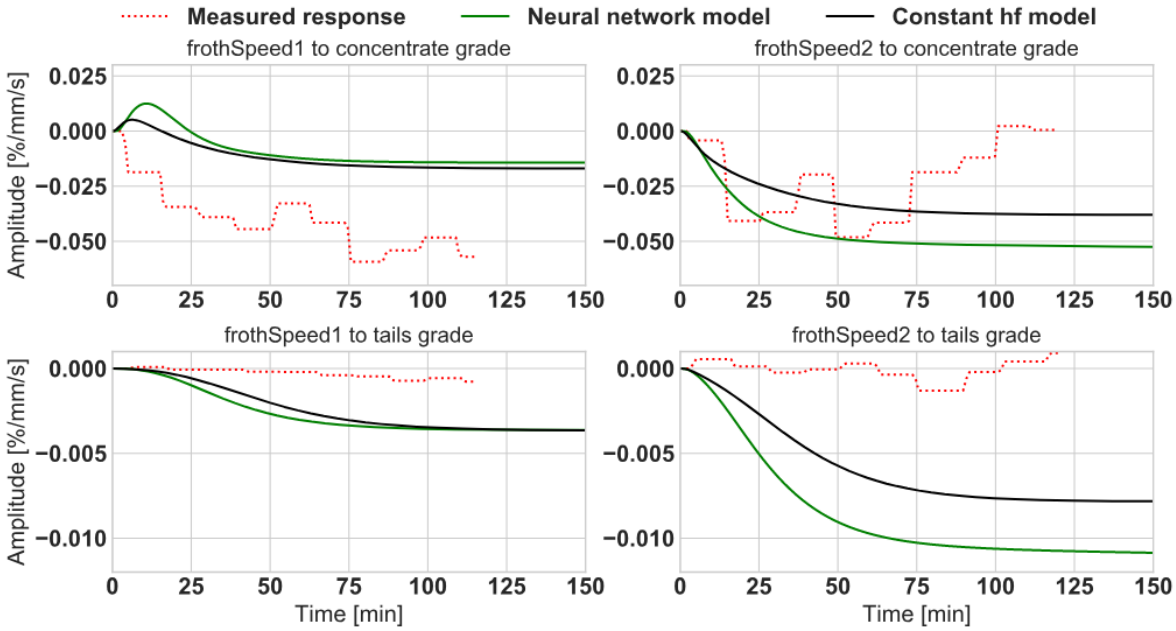

Figure 62. Comparison of responses with the neural network and the constant h_f models using the original simulation model.

When the emphasis is set on the front of the bank, the situation turns on itself and the gain differences can only be seen in frothSpeed1. Thus, it is essential to have correct balance of recovery, as having the balance wrong means that the air flowrate's effect is dampened, and the gains remain low. It should also be noted that the lower gain in concentrate lead to lower gain in tailings.

6.5. Effect of the flotation kinetics in the simulation

Flotation kinetics is the most important factor in fitting the model and getting the correct results as they have an impact on both the recovery balance and the effectiveness of the air flowrate. When a mineral has high flotation rate, more of it is recovered at the front of the bank and vice versa. This change in recovery balance makes frothSpeed2 less ideal and allows frothSpeed1's gain to increase when larger changes to the air flowrate are made.

The kinetics also affect the pulp phase recovery through collection zone flotation rate k_c. As the air flowrate is changed, the changes in mineral specific flotation rates are proportional. This means that when the air flowrate is decreased, a flotation rate of 3 1/min has a larger absolute decrease than if it was 1 1/min.

Fig. 63 shows both the iron and copper grades during step 3 of the plant test and it can be observed that copper and iron have a 1 to -1 relationship in concentrate and a 1 to 50 in tailings. In the simulation model however, the relationships are 1 to -0.2 and 1 to 15 respectively. This means that when a step to frothSpeed1 is done in the simulation, less iron than expected is moved into the tailings. If the ratios are improved, the amount of iron would decrease faster in the concentrate, thus increasing the gain in the concentrate, and the amount of iron in the tailings would increase faster, thus decreasing the gain in the tailings.

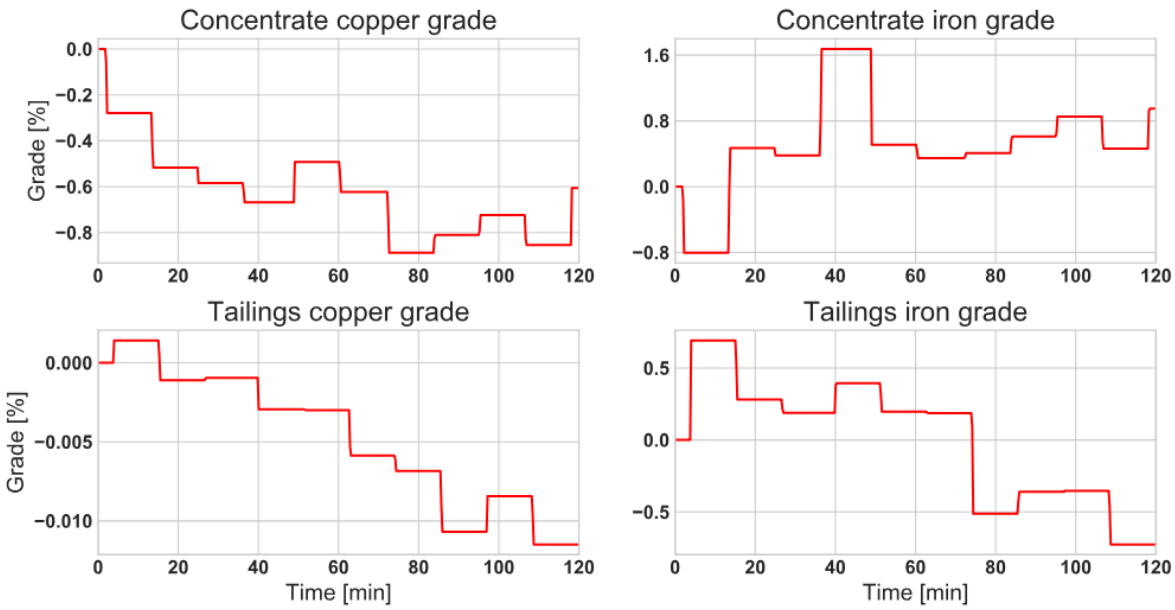

Figure 63. Iron and copper grade changes during the step 3 made to frothSpeed1 at the plant.

The ratio between copper and iron grade changes can be improved by decreasing pyrite's maximum flotation rate $kmax$ to move its recovery balance towards the end of the bank. Fig. 64 shows that when the ratio was improved to 1 to -0.3 and 1 to 20 in concentrate and tailings respectively, the concentrate gains follow the measured responses.

The tailings gains are still high, but they decreased whilst the concentrate gains increased, which could not be achieved with other methods. During the experimentation, the differences in the tailings could not be completely removed and the closest gain simulated was -0.0016 for frothSpeed1 while frothSpeed2 had -0.045. The large differences are likely caused by calibration errors and the difficulty of measuring very low grades at the plant.

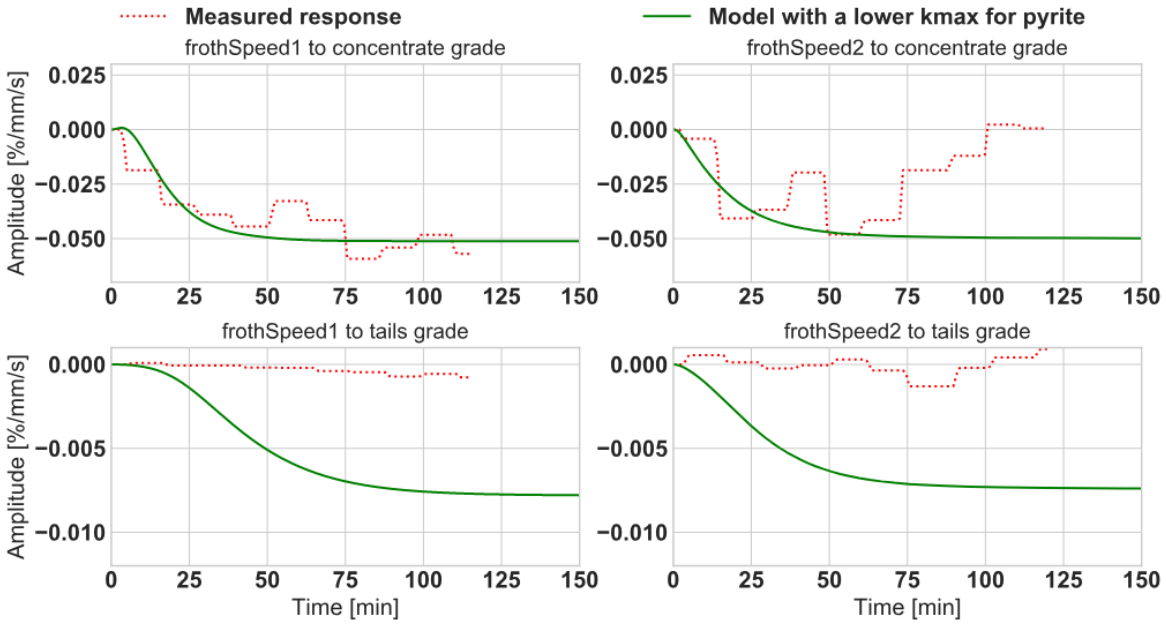

Figure 64. Reduced maximum flotation rate for pyrite allows copper grade to change more, thus making it possible to get correct gains. Gain for frothSpeed2 now fits the measured response.

6.6. Summary of the results

Correct flotation kinetics are the basis for a good flotation model as having the wrong kinetics makes fitting of the other parameters impossible. The model also applies the kinetics at the beginning of the circuit and they stay the same trough out the model whereas in the actual plant they can be affected by reagents in the middle of the circuit. Having too high flotation rates can make the last cells obsolete as all the particles are recovered in front but on the other hand too low flotation rate leaves the recovery too low. This also affects the importance of air flowrate as a change made to an obsolete cell does not affect the final concentrate or tailings. Getting good enough flotation kinetics however, requires more data for analysis than was available.

The differences in the tailings gains remain high even after using exaggerated flotation kinetics. The lowest the gain got is -0.0015 which is still relatively high in comparison to the measured. This could however be achieved for only frothSpeed1, by making chalcopyrite's flotation rate multiple times higher, which ensured that when a step was done to frothSpeed1, frothSpeed2 would recover all the lost copper without sending any to tailings. Since even the unrealistic flotation rates could not fix the error, the tailings measurements may be poorly calibrated. Whatever is the issue, the simulated and the measured responses cannot line up with each other.

The original model has a good fit for frothSpeed2 to concentrate but frothSpeed1 to concentrate has a non-minimum phase response which can be seen in two of the failed plant step tests but not in the succeeded step and its gain is half of that of the measured. It also must be noted that the plant step test made to frothSpeed2 did not fully reach the set points and thus the measured gain is lower than it should be. The simulated gain is however in an appropriate range. The tailings responses have large differences in their gains, but as the measurements are considered to have calibration errors their actual fit is hard to estimate.

Thus, HSC could not produce three out of the four responses with the plant data in use. The dynamics are similar to those seen in the measurements, but the gains have large errors. The combination of correct bank volume, input flowrate, cells' mechanical parameters and correctly tuned froth speed control can produce dynamics which are close to correct but correct gain requires having correct flotation kinetics which are further impacted by the air flowrate. Having the correct kinetics can remove the error between the simulated frothSpeed1 to concentrate response and the measurement, and they can reduce the difference to some extent in tailings responses while the concentrate gains remain correct. Getting the correct kinetics however, requires more extensive analysis of the process as they cannot be interpreted from only the final concentrate, tailings and the input feed measurements. Therefore, a model fitted based on insufficient plant data cannot produce the correct gains.

7. Discussion About the Results

In this section, thought is given to possible missteps in making the model which could affect the results. The focus is on the froth speed model, operating point of the circuit and the kinetics.

The froth speed model greatly impacts the resulting gain as it dictates the change in air flowrate which produces the correct step in froth speed. The datasets the models were trained on was relatively small, consisting of 10 000 datapoints on average which was not rich as third of the data had control on. From the plant data it was estimated that an appropriate change in air flowrate to produce a ± 5 mm/s step to froth speed is between 0.5 and 1.5 m3/min. During the step tests which were used in the comparison, the range was from 0.5 to 3.0 m3/min and especially cells 3 and 4 had large differences. This results in lower gains and means that the network's predictions are off at certain operating points.

The relationship between the air flowrate and the froth speed is non-linear in the neural network and therefore the size and the starting point of the froth speed step matters. This can be seen from Fig. 54, where flowrate curves have few different slopes throughout the air flowrate range. Thus, making a larger change in froth speed may result in the air flowrate curve switching from one slope to another, where the required air flowrate change is different.

The same step to air made at different level also produces different results as does a step made with different starting air flowrates. The cell levels during the simulation were the nominal operating levels and they were all within ± 10 mm of those during the plant tests except on cell 6 where it was off by 30 mm. The starting air flowrates however, had larger differences in them. The flowrates in the first four cells were all 1 m3/min lower during the plant test and for the last four cells they were 1 m3/min higher, which may explain the different air flowrate change ranges, discussed earlier.

Figs. 65 and 66 shows how steps made at different operating points change the responses to the concentrate and tailings grades. The steps were made to only to the first cell of the series. Response with higher starting air flowrate has lower overshoot at the start and stabilize to lower gain in concentrate. In the tailings, the responses stabilized to -0.0075 when the bubble surface area flux corresponding to the air flowrate was close to nominal bubble surface area flux and to -0.006 when the air flowrates were higher. When the level was varied, the responses in both the concentrate and tailings stabilized to higher negative gains the lower the level was.

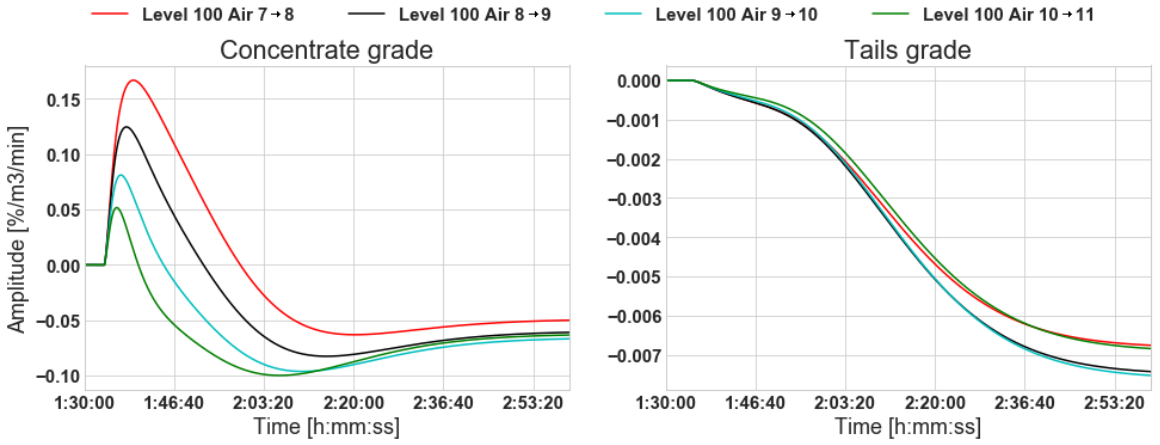

Figure 65. Steps to air with the same level. The overshoot at the start of concentrate increases considerably the smaller the air flowrate is, all the responses stabilize between -0.05 and -0.07. For the tailings the responses stabilize to −0.006 and -0.0075. The steps made at 8 and 9 m3/min were closer to the nominal Sb and stabilize lower than the steps made at 7 and 10 m3/min.

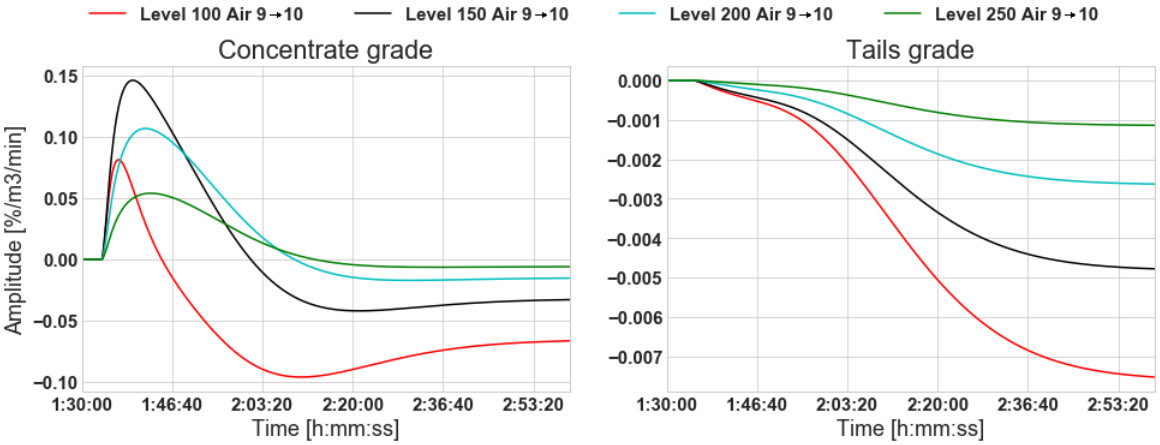

Figure 66. The same step to air made at different levels. The lower the level the higher gain in both the concentrate and tailings.

From the figures it can be seen that the level could have a large impact on the tailings grade. The levels in the simulation however, were close to those during the plant testing and the small differences in all cells except one are not enough to produce the difference in tailings gains. Starting air flowrate differences on the other hand cannot explain the differences in tailings gains as the responses stabilized close to each other regardless of the starting point.

The biggest problem affecting the results are the kinetics. They are typically tested in mineral processing laboratories by mainly using two kinds of tests: locked and open cycle. The locked cycle tests can provide the kinetics for a full-scale industrial plant and it is the preferred method for kinetic testing (Isaksson, A., 2018), but the open circuit testing can be used in open circuit roughing where no feedbacks from regrinding are added to the feed, as was the case in the plant under experimentation (Fragomeni, D., 2006).

The kinetics from both the open and locked cycle tests are depicted in Table 7 and the locked cycle results are the ones used in the model. Experimentation to remove the error in concentrate gains showed that the open cycle kinetics have more fitting results, as the $kmax$ for chalcopyrite is higher than in the locked test and lower for pyrite. These two changes would lead to results which are closer to Fig. 64, as an increase in chalcopyrite's $kmax$ slightly increases recovery of the frothSpeed1 whilst a decrease in pyrite's $kmax$ would further improve the ratio between iron and copper grade changes. NSG has also large differences in its constants, but they produce similar results. This is because the NSG ends up in tailings with both kinetics as the locked cycle limits the recovery by low infinite recovery while the open cycle limits it with the low flotation rate. Choosing the more fitting kinetics without knowing the measured response however, is not simple.

Table 7. Infinite recoveries and maximum flotation rate constant from both the open and the locked cycle tests.

	Infinite recovery [%]				Maximum flotation rate [1/min]			
	Ccp	Sp	Py	NSG	Ccp	Sp	Py	NSG
Open cycle	98.992	92.24	100	74.84	3.756	1.936	1.068	0.003
Locked cycle	99.9	97.2	100	2.4	3.39	1.845	1.467	0.897

Another uncertainty in the kinetics fitting is the reagent addition. Lime is added to the slurry in the first conditioner and cell 5 and it could affect pyrite's kinetics negatively. PAX is added to the circuit from conditioner 1 and cells 3 and 6, which is likely to affect chalcopyrite's kinetics positively. This however, is not accounted for in the model and as the kinetics are applied in the conditioners and they are not changed in the middle of the circuit.

PAX has been found to increase the infinite recovery while the flotation rate constant stays constant (Maree, W., et al., 2017). As the infinite recovery of chalcopyrite is already 99.9 %, the simulation with 100 % would not cause much of a change, meaning that changing the chalcopyrite kinetics in the middle of the circuit in order to simulate PAX addition, would not impact the results much.

Lime is mainly used to control the pH level of the slurry, but it is also known to depress pyrite at high pH levels (Zanin, M., et al. 2019). The pH level during the testing was kept low at 8.75 which is too low for pyrite rejection to occur which would lead to larger errors in its infinite recovery. Therefore, the infinite recovery for pyrite can be assumed to be high as is the case in both the locked and open cycle kinetics.

8. Conclusion

This thesis was conducted in order to find out whether HSC could be used to produce response models for the GRO when a model parameterization is based on real plant data when no additional laboratory campaigns are done. The dynamics of the flotation process were also studied in order to understand the response models for the GRO.

The study concludes that the HSC Sim is not capable of producing the response models from the plant data and better results require that the additional laboratory campaigns are conducted. The fit estimation is however limited by calibration errors and difficulty of measuring very low grades in the tailings.

The HSC Sim can produce dynamics which are like those seen in the measurements but achieving the correct gain is difficult. The gain is mostly affected by the kinetics and the froth speed model as it dictates the changes in air flowrate. As the dynamics are sufficient, HSC could be used as a tool for creating a priori models, but the gain would have to be fitted with plant step tests as the kinetics cannot be fitted from only the input, tailings and final concentrate measurements.

Making the model more accurate requires more comprehensive measurements and on-site analysis. Fitting of the kinetics requires more analyzed elements and assays from all the concentrate streams and fitting of the froth recovery exponent requires laboratory analysis of each cell's froth recovery.

The study of the flotation dynamics concludes that cell level's and air flowrates effects are well understood but froth's behavior makes the flotation process uncertain as a whole. The fact that the froth's behavior is unpredictable, makes modeling of froth speed difficult.
The neural network models for froth speed models are cell specific and they do not work as general froth speed models. Some of the models require richer data as some of the cells' air flowrate measurements moved within a very small range, making it difficult to get an understanding how the air flowrate affected the froth speed in those cells. In comparison to the averages from all the plant data, the neural network models produced sufficient air flowrate changes but in comparison to the succeeded plant step, the changes were low for the first four cells.

Thus, accurate fitting of the flotation and froth speed models would require a lot more work and analysis. Based on these results, making an HSC model for purely response test purposes is not worth the effort as the gain fitting and froth speed modeling both require the plant testing.

Even though the response gains have large errors, the dynamics are promising. Further research should be done with other plants to see whether different results are obtained. The froth speed models should also be studied more as the current model can only predict values within the training set, and more general model would be required if simulations were to be used in future to obtain the response models. As the kinetics were the biggest issue in the model, it should be studied how much work it requires to get more accurate kinetic constants from the plant. The copper recovery responses during the plant steps should also be studied as they may be used to acquire estimates for the froth recovery exponents.

References

AMETEK, XR-100CR Si-PIN X-Ray Detector – documentation, application manual. Available at: https://www.amptek.com/products/si-pin-x-ray-detectors-for-xrf/xr-100cr-si-pin-x-ray-detector#Documentation [Accessed: 5 September 2019].

Ata, S. (2012). Phenomena in the froth phase of flotation – A review, *International Journal of Mineral Processing*, 102 - 103, pp. 1-12

Boyes, W. (2010). Instrumentation reference book. 4th ed. Amsterdam: Butterworth-Heinemann/Elsevier, pp. 30-45.

Bunyak, D. (2000). To Float or Sink: A brief history of flotation milling. *The Mining History Journal*, 7, pp. 35-44.

Calvo, G., Mudd, G., Valero, A. and Valero, A. (2016). Decreasing ore grades in global metallic mining: A theoretical issue or a global reality? *Resources*, 5(4), p. 36.

Chao, L. (2016). An Investigation of Flotation Froth Rheology. Ph.D. The University of Queensland.

Chau, T.T., et al., (2009). A review of factors that affect contact angle and implications for flotation practice. *Advances in Colloid Interface Science*. 150 (2), pp. 106-115.

Clift, R., Grace, J. R. and Weber, M. E. (2005). Bubble, Drops, and Particles. Dover Publications Inc., Mineola, NY, USA, pp. 169-202.

Coleman, R. (2009). Flotation cells: Selecting the correct concentrate launder design. *Filtration & Separation*, 46(6), pp. 36-37.

Dahlke, R., Gomez, C. and Finch J. A. (2005). Operating range of a flotation cell from gas holdup vs. gas rate. *Minerals Engineering*. 18 (9), pp. 977-980.

Duan, J., Fornasiero, D. and Ralston, J. (2003). Calculation of the flotation rate constant of chalcopyrite particles in an ore. *International Journal of Mineral Processing*, 72(1-4), pp. 227-237.

Farrokhpay, S. (2011). The significance of froth stability in mineral flotation- A review. *Advances in Colloid and Interface Science*, 166, pp. 1-7.

Finch, J. A. and Dobby, G. S. (1990). Column Flotation. Pergamon Press, Oxford, UK.

Fragomeni, D., Hoffman, M., Kelly, A., Yu, S., Lotter, N. O. (2006). Flotation Mini Pilot Plant Experience at Falconbridge. *Mineral Processing Modeling, Simulation and Control Conference*, Ontario, Canada, 6 – 7 June.

Fuerstenau, M., Jameson, G. and Yoon, R. (2009). *Froth flotation*. Littleton, Colo.: Society for Mining, Metallurgy, and Exploration.

Gharai, M. and Venugopal, R. (2015). Modeling of flotation process – an overview of different approaches. *Mineral Processing and Extractive Metallurgy Review*, 37(2), pp. 120-133.

Gómez, C., Mesías, J. and Álvarez, J. (2017). Bubble Surface Area Flux and Performance in Laboratory Flotation Testing. *International Mineral Processing Congress Proceedings*.

Gorain, B.K., Harris, M.C., Franzidis, J.P. and Manlapig, E.V. (1998). The effect of froth residence time on the kinetics of flotation. *Minerals Engineering*, 11, pp. 627-638

Gorain, B.K., Harris, M.C., Franzidis, J.P. and Manlapig, E.V. (1998).Validation of k-Sb relationship and effect of froth depth. *Minerals Engineering*, 11, pp. 615-626

Gu, G., Xu, Z., Nandakumar, K. and Masliyah, J. (2003). Effects of physical environment on induction time of air-bitumen attachment. *International Journal of Mineral Processing*, 69 (1-4), pp. 235-250.

Hadler, K. and Cilliers, J. (2009). The relationship between the peak in air recovery and flotation bank performance. *Minerals Engineering*, 22(5), pp. 451-455.

Hadler, K., Greyling, M., Plint, N. and Cilliers, J. (2012). The effect of froth depth on air recovery and flotation performance. *Minerals Engineering*, 36 (38), pp. 248-253.

Hadler, K., Smith, C. and Cilliers, J. (2010). Recovery vs. mass pull: The link to air recovery. *Minerals Engineering*, 23 (11-13), pp. 994-1002.

Harris, A., Venkatesan, L. and Greyling, M. (2013). A practical approach to plant-scale flotation optimization. *Journal of the Southern African Institute of Mining and Metallurgy*, 113 (3), Available at: http://www.scielo.org.za/scielo.php?script=sci_arttext&pid=S2225-62532013000300016 [Accessed 22 October 2019].

Harris, M., C. (2013). Modelling the Froth Transport Zone in a Flotation Cell. AMIRA P9P Discussion Document (unpublished).

Health, J. (2016). Optimizing froth area of the flotation cell [Webinar]. Available at: https://www.911metallurgist.com/blog/wp-content/uploads/2016/06/Flotation-Cell-Froth-Area-Optimization-by-Crowding.pdf [Accessed 16 September 2019].

ISA95 (2019). International standard from the International Society of Automation. Available at: https://www.plm.automation.siemens.com/global/en/our-story/glossary/isa-95-framework-and-layers/53244 [Accessed 19 November 2019].

Isaksson, A. (2018). Evaluation of Scale-up Model for Flotation with Kristineberg Ore, Ph. D.

Jameson, G.J. (2012). The effect of surface liberation and particle size on flotation rate constants. *Minerals Engineering*. 36-38, pp. 132-137.

Johansson, G. and Pugh, R. (1992). The Influence of Particles Size and Hydrophobicity on the Stability of Mineralized Froths. *International Journal of Mineral Processing*, 34, pp. 1-21.

Jovanović, I. and Miljanović, I. (2015). Modelling of Flotation Processes by Classical Mathematical Methods – A Review. *Archives of Mining Sciences*, 60 (4), pp. 905-919.

Kawatra, S. and Young, C. (2019). SME mineral processing & extractive metallurgy handbook. 1st ed. Society for Mining, Metallurgy, and Exploration, pp. 1053-1062.

Kejonen, I., Haavisto, O., Martikainen, J., Suontaka, V. and Musuku, B. (2018). Improving grade control efficiency with rapid on-line elemental analysis. *Minerals Engineering*,

124, pp. 68-73.

King, R. (2012). Modeling and Simulation of Mineral Processing Systems. 2nd ed. Society for Mining, Metallurgy, and Exploration, pp. 351-415.

Klimpel, R. R. (1980). Selection of chemical reagents for flotation. Mineral Processing Plant Design, 2nd ed. AIME, New York, pp. 907-934.

Klimpel, R. R., Isherwood, S. (1991). Some industrial implications of changing frother chemical structure. *International Journal of Mineral Processing*. 33 (1-4), pp. 369-381.

Laurila, H., Karesvuori, J., and Tiili, O. (2002). Strategies for Instrumentation and Control of Flotation Circuits. Mineral Processing Plant Design, Practice, and Control. 1st ed. Society for Mining, Metallurgy, and Exploration, pp. 2174-2195.

Law, K. (2014). Definitions for Hydrophilicity, Hydrophobicity, and Superhydrophobicity: Getting the Basics Right. *The Journal of Physical Chemistry Letters*, 5(4), pp. 686-688.

Liu, J., Gui, W. and Tang, Z. (2013). Flow velocity measurement and analysis based on froth image SIFT features and Kalman filter for froth flotation. *Turkish Journal of Electrical Engineering & Computer Science*, 21, pp. 2378-2396.

Liu, C., Chen, Y., Song, S. and Li, H. (2018). The effect of aluminum ions on the flotation separation of pentlandite from lizardite. *Colloids and Surfaces A: Physicochemical and Engineering Aspects*, 555, pp. 708-712.

Lundh, M., Gaulocher, S., Pettersson, J., Lindvall, H. and Gallestey, E. (2009). Model Predictive Control for Flotation Plants. Available at: https://library.e.abb.com/public/d3579dd3cbc2fe5bc125762e0043dec2/Sudbury_MPC_Flotation_2033.pdf [Accessed 28 June 2019]

Malewski, J. and Krzeminska, M. (2012). Dependence of mine revenue on the grade of copper concentrate. *Physicochemical Problems of Mineral Processing*, 48(2), pp. 559-568.

Maree, W., Kloppers, L., Hangone, G. and Oyekola, O. (2017). The effects of mixtures of potassium amyl xanthate (PAX) and isopropyl ethyl thionocarbamate (IPETC) collectors

on grade and recovery in the froth flotation of a nickel sulfide ore. *South African Journal of Chemical Engineering*, 24, pp. 116-121.

Meinert, L., Robinson, G. and Nassar, N. (2016). Mineral Resources: Reserves, Peak Production and the Future. *Resources*, 5 (1), p.14.

Miettunen, J. (1983). The Pyhäsalmi Concentrator – 13 Years of Computer Control. *International Federation of Automation Control Proceedings Volumes*, 16 (15), pp. 423-433.

Mintek (2011). Measurement and Control Solutions – FloatStar. Available at: https://www.mintek.co.za/technical-divisions/measurement-and-control-solutions-mac/control-solutions/floatstar/ [Accessed 19 November 2019].

Nazari, S. and Cristonffanini, C. (2019). Digital Twin in Mineral Processing. In: *Canadian Mineral Processors*. Richmond, BC: Andritz, pp. 92-101.

Neethling, S. and Cilliers, J. (2012). Grade-recovery curves: A new approach for analysis of and predicting from plant data. *Minerals Engineering*, 36-38, pp. 105-110.

Nguyen, A. (2007). FLOTATION. Encyclopedia of Separation Science, pp.1-27.

Oliver, S. and Tooher, R. (2018). Optimising flotation plant operation by using a digital twin in the control room. *AusIMM Mill perators' Conference*. Victoria: The Australasian Institute of Mining and Metallurgy, pp. 93 - 101.

Outotec (2015). HSC Chemisty history. Available at: https://www.outotec.com/products/digital-solutions/hsc-chemistry/hsc-chemistry-history/ [Accessed 5. November 2019].

Outotec (2018). Flotation launder design. Outotec south east asia pacific region customer eNewsletter, 3, pp.5-7, Available at: https://www.outotec.com/globalassets/newsletters/output/2018-3/3.-flotation-launder-design.pdf [Accessed 16 September 2019].

Outotec (2019a). Basics in Mineral Processing, [online course by Outotec]

Outotec (2019b). Advanced Control Solutions for Concentrator Plants – OUTOTEC INTERNAL material

Park, S. and Seo, M. (2011). Interface Science and Composites. *Interface Science and Composites*, 18, pp. 1-3.

Pugh, R. (2016). Bubble and foam chemistry. 1st ed. Cambridge University Press, p.3.

Remes, A., Izart, C., et al., (2019). HSC – Sim MinPro Unit Models: Flotation Cell: MU-310-11. pp. 128-145.

Remes, A., Kongas, M., Saloheimo, K. and Jämsä-Jounela, S. (2005). Economical Effects of On-line Elemental Analysis Performance on Flotation Control.

Remes, A., Tommiska, J., and Lamberg, P. (2019). Mass Balance Module, Available at: https://www.outotec.com/globalassets/products/digital-solutions/hsc/51-Mass-Balance.pdf [Accessed 4 September 2019]

Savassi, O.N., Alexander, D.J., Johnson, N.W., Franzidis, J.P., Manglapig, E.V. (1997). Measurement of froth recovery of attached particles in industrial flotation cells. *Mill Operators Conference Proceedings*, 6, pp. 149–155.

Savassi, O. N., Alexander, D, J., Franzidis, J. and Manlapig, E. (1998). An empirical model for entrainment in industrial flotation plants. *Minerals Engineering*, 11 (3), pp. 243-256.

Sbárbaro, D. and Del Villar, R. (2010). Advanced control and supervision of mineral processing plants. 1st ed. London: Springer, pp. 287-308.

Shean, B. and Cilliers, J. (2011). A review of froth flotation control. *International Journal of Mineral Processing*, 100 (3-4), pp. 57-71.

Shi, F. and Zheng, X. (2003). The rheology of flotation froths. *International Journal of Mineral Processing*, 69 (1-4), pp. 115-128.

Shumba, T. (2014). Relationship between flotation operational factors and froth behaviour. BSc. University of Cape Town.

Suichies, M., Leroux, D., Dechert, C. and Trusiak, A. (2000). An implementation of generalized predictive control in a flotation plant. *Control Engineering Practice*, 8 (3), pp. 319-325.

Supomo, A., Yap, E., Zheng, X., Banini, G., Mosher, J. and Partanen, A. (2008). PT Freeport Indonesia's mass-pull control strategy for rougher flotation. *Minerals Engineering*, 21(12-14), pp.808-816.

Subrahmanyam, T. and Forssberg, E., (1988). Froth stability,particle entrainment and drainage in flotation. *International Journal of Minerals Processing*, 23, pp. 33-53.

Trahar, W.J., 1981. A rational interpretation of the role of particle size in flotation. *International Journal of Mineral Processing*, 8 (4), pp. 289-327.

Wang, L., Peng, Y., Runge, K. and Bradshaw, D. (2015). A review of entrainment: Mechanisms, contributing factors and modelling in flotation. *Minerals Engineering*, 70, pp. 77-91.

Willard, T. (2010). Mining Chemical Handbook. Cytec Industries Inc.

Wills, B. and Finch, J. (2015). Wills' mineral processing technology: an introduction to the practical aspects of ore treatment and mineral recovery. 8th ed. Oxford: Butterworth-Heinemann, pp. 1-27, 41-90, 265-380.

Wills, B. and Tim Napier-Munn, (2006). Will's mineral Processing Technology. Massachusetts: Elsevier Science and Technology Books.

Welsby, S. D. D. (2014). Pilot-scale froth testing at Highland Valley Copper. *Canadian Mineral Processing Conference Proceedings*, Ottawa, Canada, pp. 301-314.

Zanin, M., Lambert, H. and du Plessis, C. (2019). Lime use and functionality in sulphide mineral flotation: A review. *Minerals Engineering*, 143, 105922.

Zhang, W., Nesset, J. E. and Finch, J. A. (2010). Water recovery and bubble surface area flux in flotation. *Canadian Metallurgical Quarterly*, 49 (4), pp. 353-362.

Zheng, X., Franzidis, J. and Manlapig, E. (2004). Modelling of froth transportation in industrial flotation cells. *Minerals Engineering*, 17 (9-10), pp. 981-988.

Yianatos, J., Moys, M., Contreras, F. and Villanueva, A. (2008). Froth recovery of industrial flotation cells. *Minerals Engineering*, 21 (12-14), pp. 817-825.

Yianatos, J. and Berg, L. (2013). Control of rougher flotation circuits aided by industrial simulator. *Journal of Process Control*, [online] 23(2), pp. 140-147.

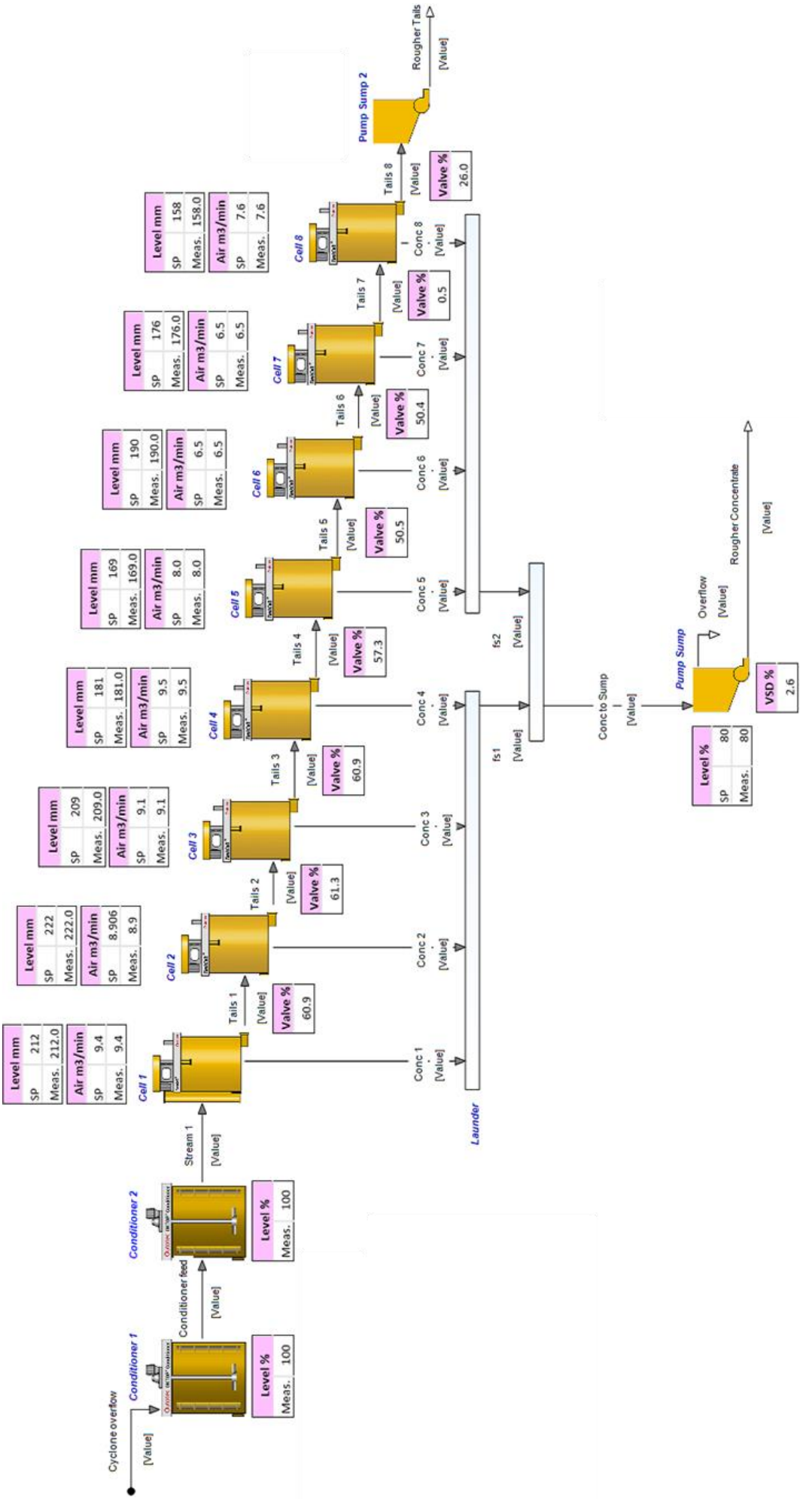
Cyclone overflow
[Value]
Conditioner 1
Level %
SP
Meas. 100
Conditioner feed
[Value]
Conditioner 2
Level %
SP
Meas. 100
Stream 1
[Value]
Launder
Cell 1
Level mm
SP 212
Meas. 212.0
Air m3/min
SP 9.4
Meas. 9.4
Conc 1
[Value]
Tails 1
[Value]
Valve % 60.9
Cell 2
Level mm
SP 222
Meas. 222.0
Air m3/min
SP 8.906
Meas. 8.9
Conc 2
[Value]
Tails 2
[Value]
Valve % 61.3
Cell 3
Level mm
SP 209
Meas. 209.0
Air m3/min
SP 9.1
Meas. 9.1
Conc 3
[Value]
Tails 3
[Value]
Valve % 60.9
Cell 4
Level mm
SP 181
Meas. 181.0
Air m3/min
SP 9.5
Meas. 9.5
Conc 4
[Value]
Tails 4
[Value]
Valve % 57.3
Cell 5
Level mm
SP 169
Meas. 169.0
Air m3/min
SP 8.0
Meas. 8.0
Conc 5
[Value]
Tails 5
[Value]
Valve % 50.5
Cell 6
Level mm
SP 190
Meas. 190.0
Air m3/min
SP 6.5
Meas. 6.5
Conc 6
[Value]
Tails 6
[Value]
Valve % 50.4
Cell 7
Level mm
SP 176
Meas. 176.0
Air m3/min
SP 6.5
Meas. 6.5
Conc 7
[Value]
Tails 7
[Value]
Valve % 0.5
Cell 8
Level mm
SP 158
Meas. 158.0
Air m3/min
SP 7.6
Meas. 7.6
Conc 8
[Value]
Tails 8
[Value]
Valve % 26.0
Pump Sump 2
Rougher Tails
[Value]
fs1
[Value]
fs2
[Value]
Conc to Sump
[Value]
Pump Sump
Level %
SP 80
Meas. 80
Overflow
[Value]
Rougher Concentrate
[Value]
VSD %
2.6

Step 1 – frothSpeed1

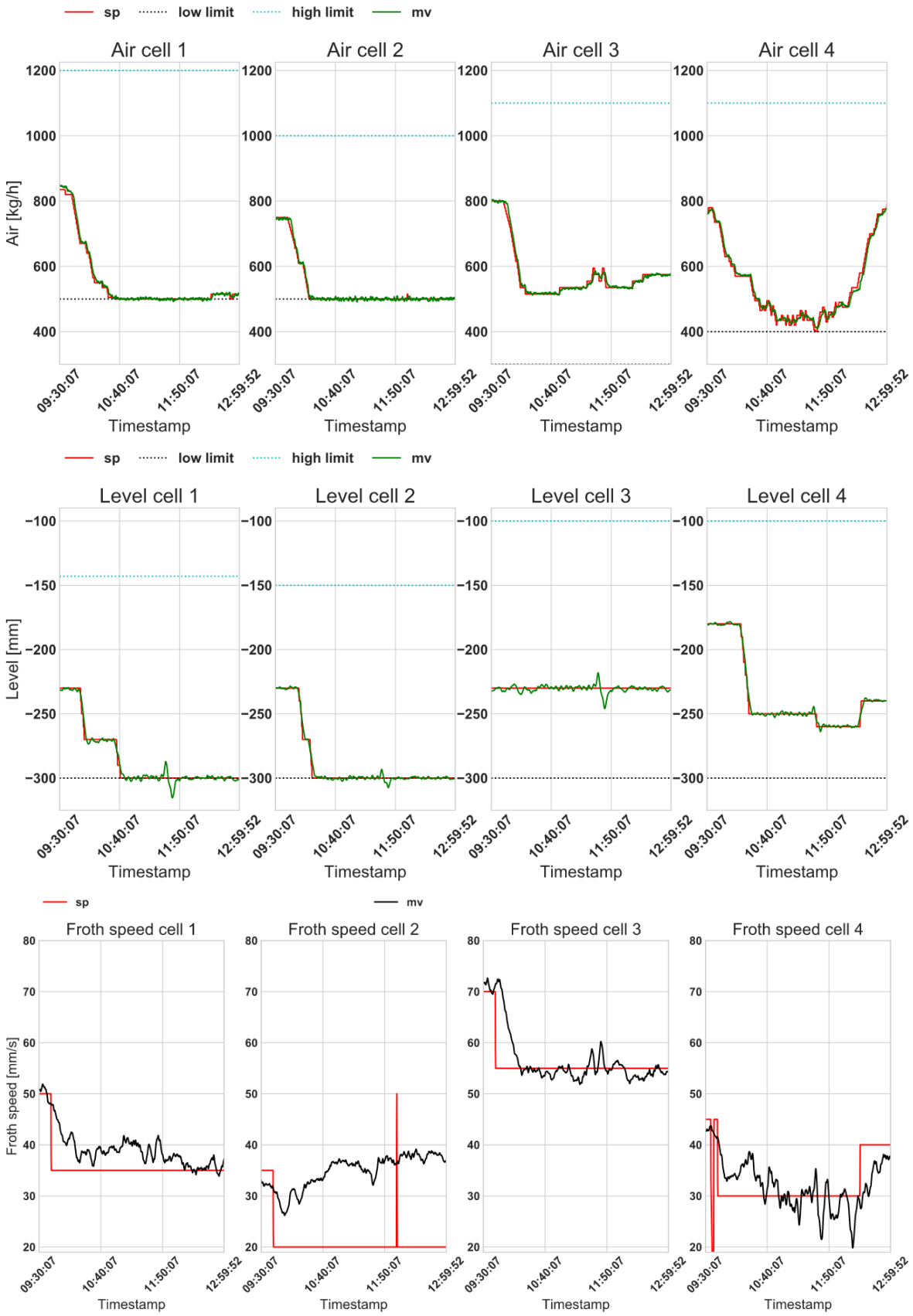

Step 2 – frothSpeed1

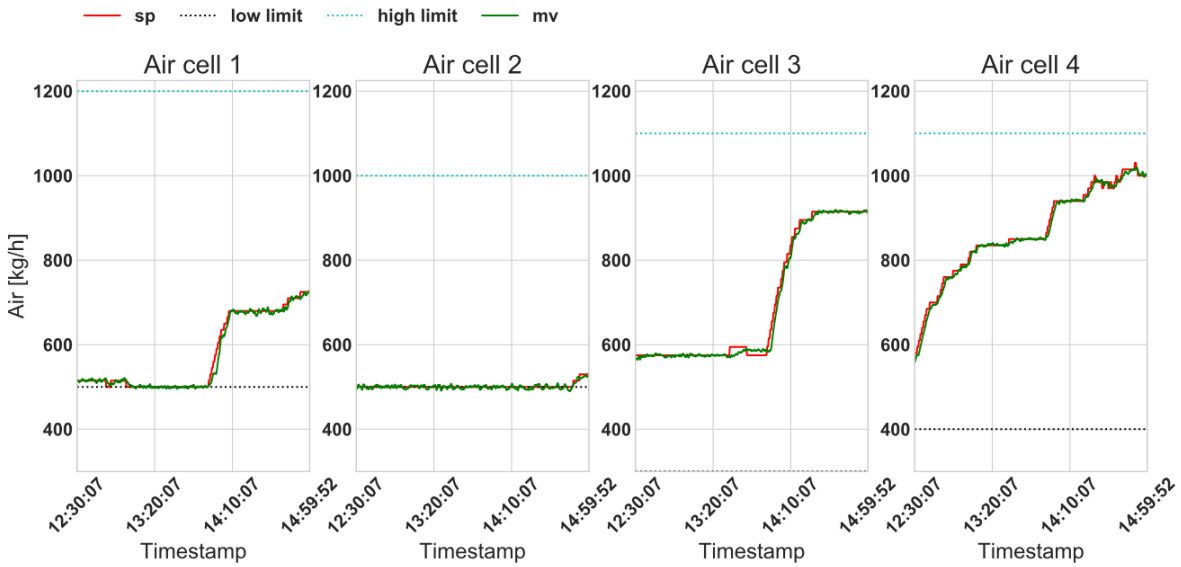

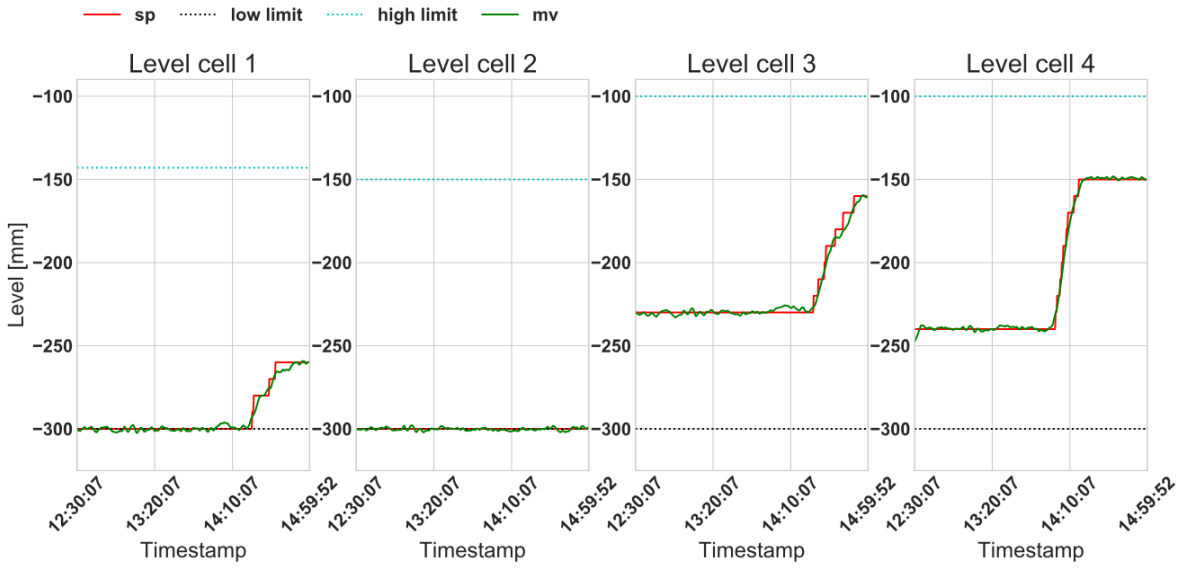

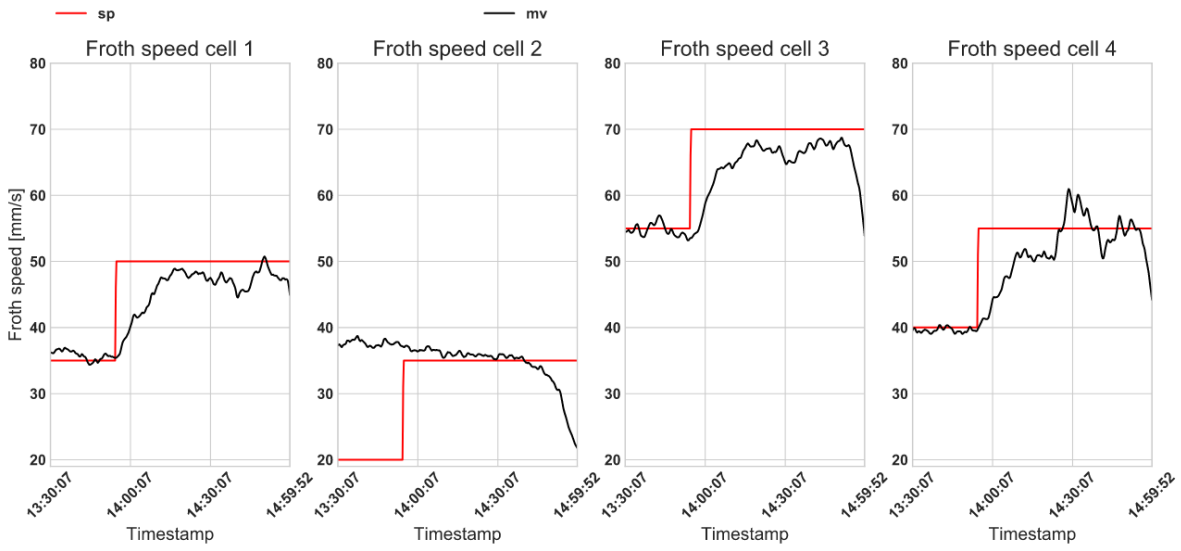

Step 3 – frothSpeed1

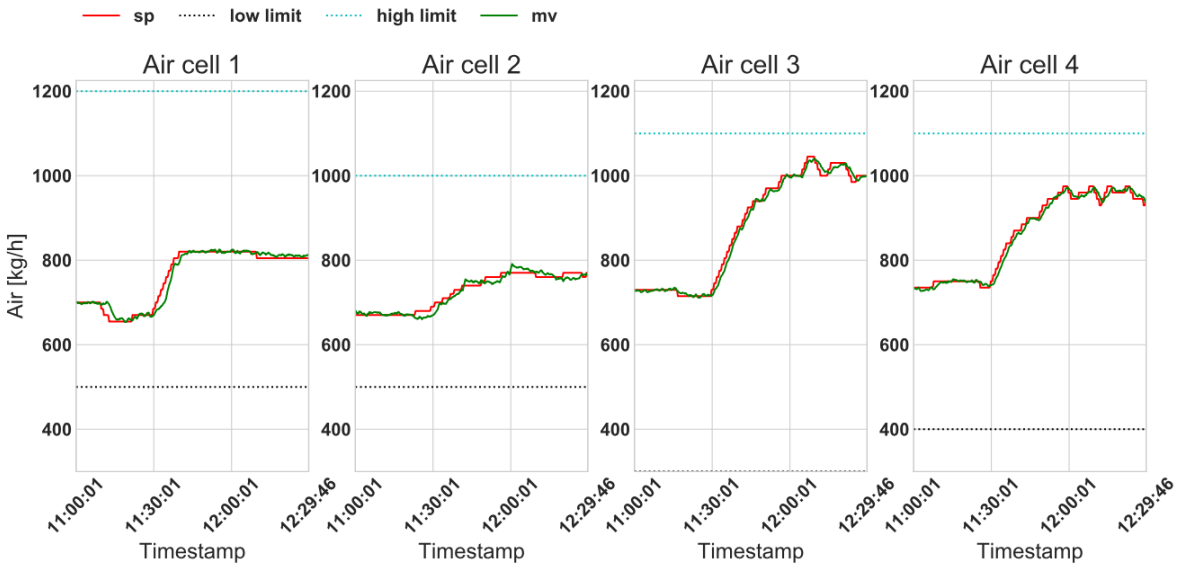

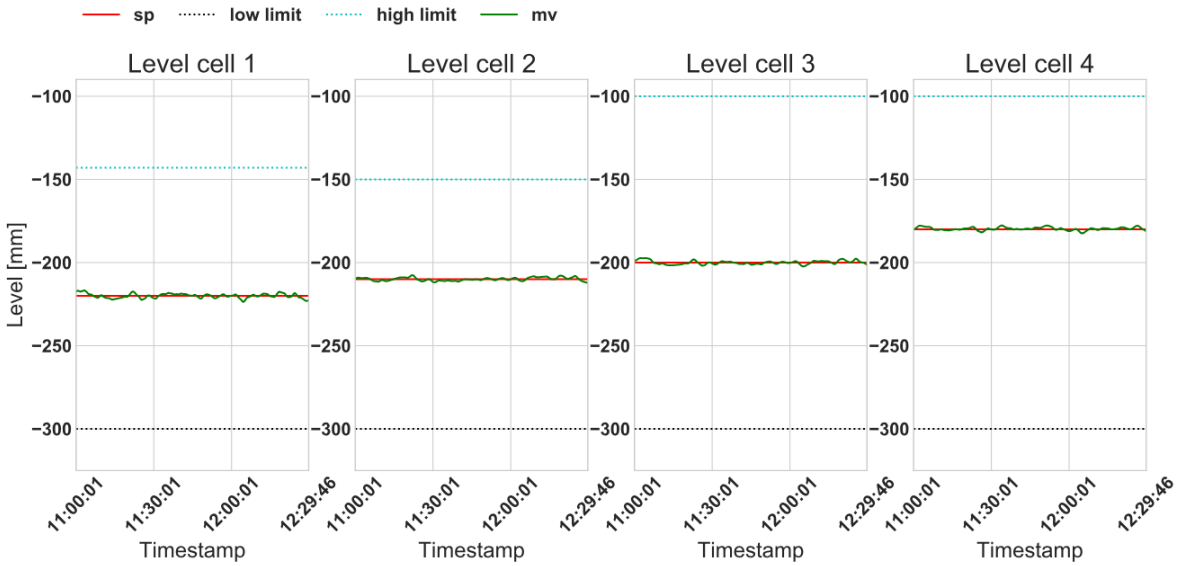

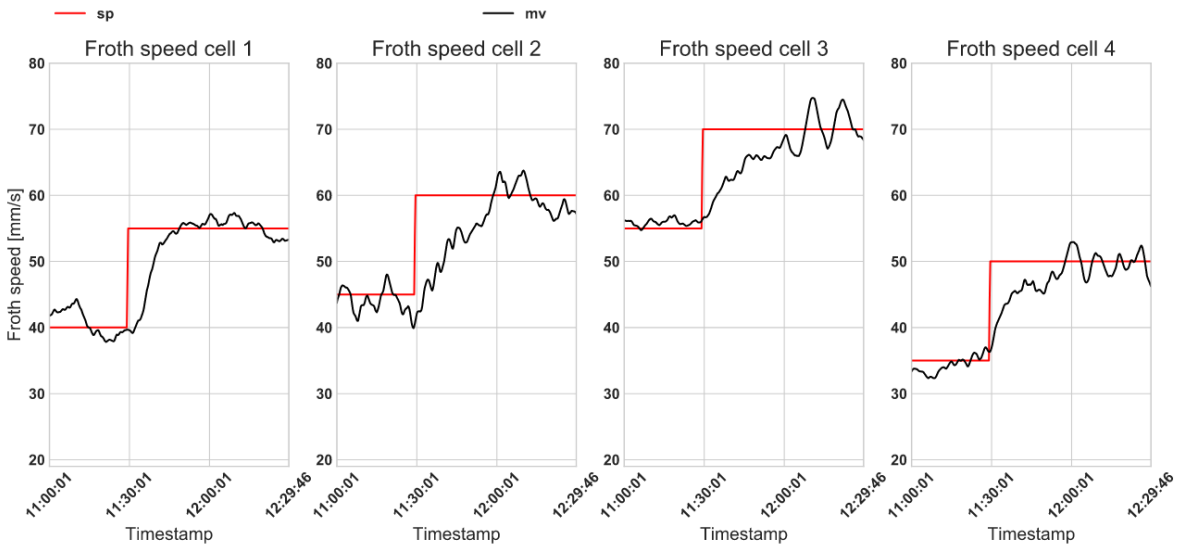

Step 4 – frothSpeed1

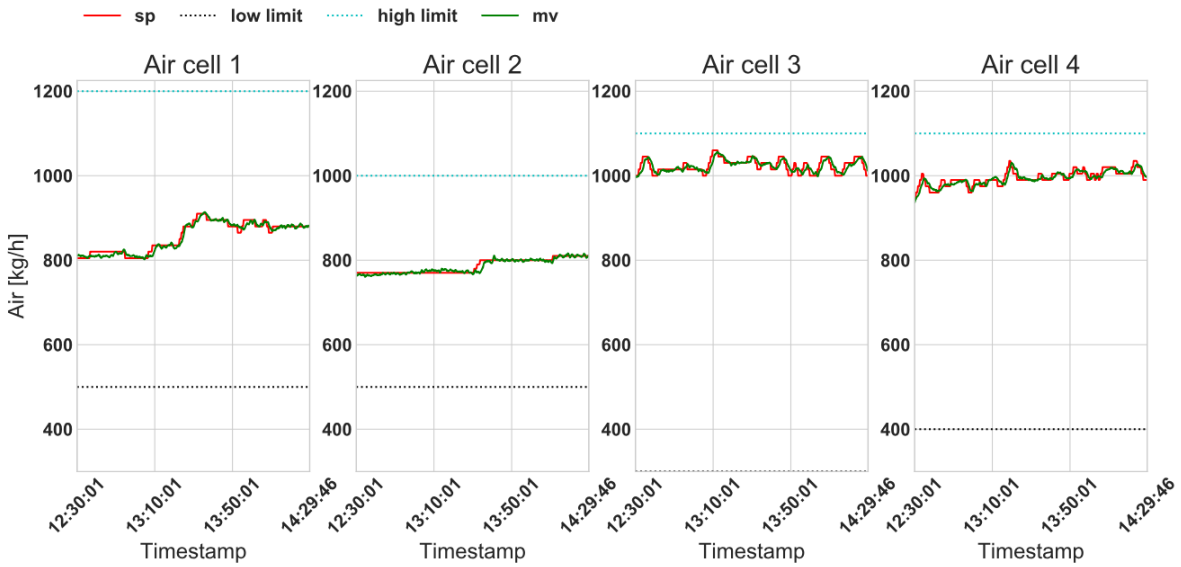

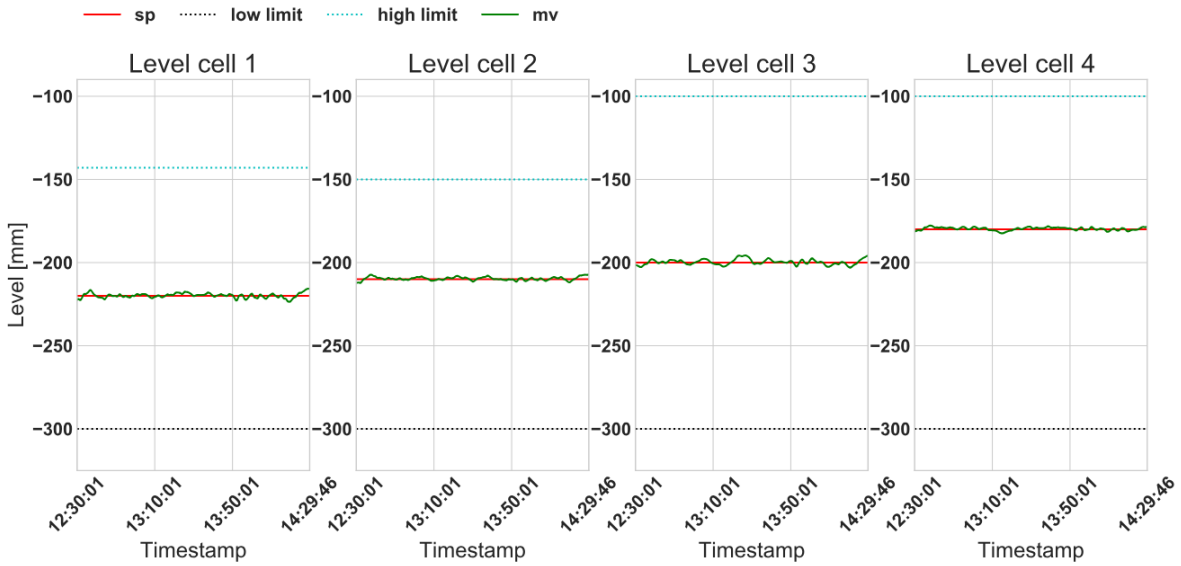

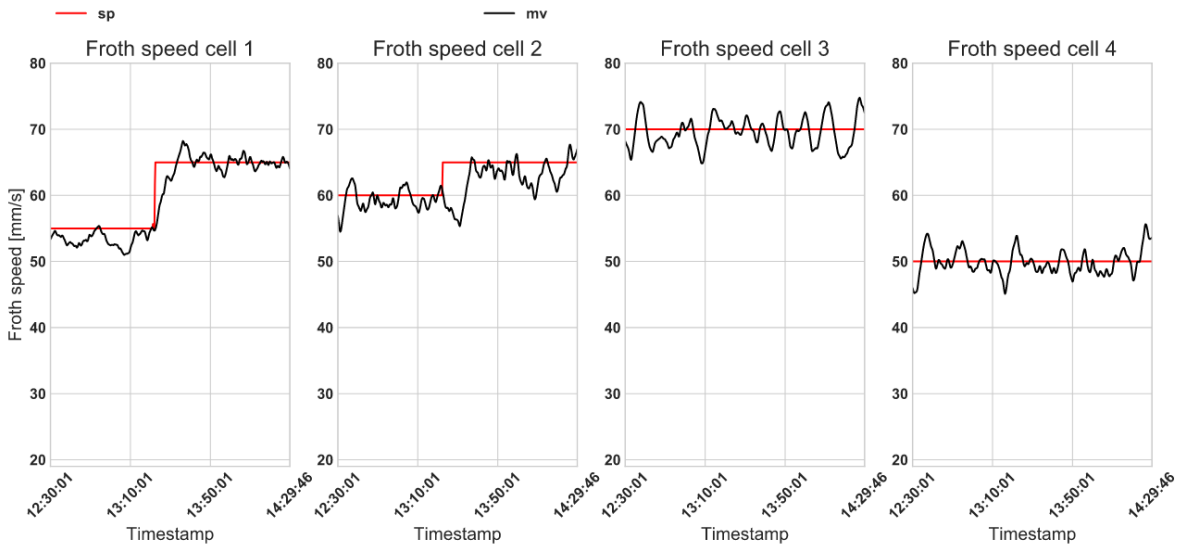

Step 5 frothSpeed2